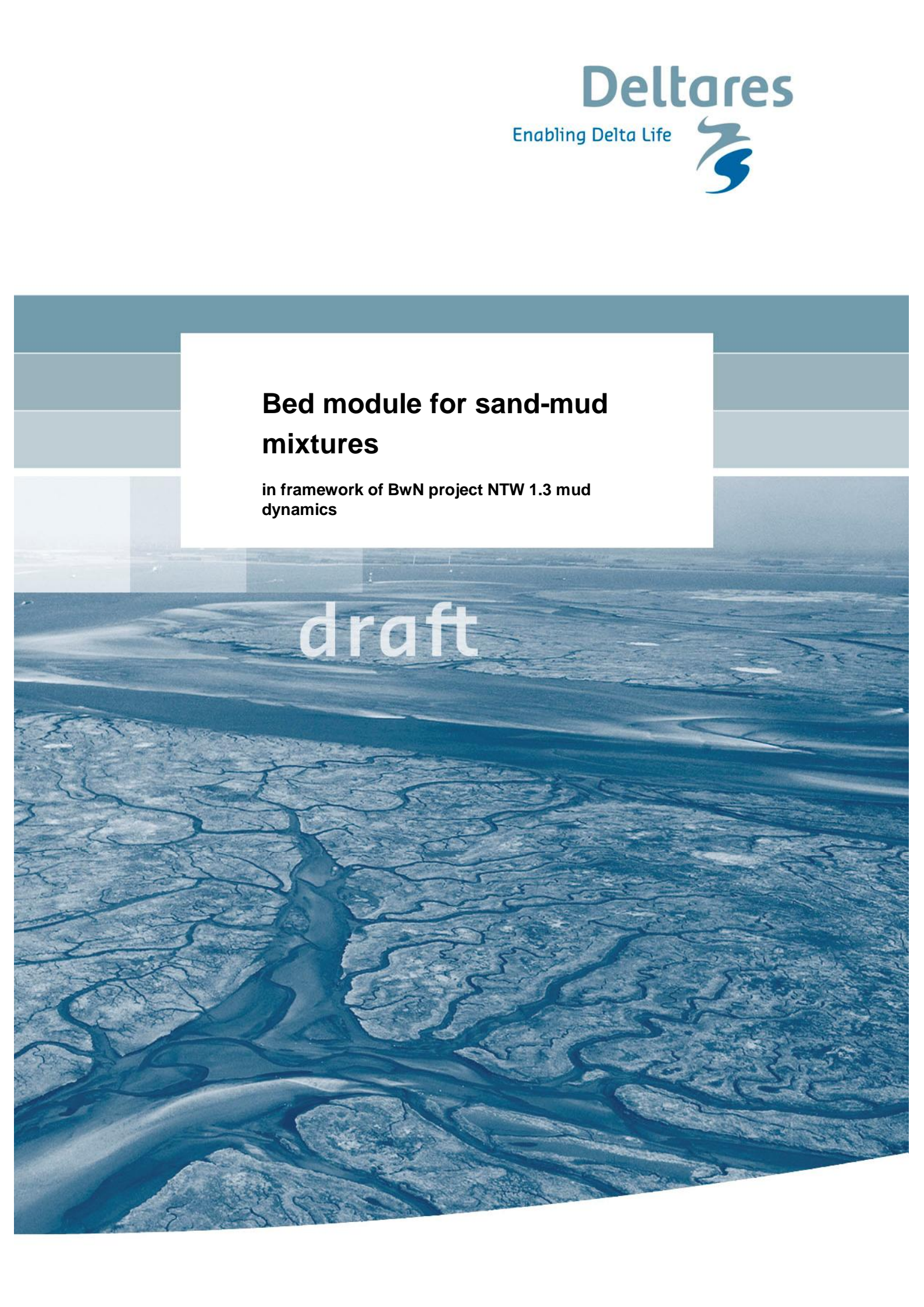


## **Bed module for sand-mud mixtures**

in framework of BwN project NTW 1.3 mud dynamics

draft





## **Bed module for sand-mud mixtures**

**in framework of BwN project NTW 1.3 mud dynamics**

Thijs van Kessel  
Aukje Spruyt-de Boer  
Jebbe van der Werf  
Luca Sittoni  
Bram van Prooijen  
Han Winterwerp

1200327-000



**Title**

Bed module for sand-mud mixtures

**Client**

Ecoshape

**Project**

1200327-000

**Reference**

1200327-000-ZKS-0013

**Pages**

111

**Keywords**

sand-mud mixtures bed module Delft3D

**Summary**

This report described the development and application of a bed module for sand-mud mixtures. The open-source module is available as both stand-alone Fortran module and fully integrated in Delft3D. To steer the stand-alone version, a simple Matlab interface is available. The Delft3D version uses the existing user interface. Both versions are available from the web.

**References**

Building with Nature Project NTW 1.3 Mud Dynamics

Version	Date	Author	Initials	Review	Initials	Approval	Initials
1	sep. 2012	Thijs van Kessel		Johan Boon		Tom Schilperoort	
		Aukje Spruyt-de Boer					
		Jebbe van der Werf					
		Luca Sittoni					

**State**

draft

This is a draft report, intended for discussion purposes only. No part of this report may be relied upon by either principals or third parties.



## Contents

<b>1</b>	<b>Introduction</b>	<b>1</b>
<b>2</b>	<b>Literature review</b>	<b>3</b>
2.1	Introduction	3
2.2	Mud infiltration mechanisms	3
2.2.1	Sedimentological processes	3
2.2.2	Bioturbation	4
2.2.3	Advective transport	5
2.2.4	Turbulent diffusion	6
2.2.5	Modelling	7
2.3	Residence time & infiltration rates	7
2.3.1	Infiltration rates	7
2.3.2	Mixing rates & diffusion coefficients	8
2.3.3	Residence time	9
2.3.4	Measurement methods	9
2.4	Erosion rate of sand-mud mixtures	10
2.5	The North Sea	11
2.5.1	Mud content	11
2.5.2	Bioturbation	11
2.5.3	Pore water flow	12
2.6	Discussion and conclusion	15
<b>3</b>	<b>Description of bed module</b>	<b>19</b>
3.1	Introduction	19
3.2	Mixed Eulerian-Lagrangian approach	20
3.2.1	Delft3D input files	21
3.2.2	Examples	22
3.3	Mixing between layers	26
3.3.1	Delft3D input files	28
3.3.2	Examples	30
3.3.3	Changes in the source code	35
3.4	Fluff layer concept	36
3.4.1	Method 1	37
3.4.2	Method 2	39
3.4.3	Delft3D input files	40
3.4.4	Changes in the source code	41
3.5	Formulations for sand-mud interaction	43
3.5.1	Non-cohesive regime ( $p_m < p_{m,cr}$ )	44
3.5.2	Cohesive regime ( $p_m > p_{m,cr}$ )	44
3.5.3	Results	46
3.5.4	Implementation in Delft3D	49
3.5.5	Delft3D input files	50
3.5.6	Examples	50
3.5.7	Changes in the source code	54

<b>4 Idealised Tests</b>	<b>55</b>
4.1 Introduction	55
4.2 Test 1: General test	55
4.3 Test 2: Vertical diffusion	65
4.4 Test 3: Fluff layer	73
4.5 Test 4: Sand-mud interaction	78
<b>5 Practical Application</b>	<b>81</b>
5.1 Introduction	81
5.2 Model and Model Outputs Description	81
5.3 Parameters Setting and Variations	82
5.4 Results	83
5.4.1 Group 1	84
5.4.2 Group 2	86
5.4.3 Group 3	92
5.4.4 Group 4	95
5.4.5 Group 5	99
5.5 Conclusions	104
<b>6 Dissemination</b>	<b>107</b>
<b>Appendices</b>	
<b>A References</b>	<b>A-1</b>
<b>B Considerations on a generic water-bed exchange module</b>	<b>B-1</b>

## 1 Introduction

This report describes the development and application of a bed module for sand-mud mixtures. Such module is important, as sediment transport is often not solely determined by the carrying capacity of the flow, but also by the sediment supply from the bed.

The sink and source terms from and towards the bed depend on sediment composition. It is therefore important that information on sediment composition is tracked within a model. The bed model described in this report includes such tracking. Also, formulations have been included that describe the erosion behaviour of the bed as a function of bed composition.

If the mud fraction of the bed remains below a critical value, the erosion behaviour of the bed is non-cohesive. However, if the critical value is exceeded, the behaviour switches to cohesive. Erosion formulations change accordingly.

The structure of this report is as follows. In Chapter 2, a literature survey is described on the most important processes playing a role in mixed sand-mud beds. In Chapter 3, the formulations are described that have been implemented into the bed module. Also the development of the module itself is described herein. In Chapter 4, schematised tests with the bed module are described. These give insight into the basic functioning of the module. In Chapter 5 practical tests are described, using an existing realistic schematisation of the Wadden Sea. Finally, the dissemination of the bed module and possible steps for further development are discussed in Chapter 6.

Depending on the aim of and time availability for the reader, he or she may step directly to the chapter(s) of his or her main interest. All chapters may be read independently.



## 2 Literature review

### 2.1 Introduction

Research on the impact of large-scale sand mining in the Dutch coastal zone in the framework of Maasvlakte-2 land reclamation has demonstrated the influence of the assumed buffer capacity of fines in the sandy seabed on the long-term behaviour of the dispersion of fines (Van Kessel et al. & Van Prooijen et al., 2007). As insufficient knowledge on this buffer capacity exist, a literature review was made as a first step towards increasing the accuracy of fine sediment dispersion models.

Fine sediments penetrate into or are released from a sandy substrate, depending on the hydrodynamic conditions. Release of fine sediments results in an increasing sediment concentration in the upper water column, while penetration of fines into the bed lowers the suspended sediment concentration. This so-called buffering of fines into a sandy substrate has been demonstrated to influence the annual variation of the suspended sediment concentration: In the North Sea, the mud concentrations 2 km offshore are larger during and after storms than before storms. It takes days to weeks for the concentrations to return to pre-storm values. The autumn sediment concentrations are lower than the spring sediment concentrations, during similar hydrodynamic conditions (Kleinhans et al., 2005).

The physical processes responsible for the buffering of fine sediments still remain to be further explored. This literature review aims to summarize the mud infiltration mechanisms in subtidal marine sediment beds, estimates of mixing rates and residence times of mud in sand beds, and state-of-the-art modelling efforts. Although primarily generic, this review is also regionally focusing on the North Sea area. The infiltration mechanisms in intertidal areas such as swash on sloping beaches (i.e. Turner and Masselink, 1998) or sand banks (Gibbes et al. 2008s, 2008b) are not evaluated here.

### 2.2 Mud infiltration mechanisms

In muddy, cohesive sediment, solutes are mainly transported by molecular diffusion, and possibly by benthic fauna. Interstitial flow is much faster in permeable sands, resulting in higher advective transport rates (see Figure 2.1). Advective transport is flow-induced material transport through sediment pores, driven by pressure gradients. Especially in the presence of bedforms, advective transport in permeable sediments may be high. Furthermore, fine sediment may be mixed or released from a sand bed through bedform migration. These mechanisms can be summarized as (1) sedimentological processes, (2) biological processes, (3), advective transport, and (4) molecular diffusion, which will be elaborated hereafter.

#### 2.2.1 Sedimentological processes

The entrainment of muds into suspension is coupled to bedform dynamics. Mobile bedforms create an active layer of sediment with a thickness approximately equal to the bedform height, to be mobilised during one or a few storms. On a timescale of 1-10 years, bedforms smaller than sandwaves, macrobenthos, and fishing determine the mobility depth (Kleinhans et al, 2005).

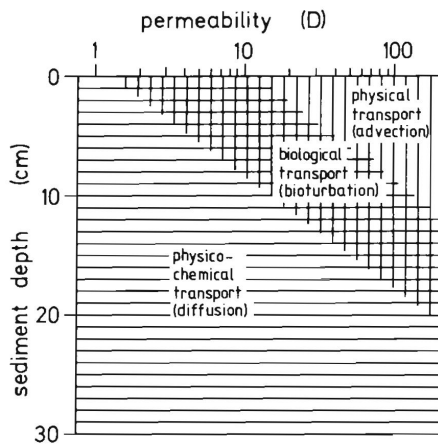


Figure 2.1 Mixing process as a function of depth and permeability ( $D$ , in  $10^{-13} \text{ m}^2$ ). From Huettel and Gust, 1992.

Mud infiltrates a sand bed by bedform dynamics through two mechanisms:

- 1 Mud drapes (consolidated or not) are covered by bedforms. In the North sea, these drapes are typically 1-5 mm thick (Kleinhans et al., 2005). Such mud drapes can probably only form during summer neap tides. Burial by large bedforms, such as sandwaves, may lead to residence times of the mud in the sand bed of 1 century.
- 2 The upper part of a sediment bed is permanently mobilised by ripples (the active layer), even during fairly tranquil conditions during which a substantial amount of fine sediment may settle towards the bed. In the North Sea, ripples generated by tidal currents bury fine sediment up to a depth of 5 cm (Kleinhans et al., 2005). Most organisms must migrate below the active layer to survive highly energetic conditions (Kleinhans et al., 2005).

Marinelli et al (1998) measured a 'reset' of tracer concentrations during the winter storm season. A single hurricane was insufficient to vertically mix and lower the tracer concentrations, from which they assumed that longer term energetic conditions are needed to reset the profile.

## 2.2.2 Bioturbation

Organisms influence sediment beds mainly through biodeposition, biostabilization, and bioturbation. Biodeposition results in increased sedimentation rates, biostabilization in reduced erosion rates, and bioturbation in increased mixing rates (which, usually, increases the erosion rate). Modelling results by Paarlberg et al. (2004) suggest that destabilizing organisms reduce the mud content in a bed, whereas stabilizing organisms may cause an increase in the mud content.

Biodeposition through faeces production is different for deposit feeders, which only change the characteristics of existing sediment, and filter feeders, which add new material to the sediment (Lee and Swartz, 1980). Bed sediment is stabilized through microbial binding (micro-organisms, especially polysaccharides), tubes (especially species that burrow firm tubes), roots by aquatic vegetation, and by benthic macroalgal mats. Bioturbation results in the vertical mixing of surface sediment. Mixing rate and burial depth depend on the species that occur at a typical site, which in turn relate to the hydrodynamic conditions, sediment available, nutrients and temperature. Hence, the variation of mixing by bioturbation is large.

An extensive review of reworking rate and penetration depth is given by Lee and Swartz (1980).

### 2.2.3 Advective transport

Advective transport is the transport of fines by interstitial porewater flow in stationary sediment beds. Fines and the coarser sediment matrix are therefore not physically mixed: the sand matrix through which the fines percolate remains unchanged. Mechanisms of advective transport are (Huettel and Webster, 2001):

- Current-topography interaction by steady flow as well as by oscillating wave-generated currents.
- Wave-generated pressure gradients.
- Haline or thermal convection.

#### 2.2.3.1 Current-topography interaction

Pressure differences generated by bedforms cause inflow into the bedform troughs and outflow from the bedform crests (see Figure 2.2). Infiltration rates are highest for fines with a grain size of  $1\ \mu\text{m}$  as smaller grain sizes adhere to particles, while coarser are blocked by the pores (Huettel et al., 1996). In a shallow but calm environment (0.5 m deep, wave height less than 0.1 m), the bulk porewater flow velocity decreases from nearly 50 cm/hr or  $140\ \mu\text{m/s}$  (near-surface) to 20 cm/hr at a depth of 5 cm (Precht and Huettel, 2004). In addition to bedforms, bioroughness may also generate pressure differences sufficiently high to generate pore water flows (Huettel and Gust, 1992). Thibodeaux and Boyle (1987) measured inflow velocities of around  $50\ \mu\text{m/s}$ , and intrusion depth 5 times the bedform height. Wilson et al. (2008) estimate that under typical shelf conditions, bottom currents induce pressure gradients up to 2 Pa/cm across seafloor ripples and similar seafloor features. Resulting porewater flows can reach the upper 30 cm of sediments below the seafloor. The magnitude of this flow depends on the permeability of the sediments in question, and laboratory studies suggest that this type of flow does not affect biogeochemical processes significantly below a permeability of roughly  $10^{-12}\ \text{m}^2$  (Wilson et al., 2008).

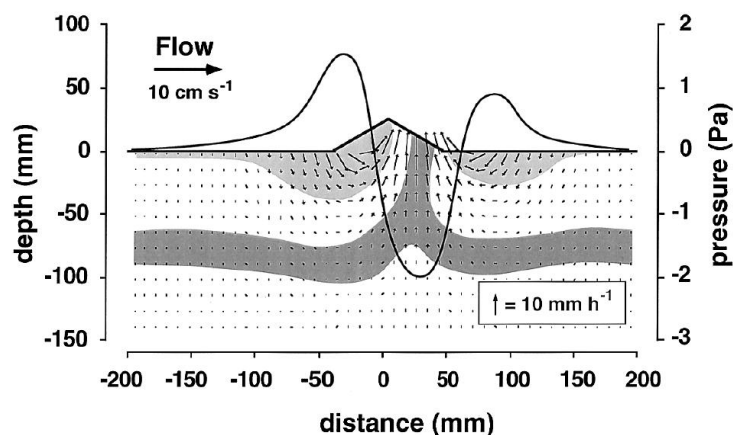


Figure 2.2 Infiltration and outflow due to pressure variations over bed-topography interaction in steady uniform flow. From Huettel et al., 1998.

### 2.2.3.2 Wave-generated pressure gradients

Alternatively, mud infiltration into sand beds may be substantially increased by wave-generated pressure gradients (Riedl et al, 1972, Harrison et al., 1983, Shum, 1993). The dynamic pressure gradients generated by waves creates oscillating horizontal near-bed flows, as well as oscillating pressure gradients. The horizontal flow velocities produce inflow of pore water when interacting with morphologic perturbations, which is basically the mechanism described in section above. The focus here is on the effect of the time-varying pressure gradients near the bed, generating inflow and outflow of pore water.

Wave –generated pressures are highest under the wave crest, resulting in inflow, while water flows upward under the wave trough. The result is an elliptical trajectory of the porewater within the bed, more analogue to eddy diffusion than to advection (Riedl et al., 1972, Harrison et al., 1983). The resulting exchange velocity between the bed and the water column depends on wave characteristics (wave height, and length), fluid viscosity, bed permeability which was elaborated in detail by Riedl et al. (1972). The depth to which the porewater penetrates as a result of wave-driven pressure difference is not quantified. Transport of porewater within the sand bed itself were addressed by Harrison et al. (1983) and Rutgers van der Loeff (1981) Harrison et al. (1983) quantified the wave-driven mechanical dispersion whereby wave-enhanced transport is simulated with an empirical diffusion coefficient. Wave-driven mechanical dispersion is favored by large grain size or high permeability, large sediment thickness, large wave amplitude, and shallow water. However, the mechanisms by which an oscillatory flow generates net advective transport are not obvious. Solute transport in a porous medium forced by an oscillatory flow may be caused by rotational dispersion or by shear dispersion (Webster, 2003). Rotational dispersion requires that the pore water excursion exceeds the grain size diameter, and therefore there is a minimum wave height, grain diameter, and penetration depth for which this mechanism effectively contributes to pore water mixing. Shear dispersion (Webster, 2003) creates a radial concentration gradient of a solute transported by the pore water flow within the pores itself. This gradient is reduced by molecular diffusion, resulting in mixing along the length of the pores. Shear dispersion is effective for mixing of solutes within pores to greater depths than rotational dispersion, even if these may dominate the mixing close to the water-bed interface (Webster, 2003).

### 2.2.3.3 Density-driven convection

Haline or thermal convection may play a role in areas with substantial temporal variations in salinity or temperature. When the water above the water-bed interface is more saline or colder than the porewater, the water in the upper layer enters the permeable bed as plumes, while the fresher and/or warmer porewater is expelled. Mixing rates by haline convection are substantially larger than mixing rates by molecular diffusion (Huettel and Webster, 2001).

### 2.2.4 Turbulent diffusion

In absence of other mixing processes, fines transported in pore waters may be mixed within the sand matrix by turbulent diffusion. However, turbulent diffusion is probably several orders of magnitude lower than any of the other mechanism, and is therefore of minor importance. Advective transport dominates over diffusion processes when the Péclet Number exceeds unity. In coarse-grained ( $d = 2$  mm), shallow areas ( $H = 5$  m) with relatively large waves ( $H_s = 0.5$  m)), the wave-driven diffusivity increases 4 orders of magnitude compared to the molecular diffusivity (Harrison et al, 1983). In a shallow area in the Mediterranean Sea with very low wave heights ( $H = 0.7$  m and  $H_s = 0.1$  m), the advective transport was observed to

exceed transport by molecular diffusion by at least 3 orders of magnitude (Precht and Huettel, 2004). The importance of molecular diffusion is higher at impermeable sediments and absence of biological and/or physical mixing mechanisms (see also Figure 2.1).

### 2.2.5 Modelling

Several numerical models exist that compute the grain size distribution of sediment beds using different sediment fractions. In these models, sediment is deposited as distinct layers which are vertically mixed within the bed through a diffusion coefficient representing bioturbation. Harris and Wiberg (1996), for instance, apply a double-layer sediment transport model to account for the effect of bed armouring. The upper layer may be resuspended, while sediment from the lower layer may be mixed upward by biodiffusion. The depth of the active layer is related to the excess shear strength and the grain size. Sanford (2008) developed a 1DV numerical (MATLAB) model simulating the effect of bioturbation on the vertical distribution of sand and mud. Van Ledden (2003) developed a sand-mud model as part of the Delft3D model suite that model the vertical and spatial segregation of sand-mud mixtures. A distinguishing aspect of van Ledden's model is that it also models the effect of mixtures on erosion rates. Paarlberg et al (2004) extended the sand-mud model developed by Van Ledden (2003) with biotic stabilization and mixing.

A two layer mud buffering model is developed by van Prooijen et al. (2007) and van Kessel et al. (submitted) to simulate fine sediment transport in a sandy environment. The first layer is representative for the thin fluff layer on the bed surface that forms during slack tide and that is easily resuspended by tidal currents. The total sediment mass in this layer tends to be small and the residence time of sediment in this layer is short because of the large flux between the fluff layer and the water column. The second layer is representative for the sandy seabed into which fines may entrain and temporarily be stored. Resuspension from this buffer layer is only significant during highly dynamic conditions, such as spring tide or storms. A user-defined fraction of the fine sediment is transported from the water column into the layer 1 and 2, and eroded when the bed shear stress exceeds a critical value  $\tau_{cr}$ . Since  $\tau_{cr}$  of the layer 2 (lower layer) is higher than the layer 1 (upper layer), sediment is transported from layer 1 to layer 2 when  $\tau_{cr,1} < \tau < \tau_{cr,2}$ . An alternative method to transport sediment from layer 1 to layer 2 is through a so-called burial term in which a user defined percentage of fines in the upper layer is transported to the deeper layer. This latter is more in analogy to diffusion coefficients representing bioturbation used in other models. The erosion rates in van Kessel's and van Prooijen's model is not influenced by the composition of the sand-mud mixtures. Also, it only simulates the transport of mud, and not of sand.

## 2.3 Residence time & infiltration rates

### 2.3.1 Infiltration rates

Infiltration rates are highest for fines with a grain size of 1  $\mu\text{m}$  because smaller grain sizes adhere to particles, while coarser are blocked by the pores (Huettel et al., 1996). Field measurements of Reimers et al. (2004) of flow intrusion at a water depth of 13 m yielded intrusion velocities up to 53 cm/hr near the seabed surface, decreasing rapidly to nearly 0 approximately 2 cm below the seabed surface. The intrusion velocity is episodic, depending on the wave height and current velocity. Intrusion velocities rapidly decline with depth and time. Thibodeaux and Boyle (1987) measured inflow velocities of around 50  $\mu\text{m/s}$  in the field.

Measured inflow velocities are lower in laboratory conditions: intrusion velocities over 1 cm/hour near the surface were measured by Huettel et al. (1996, 1998) due to flow-topography interactions. More typical inflow velocities are displayed in Figure 2.3 (Precht and Huettel, 2004).

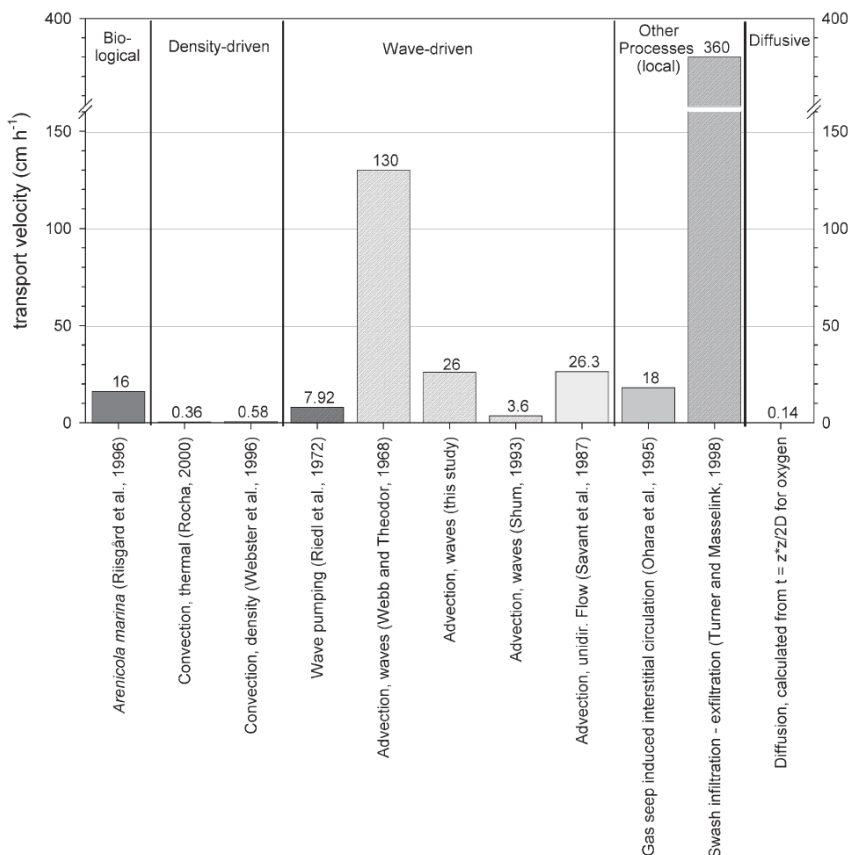


Figure 2.3 Flow velocity in permeable sediment, based on different sources (Precht and Huettel, 2004).

Infiltration rates are determined by hydrodynamics and sediment dynamics. Especially the permeability is important for the inflow velocity. The inflow velocity scales linearly with permeability, but at different locations around the world the permeability differs several orders of magnitude. Wilson et al. (2008) related existing measurements of permeability obtained worldwide to the grain size. The permeability correlates reasonably with grains size as long as the nearshore zone (< 10 m water depth) is separated from the continental shelf (>10 m water depth). The lowest permeability observed in undisturbed samples is  $2 \cdot 10^{-12}$  m/s (at a median grain size  $D_{50}$  of 150  $\mu$ m). The permeability in the nearshore zone is consistently lower than that on the continental shelf, despite a similar grain size class.

### 2.3.2 Mixing rates & diffusion coefficients

Dellapenna et al. (1998) measured mixing coefficients in two strongly contrasting environments. One site had biological mixing rates of 80 to 172 cm<sup>2</sup>/year, with mixing depths of 17 to 25 cm. The other site had less intense mixing rates of 6-30 cm<sup>2</sup>/year, but mixing depths were greater, 21-40 cm. Heberta et al. (2007) measured in situ pore water mixing at a depth of 10 m below the water surface on a flat sandy seafloor. No infaunal burrows were

observed in cores. The wave height was up to 1.2 m, and near-bed current velocities less than 20 cm/s. The measured diffusivity scales reasonably with the wave height, and is 3-4 orders of magnitude higher than the molecular diffusion rate: between  $10^{-2}$  to  $10^{-3}$  m<sup>2</sup>/hr. A field study on an intertidal mud flat by Rusch et al (2000) on the seasonal dynamics of Particulate Organic Matter in the top sediment layer resulted in a  $D_s$  between  $0.18 \cdot 10^{-6}$  and  $1.43 \cdot 10^{-6}$  cm<sup>2</sup>/s. They concluded that in an area with only minor influence of macrofauna, the biodiffusion coefficient of  $1.85 \cdot 10^{-6}$  cm<sup>2</sup>/s is responsible for half of the total mixing rate. Forster et al. (1999) measured a diffusion coefficient  $D_s$  around  $6.5 \cdot 10^{-6}$  cm<sup>2</sup>/s by applying a Bromide Tracer to measure benthic mixing in the bed sediments of the Skagerrak and the North Sea.

### 2.3.3 Residence time

The time that fines remain buried in the bed can be expressed in terms of a half life, and as a residence time. Decadal measurements of various contaminants have been used by Laane et al. (1999) to compute an average half life of sediments in the active layer of the North Sea. For the Dutch coastal zone North of the Rhine, the half life is 1.9 years. This means that half of the sediment in the active layer is resuspended in 1.9 years. This is a fundamentally different approach from the residence time used by Dellapenna (1998), which is defined as the time for sediments to be permanently buried. This residence time is estimated by dividing the mixing depth by the accumulation rate. Hence, the residence time is defined as the time required for the sediments to be permanently deposited.

From a geological point of view, bioturbation is a slow and continuous process, and therefore biological mixing dominates sedimentary strata on longer timescales (Dellapenna, 1998). The duration, depth, and degree of sediment disturbance by biological processes depend on the benthic community structure and its temporal and spatial variability. Physical mixing is episodic (event-driven), and modulated on a variety of frequencies and depths, depending on the driving forces (e.g. wind, waves, tides, surges).

### 2.3.4 Measurement methods

Measurement methods which can be used to measure the flux of mud into or out of the sediment bed are basically (1) to determine the mixing rates from sediment cores, using some sort of natural tracer, (2) active field measurements during which the decay of a substance injected into the bed is monitored, and (3) indirect measurements such as sediment concentration time series.

Examples of the first are Dellapenna et al. (1998, 2003), who measured particle residence time and mixing using radioactive tracers. Biological mixing is identified by a constant decrease in tracer activity with depth, while the absence of biological mixing results in distinct layers of constant or decreasing activity. Laane et al (1999) used existing decadal measurements of various contaminants to compute an average half life of sediments in the active layer of the North Sea. Rusch et al. (2000) used profiles of particulate organic matter concentrations to estimate the porewater flows and mixing rates in an area relatively little influenced by macrofauna.

The redox potential discontinuity (RPD) layer separates the oxidized surface water from the reduced pore water, resulting from the balance between metabolic demand of sediment biota oxidizing organic matter, and the delivery rate of nutrients. The RPD is therefore a proxy for

the penetration depth of the seawater (Riedl et al., 1972). In the North Sea, the RPD layer is approximately 2.5 cm below the seabed (Rutgers van der Loeff, 1980). Near Hawaii, at a site exposed to large swell waves, the depth of the RPD layer was between 15 and 50 cm (Falter and Sansone, 2000). More moderate depths of around 10 cm were observed by Marinelli et al (1998) in the South Atlantic Bight. Riedl et al. (1972) use the depth of the redox potential discontinuity layer as an indication of the penetration depth, which in their study area (the West Atlantic shelf North of Florida) amounts to 20 cm at shallow depth (3 m) to 2-5 cm at 10 m water depth, and less further offshore.

Field experiments during which the decay of an injected substance is measured vary considerably. Forster et al. (1999) applied a Bromide Tracer to measure benthic mixing in the bed sediments of the Skagerrak and the North Sea, and Marinelli et al (1998) et al used Bromide in the South Atlantic Bight (US). Heberta et al. (2007) injected a neutrally buoyant dye 15 cm below the bed level, and the concentration decay measured with a spectrometer attached on a tripod. Reimers et al. (2004) executed field measurements of flow intrusion in the top 2 cm of the seabed using iodide injected from a tripod, at a water depth of 13 m. Precht and Huettel (2004) injected dye in a sandy substrate in a shallow water and low energy environment, and measured the concentration decay with optical instruments.

Krishnappan and Engel (2006) measured the entrapment of fines in coarse sediment beds in the laboratory using an annular flume. With a calibrated flocculation and settling model the concentration variation in the flume as a function of time could be reproduced. A systematic study is planned to determine the entrapment coefficient for various bed material types and bulk hydraulic parameters.

Sediment concentration measurements can be used as an indirect method to determine the buffering of fines through data analysis (Kleinhaus et al., 2005) or in combination with numerical modelling tools (van Kessel et al., submitted, and van Prooijen et al., 2007).

## 2.4 Erosion rate of sand-mud mixtures

The network structure of a sediment bed determines the erosion type and rate significantly. A conceptual framework for the erosion behaviour of sand–mud mixtures was proposed by van Ledden et al. (2004), identifying a cohesive and non-cohesive sand-dominated network structure, a cohesive and non-cohesive silt-dominated network structure, a non-cohesive mixed structure, and a cohesive clay-dominated structure. The transitions between silt–sand–clay domination are determined by the volume fractions of the different sediment types, and the total water content  $n$ . The behaviour of the sediment bed is dominated by a sand skeleton when at least 40% of the volume fraction (including sediment and water) consists of sand. The sand content needed for a sand-dominated skeleton increases with porosity (or water content), see van Ledden et al. (2004) or Winterwerp & van Kesteren (2004) for more details. Mastbergen & van den Berg (2003) analysed the effect of permeability on the erosion rate of sand beds. A moderately packed sand bed needs to increase its pore volume in order to release individual sand particles (shear dilatancy). This shear dilatancy results in negative pore pressures, which decrease the effective erosion rate of the bed. Sediment beds with a low permeability are compacted silts or very fine sands, but also sand in which the pores are blocked by clay.

The critical clay or mud content for a sediment bed to become cohesive can be determined through experiments. Both Mitchener & Torfs (1996) and Houwing (1999) used the mud

content ( $D_{50} < 63 \mu\text{m}$ ) as a discriminator, finding critical mud contents of 3% to 15% and 20%, respectively. However, cohesive properties are determined mainly by the clay fraction (defined as  $D_{50} < 4 \mu\text{m}$ ) and the clay mineral and, therefore, the clay content is probably a better discriminator than the mud content. Experimental results show that the critical clay content varies from 5% to 10% (Mitchell, 1976; Raudviki, 1990) to 11% to 14% (Panagiotopoulos et al., 1997). Van Ledden et al. (2004) concluded that a clay fraction of 7.5% results in a transition of cohesive to non-cohesive properties.

In addition to the clay content or mud content, the erosion rate is also strongly influenced by biological activity. Biostabilization (i.e. by micro-organisms, vegetation, and algae mats) reduce erosion rates, while bioturbation increases the mixing rate (which, usually, increases the erosion rate). The biological activity therefore also influence the sediment composition of the bed: destabilizing organisms reduce the mud content in a bed, whereas stabilizing organisms *may* cause an increase in the mud content (Paarlberg et al., 2004).

## 2.5 The North Sea

### 2.5.1 Mud content

The mud content in the top one meter varies of a larger part of the Dutch nearshore zone varies between 0.25 and 4% (Figure 2.4 and Figure 2.5); it may exceed 10% or locally 20% close to the shore line (Figure 2.4). The mud content in the lower meter (1-2 m below the seabed) is slightly higher (Figure 2.5), but this may be attributed to the large number of grab samples used in the surface sampling. Fines are easily flushed out during grab sampling, resulting in underestimated fine fractions. This is supported by observations by Rutgers van der Loeff (1980) in the North Sea that the bed sediment in the nearshore region is frequently covered by a mud layer. However, this mud layer is only found when collecting samples with a box core and a Van Veen grab, because the North Sea corer disturbs the sea surface too much. Additionally the grain size analyses done previously on the cores frequently did not sample mud layers within the bed sediment. Therefore the maps in Figure 2.4 provide a lower estimate for the mud content.

Surface sediment data presented by Creutzberg (1979) of a larger part of the North Sea (Figure 2.6) shows that larger mud contents are found further north of the Dutch Coast. The location of this mud deposit is the same in winter and in summer, and was already described at that location since 1904. The distinct boundary between the mud field north of the  $53.5^\circ$  latitude and the sandy Southern Bight is principally determined by spring tide current velocities. In the mud field net deposition of mud is possible because the increase of erosion velocity by consolidation proceeds faster than the increase of current velocity after slack tide.

### 2.5.2 Bioturbation

In the North Sea, bioturbation especially occurs in the upper 10-20 cm (0.01-0.1 m for *Bivalvia*, 0.05 – 0.2 m for *Polychaeta*). Mollusca, especially bivalves (shellfish) occur on the shoreface and the sandwave troughs. *Polychaeta* (bristle worms) and *Echinodermata* (e.g sea-urchins) are found further offshore (Kleinhans et al., 2005). Typical sediment reworking rates are  $0.3 \text{ g/m}^2/\text{day}$  for *Bivalvia* to  $1 \text{ g/m}^2/\text{day}$  for segmented worms such as *Polychaeta*, but are strongly seasonally varying. Bioturbation occurs most on the shoreface and the

sandwave troughs where the Mollusca thrive. The amount of mud per  $m^2$  is estimated at  $1 \text{ kg/m}^2$ , which is probably mixed within the active layer in one week.

### 2.5.3 Pore water flow

A simple model to estimate the pore water velocity due to flow-topography interaction was introduced by Thibodeaux and Boyle (1987), which can be used to estimate pore water inflow velocities in the North Sea. Combining a simple model to account for the pressure drop behind simple bedforms with the Darcy's law yields an estimate of inflow at the seabed surface::

$$v_0 = \frac{K}{\nu} \left( \frac{c_p V^2}{\lambda} + g s \right) \quad (1)$$

where  $K$  is the permeability,  $\nu$  the pore water viscosity,  $c_p$  the pressure coefficient, estimated as  $c_p = \left( \frac{\Lambda}{2h} \right)^{3/8}$ ,  $h$  is the water depth and  $\Lambda$  the bedform height,  $\lambda$  is the bedform length,  $V$  is the flow velocity,  $s$  the water level slope, and  $g$  the gravitational acceleration. In their laboratory experiments, this formulation would yield an intrusion velocity of  $0.24 \text{ cm/s}$ , which underestimates the measured intrusion velocity with a factor 2. Using eq. 1 and typical shelf conditions with ripples (bedforms with a length of  $20 \text{ cm}$  and a height of  $2 \text{ cm}$ , a water depth  $h$  of  $30 \text{ m}$ , permeability between  $1 \cdot 10^{-10} \text{ m}^2$  and  $1 \cdot 10^{-11} \text{ m}^2$ , a flow velocity  $V$  of  $1 \text{ m/s}$ , a viscosity of  $1 \cdot 10^{-6} \text{ m}^2/\text{s}$ ,  $s = 1 \cdot 10^{-5}$ ) yields  $c_p = 0.05$  and  $v_0 = 2.5$  to  $25 \text{ } \mu\text{m/s}$ . Using the same formulation but different settings, Kleinhans et al. (2005) estimated the mud infiltration into the bed to be  $1 \cdot 10^{-6} \text{ m/s}$  (or  $1\text{-}10 \text{ m/year}$ ). But they also concluded that as pores will be blocked by the infiltrating mud, the infiltration velocity gradually decreases. A typical amount of mud on the sandy surface deposited during tranquil conditions would then take approximately one year to infiltrate into the bed. They therefore concluded that mud infiltration into the bed is primarily caused by bedform migration.

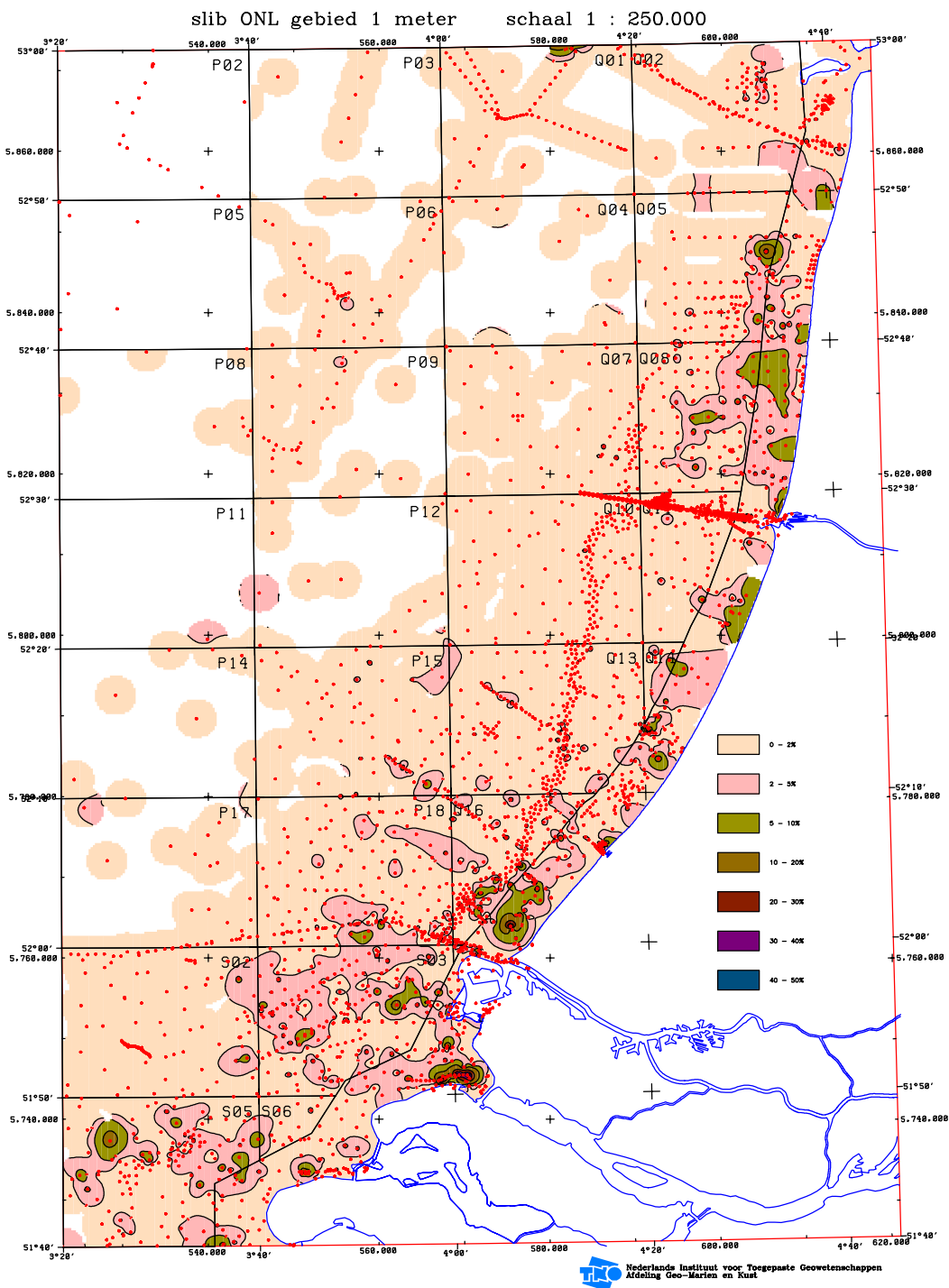


Figure 2.4 Mud content in the Dutch Coastal waters (TNO).

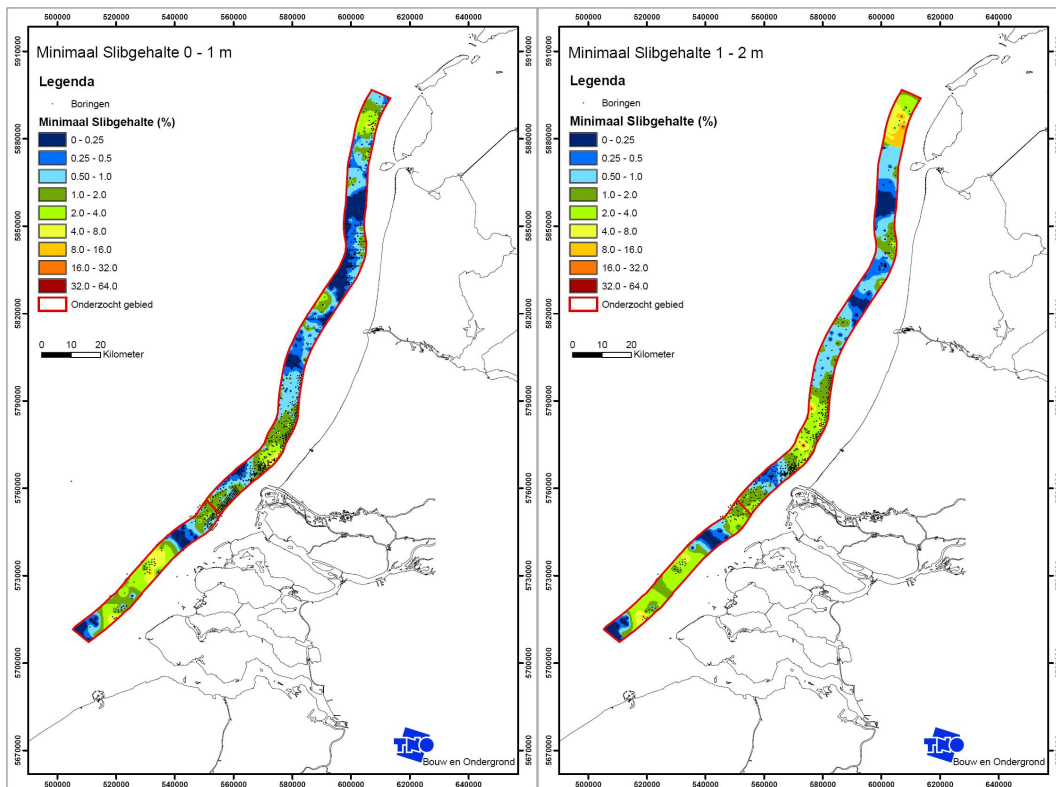


Figure 2.5 Mud content in the Dutch coastal waters between the 20 m depth contour and 7 km seaward of the 20 m depth contour (van Heteren et al., 2007)

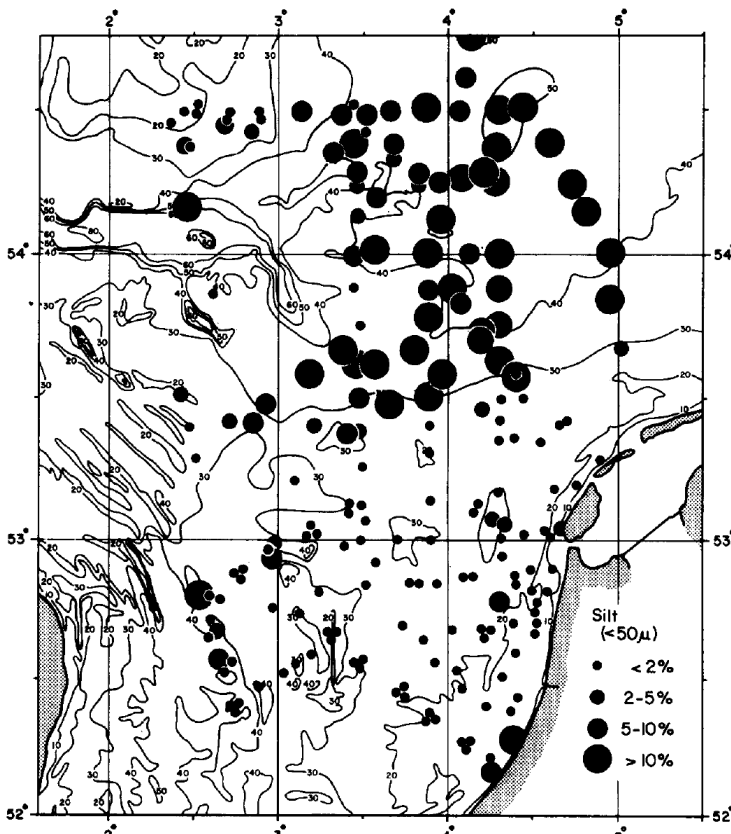


Figure 2.6 Mud content in the North Sea, from Creutzberg (1979).

Riedl et al. (1972) quantified the exchange of water between the bed and the water column through wave-generated pressure gradients. The exchange velocity between the bed and the water column depends on wave characteristics (wave height, and length), fluid viscosity, and bed permeability. The wave length can be determined from the wave period and the local water depth through linear wave theory. Considering the same shelf area as above (30 m water depth and permeability between  $1 \cdot 10^{-10} \text{ m}^2$  and  $1 \cdot 10^{-11} \text{ m}^2$ , a wave period of 6 seconds, and a wave height of 3 m, their formulations predict pore water flow velocities of 1 to 10  $\mu\text{m/s}$ . This flow velocity decreases with the wave height. At higher wave heights the upper layer of the sediment bed is probably permanently mobilised, during which sedimentological processes will probably dominate the vertical distribution of fine sediments in the bed.

It therefore seems that both flow-topography interaction and wave-generated pressure gradients in the order of 1-25  $10 \mu\text{m/s}$ , or around 0.1 to 2 m/day. This seems sufficient to transport mud into the bed. However, the permeability sand-mud mixtures increases with the mud content, and therefore mud infiltration rates are substantially less than computed with existing formulas for pore water flows.

## 2.6 Discussion and conclusion

Mud infiltration into a sand bed is caused by reworking of the bed (through bioturbation and sedimentological processes; mainly bedform dynamics) or by mixing within the pores of a sand matrix (pore water flow or diffusion). Turbulent diffusion is of lesser importance in dynamic marine areas. The question then remains to what extent release and infiltration is related to mixing processes or to interstitial pore water flows.

On the short term, interstitial pore water flows are probably important. Estimated pore water flow velocities at the sand –sea surface are in the order of 0.1 to 2 m/day in typical shelf sea conditions. However, this velocity is oscillating and does not lead to advective transports in the same order. Also, the intrusion velocity in the pores strongly depends on the permeability which strongly decreases with the mud content of the bed. This is supported by the observation that the permeability of the nearshore zone, defined by the 10 m water depth, is lower than in the open shelf, while the median grain size of the sediments is equal. The penetration depth of the pore water flow is limited, in the order of cm's to tens of cm's per year.

While pore water flow may lead to influx of mud into the bed within a relatively short time span, the amount of mud that can penetrate is probably limited because the permeability decreases. To further increase the mud content in the bed, biological and sedimentological processes are probably import. Bioturbation mixes segregated sand and mud layers, while sedimentological processes (bed form migration) lead to increased segregation. Bedforms are generated by bedload transport of sand, and therefore all mud is eroded from the upper layer when a bedform migrates. The erosion depth is determined by the size of the bedform, which may be several cm's (ripples) to decimetres (megaripples/dunes). Fine sediment eroded from the bed is brought into suspension, and deposited on the rippled bed surface. On a short timescale, this leads to a reduction of the mud content. This mud layer is subsequently slowly mixed again with the sand through percolation or bioturbation. However, if the mud layer is slightly consolidated, the mud layer may be buried by a bedform. This leads to the formation of mud layers or lenses within the sand, and is a very fast influx mechanism into the bed.

Observations and modelling shows that progressively more sediment is brought into suspension during the course of the storm season, i.e. a single storm is insufficient to rework the entire active upper layer (Marinelli et al., 1998, Kleinhans, 2005, van Kessel et al, submitted). It is not likely that subsequent storms rework progressively deeper sediment: this reworking depth is determined by the bedforms, which are in turn related to the hydrodynamics (assuming that during a storm all mud is in suspension, and the sand is non-cohesive; otherwise the bedform type and migration rate depend on the mud content). All mud present in the active layer will be resuspended during a storm, and therefore additional mechanism must play an additional role. Probably, a combination of mixing processes is responsible for the progressive increase of the sediment concentration. The most important element probably is that the sediment release depth (during a storm) is smaller (between 5 and 10 cm) than the depth up to which substantial mixing (through bioturbation or pore water flow) takes place (up to 20 to 30 cm).

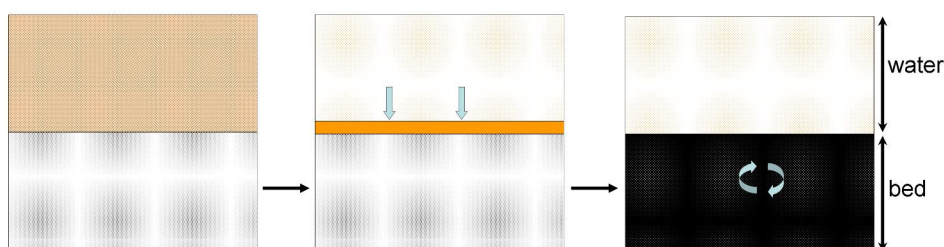


Figure 2.7 Transport of fines into the bed during summer: Suspended sediment is deposited on the clean sand bed and gradually mixed, resulting in clear water and high mud content in the bed.

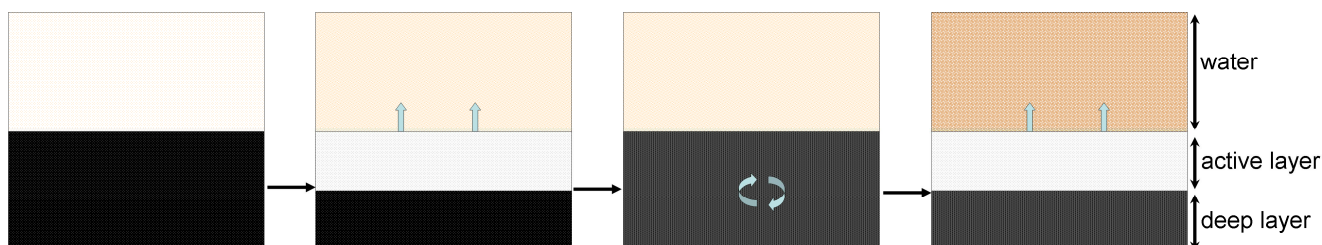


Figure 2.8 Fine sediment released during winter storms: fine sediment is washed out from the active layer, with a thickness depending on the bedform height, resulting in more turbid water, a sandy active layer, and a muddy deeper layer. Mud is transported from the muddy lower layer into the active layer through bioturbation or pore water flow. During a following storm, more fine sediment can be eroded from the upper layer, resulting in an increase in turbidity.

At the beginning of summer / end of winter, the sand bed is clean and all mud is suspended in the water column (left panel in Figure 2.7). This sediment is deposited as a thin mud layer on a clean sand bed (middle panel), which can be remobilized during spring tides or during storms only. During summer neap tides, this mud layer is mixed within the sand bed by a combination of pore water flow, bioturbation, and possibly bedform migration (right panel). During the first winter storm, all mud in the active layer (5 to 10 cm, depending on the bedform size) is washed from the sand bed due to bedform migration and brought in suspension (Figure 2.8). Due to more or less permanent higher turbulence levels in the water column, the suspended sediment concentration remains high. The upper layer devoid of fines is subsequently mixed with lower layer (between 10-20 cm), which still contains a large amounts of fines, through bioturbation or pore water flow. Overall, the mud content in the

combined upper layer is lower than at the end of summer. Because more mud is now available in the top layer, more mud can be entrained from the seabed during the following storm. Note that during slack tide some of the mud may be temporarily deposited on the sand bed in a mud layer. In contrast with summer, during which the periods that this layer exists for substantial periods of time and therefore mix with underlying sand, the period that this mud layer exists is short.

The amount of sediment in suspension can then be computed as the maximum amount of sediment the flow can at that moment carry in suspension, as long as sufficient amount of sediment is available. The sediment availability is the summation of

- 1 The amount of sediment already in suspension;
- 2 The amount of sediment available in the mud layer (if existing at that time)
- 3 The amount of mud available in the active layer. The mud content of this active layer depends on its history, and the depth on the bedform height. This bedform height can be estimated using a bedform roughness diagram (e.g van Rijn, 1993).

The amount of sediment in the active layer depends on the sedimentation / erosion flux as described above, and on supply from the deeper layer. The amount of mud transported from the deeper layer to the active layer depends on the mud fraction in both the active layer and the lower layer (sediment is transported by diffusion processes, which act on the concentration gradient), and the mixing rates. The mixing rates are determined by biological activity, wave-induced pressure gradient, or flow-topography interaction. Their relative importance varies in time and with, with diffusion due to wave-induced pressure gradients peaking in winter and bioturbation-induced mixing highest in summer. These diffusion coefficients can be computed for rotational shear due to wave-induced pressure gradients (Rutgers van der Loeff, 1981; Harrison et al., 1983; Shum, 1993), shear dispersion due to wave-induced pressure gradients (Webster, 2003), bioturbation (Lee and Schwartz, 1980; Forster et al., 1999; Rusch et al., 2000; Heberta et al., 2007), and current-bedform interaction. Although the diffusion coefficients may be based on the actual physics, for numerical modelling of mud exchange a constant value may be preferred, to be used as a calibration parameter. In somewhat different form this is the burial term in Van Kessel's model.



## 3 Description of bed module

### 3.1 Introduction

The starting point for the development of the new module has been the existing bed module within Delft3D. This module can already deal with multiple fractions and multiple layers. See the Delft3D-Flow user manual (<http://oss.deltares.nl/web/opendelft3d/manuals>) for more information, notably on page 359 ('Bed composition models and sediment availability') and page 530 ('Underlayer').

The bed module is available in two flavours:

- 1 As a stand-alone Fortran module that may be coupled to any sediment transport code (<https://svn.oss.deltares.nl/repos/openearthtools/trunk/programs/SandMudBedModule/>).
- 2 Fully integrated with Delft3D-Flow ([https://svn.oss.deltares.nl/repos/delft3d/branches/research/Deltares/20110201-BwN-mud\\_dynamics](https://svn.oss.deltares.nl/repos/delft3d/branches/research/Deltares/20110201-BwN-mud_dynamics))

For quick assessment and easy use also a simple MATLAB interface has been developed to steer the stand-alone bed module in 1DV mode. The code can be downloaded from the locations indicated above. Those wanting to use the code without any programming should use either the MATLAB interface or the integrated Delft3D version. Those wanting to integrate the bed module into their own sediment transport code should use the Fortran modules.

The philosophy behind a lot of the new features is described in the note by Bram van Prooijen ('Considerations on a generic water-bed exchange module'), which is included as Appendix B to this report. A physical explanation for the features is provided by a literature review by Han Winterwerp (see Chapter 2). New features include:

- All expressions have been rewritten in terms of mass instead of volume. This is done to facilitate error checking (mass should always be conserved) and to make the code more future-proof.
- A fully hybrid Eulerian-Lagrangian approach has been implemented. This allows to combine the advantages of both approaches (fixed active layer thickness for Lagrangian and no artificial mixing for Eulerian approach).
- Mixing in the bed has been implemented. The user-defined diffusion coefficient may vary both in vertical and horizontal direction.
- A fluff layer for the mud fraction(s) has been implemented. With the fluff layer concept, the modelling of SPM dynamics can be improved. The fluff layer provides an easily erodible pool of fine sediments.
- Sand-mud interaction has been implemented. These formulations are based on the PhD-work by Van Ledden and Jacobs. Whereas the formulations by Van Ledden apply to one sand and one mud fraction (two fractions combined), the present formulations apply to more fractions.

Apart from the first adaptation (all expressions in unit of mass), all features are described below in more detail.

## 3.2 Mixed Eulerian-Lagrangian approach

Aggradation and degradation of the bed can be treated in a Lagrangian or Eulerian framework, see Figure 3.1. In the Lagrangian framework, the thickness of the layers is constant and the set of layers moves with the aggradation/degradation by means of an artificial advection velocity. The advantage of this method is that the grid itself does not change. This means that the thicknesses of the cells can vary over the depth. In many cases it is desirable to have a high resolution near the bed surface and a coarser resolution at a larger depth. The drawback is that, depending on the numerical scheme, the movement of the grid results in artificial diffusion between the layers. Stratification will then be smoothed out.

In the Eulerian framework, the position of the layers is kept constant. The aggradation / degradation is accounted for by changing the thickness of the top layer. In case the top layer becomes too thick due to deposition, it will be split. In case the thickness tends to zero due to erosion, the layer is merged with the second layer.

The drawback of the Eulerian framework is that the top layer has no fixed thickness. As this thickness has a significant effect on the time scales of the system, it is desirable to have a top layer with a constant thickness, or a even multiple top layers with constant thickness. This implies a combination of the Eulerian and the Lagrangian framework.

In the current version of Delft3D this is partially the case, since the top layer has already a predefined thickness and it is the thickness of the second layer that changes in size. As an extension to this concept a completely mixed framework is implemented that in its limits results on the one hand in a fully Lagrangian framework and on the other hand in a fully Eulerian framework.

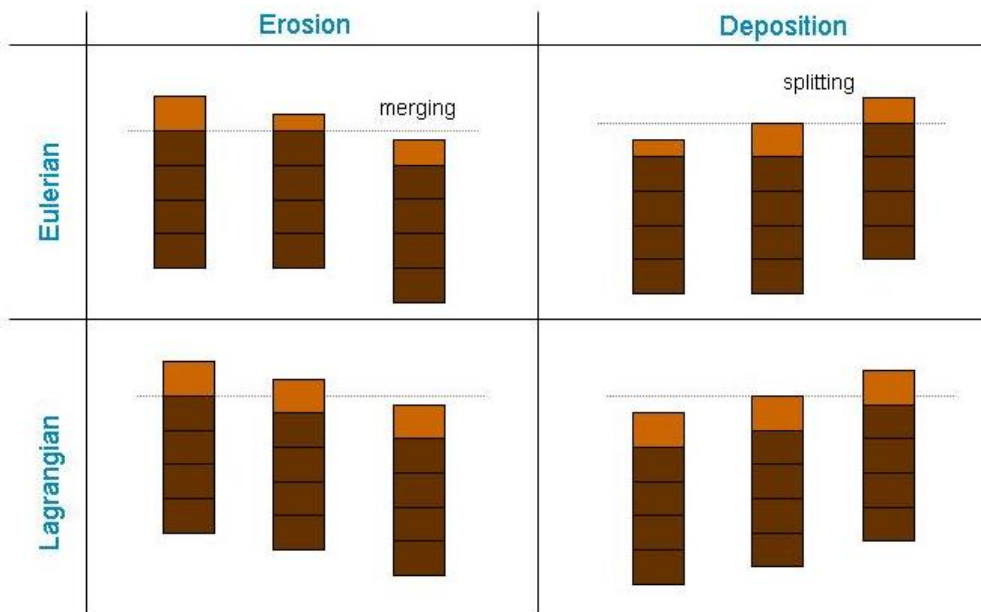


Figure 3.1 Change of grid for erosion and deposition for the Eulerian and Lagrangian framework.

### 3.2.1 Delft3D input files

#### *Keywords in the <\*.mor> file*

In the <.mor> file the `MxNuLyr` keyword is preferably replaced by the keywords `NLaLyr` en `NEuLyr`, see Table 3.1. If those latter two keywords are not present and the first one is, the framework of the current version of Delft3D is used. This means that the maximum number of Lagrangian layers is set to zero (`NLaLyr=0`) and the maximum number of Eulerian layers is set to `MxNuLyr` (`NEuLyr=MxNuLyr`).

For using a fully Lagrangian framework the number of Eulerian layers should be set to zero (`NEuLyr=0`). The Eulerian framework that is used in the current version of Delft3D (predefined thickness of top layer, variable second layer) is obtained by setting the number of Lagrangian layers to zero (`NLaLyr=0`).

It is possible to use different values for the maximum thickness of the Lagrangian and Eulerian layers. Therefore, the `ThUnLyr` keyword has to be replaced by the keywords `ThLaLyr` en `ThEuLyr`, see Table 3.1. If those latter two keywords are not present and the first one is, both the maximum thickness of the Lagrangian and Eulerian layers is set equal to `ThUnLyr` (`ThEuLyr=ThLaLyr=ThUnLyr`).

The use of Lagrangian and Eulerian layers is only possible with the new version of the <.mor> file with keywords.

Table 3.1 Overview of possible keywords and values for the use of Lagrangian and Eulerian layers in the <.mor> file.

Keyword	Value	Description
<b>Underlayer</b>		
<code>NLaLyr</code>	Integer (Default 0)	Maximum number of Lagrangian layers in case <code>IUnderLyr=2</code>
<code>NEuLyr</code>	Integer (Default <code>MxNuLyr</code> )	Maximum number of Eulerian layers in case <code>IUnderLyr=2</code>
<code>ThLaLyr</code>	Real(fp) (Default <code>ThUnLyr</code> )	Maximum thickness of Lagrangian layers in case <code>IUnderLyr=2</code>
<code>ThEuLyr</code>	Real(fp) (Default <code>ThUnLyr</code> )	Maximum thickness of Eulerian layers in case <code>IUnderLyr=2</code>

An example of the `Underlayer` chapter in the <.mor> file is given in Figure 3.2. The use of Lagrangian and Eulerian layers is only possible if more than one layer is defined (`IUnderLyr=2`).

The maximum number of Lagrangian layers is equal to 5 with a maximum thickness of 0.1 m. There are maximal 10 Eulerian layers with a maximum thickness of 0.2 m. In this example there can be totally 17 layers (1 transport layer + 5 Lagrangian layers + 10 Eulerian layers + 1 base layer).

```
[Underlayer]
  IUnderLyr      = 2           [ - ]
  ExchLyr        = false      [T/F]
  TTLForm        = 1           [ - ]
  ThTrLyr        = 0.05       [ m ]
  NLaLyr         = 5           [ - ]
  NEuLyr         = 10          [ - ]
  ThLaLyr        = 0.1        [ m ]
  ThEuLyr        = 0.2        [ m ]
  IniComp        = morlyr.inb
  UpdBaseLyr     = 1           [ - ]
```

Figure 3.2 Example of extra and changed keywords in the <.mor> file.

### 3.2.2 Examples

In the following three examples, the difference between using a Lagrangian, Eulerian and mixed framework is shown. The simulation involves a quasi-1D channel with a trench. The longitudinal cross section of the initial situation for the first sediment fraction is shown in Figure 3.3. During the simulation the location of the trench moves due to sediment deposition and erosion. The three examples differ only in the used number of Lagrangian and Eulerian layers. It can be seen that using a Lagrangian or mixed framework indeed results in more artificial diffusion between the layers.

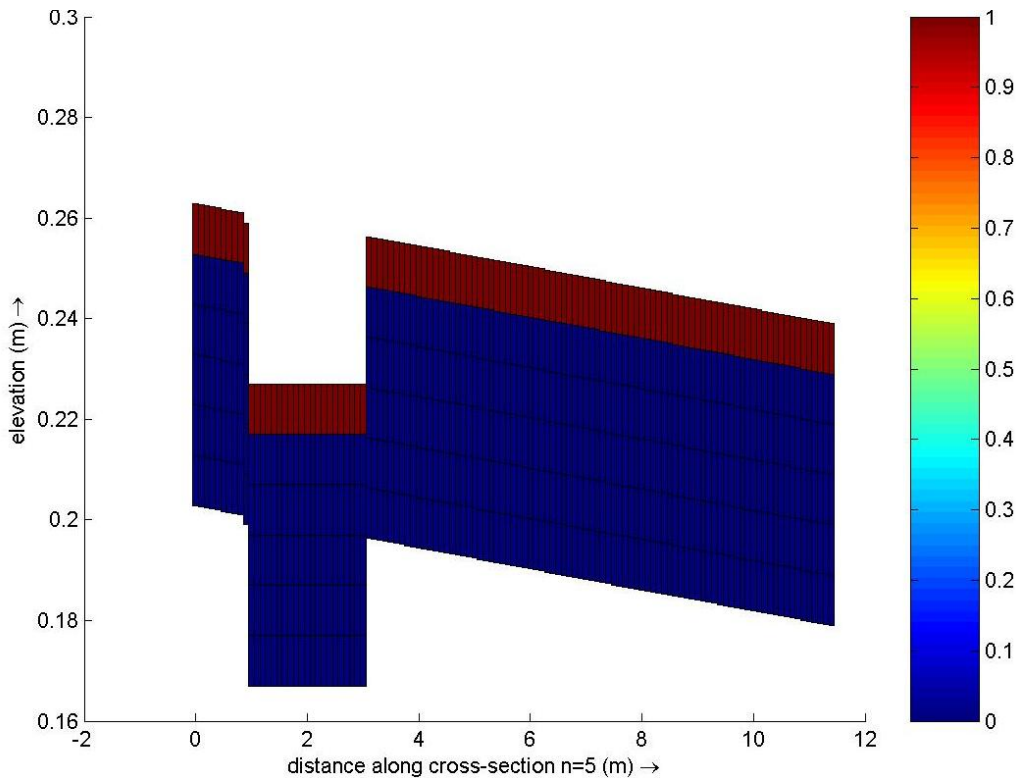


Figure 3.3 Initial situation

### 3.2.2.1 Original Delft3D framework

The thickness of the top layer is constant and there are no Lagrangian layers.

```
[Underlayer]
  IUnderLyr      = 2           [ - ]
  ExchLyr        = false      [ T/F ]
  TTLForm        = 1           [ - ]
  MxNULyr        = 10         [ - ]
  ThUnLyr        = 0.01       [ m ]
  IniComp        = morlyr.inb
```

Figure 3.4 Definition of the Underlayer chapter in the <\*.mor> file.

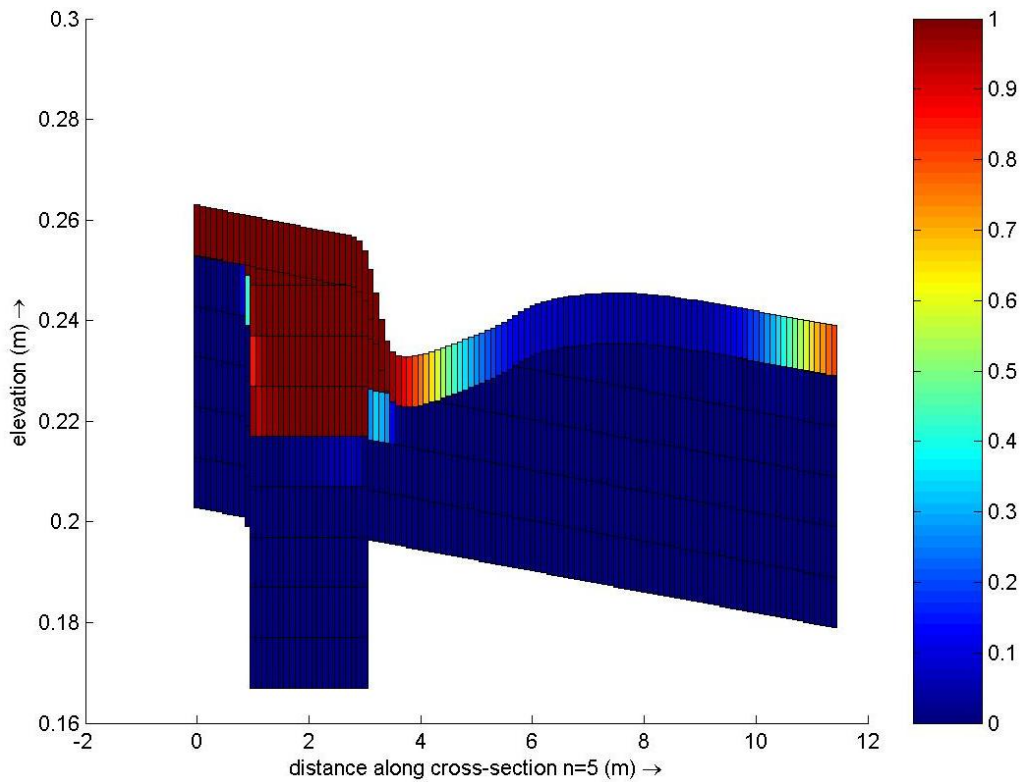


Figure 3.5 Final situation - Origina framework

### 3.2.2.2 Fully Lagrangian framework

Only Lagrangian layers are defined.

```
[Underlayer]
IUnderLyr      = 2           [ - ]
ExchLyr       = false      [T/F]
TTLForm       = 1           [ - ]
ThTrLyr       = 0.01       [ m ]
NLaLyr        = 10         [ - ]
NEuLyr        = 0           [ - ]
ThUnLyr       = 0.01       [ m ]
IniComp       = morlyr.inb
```

Figure 3.6 Definition of the Underlayer chapter in the <\*.mor> file.

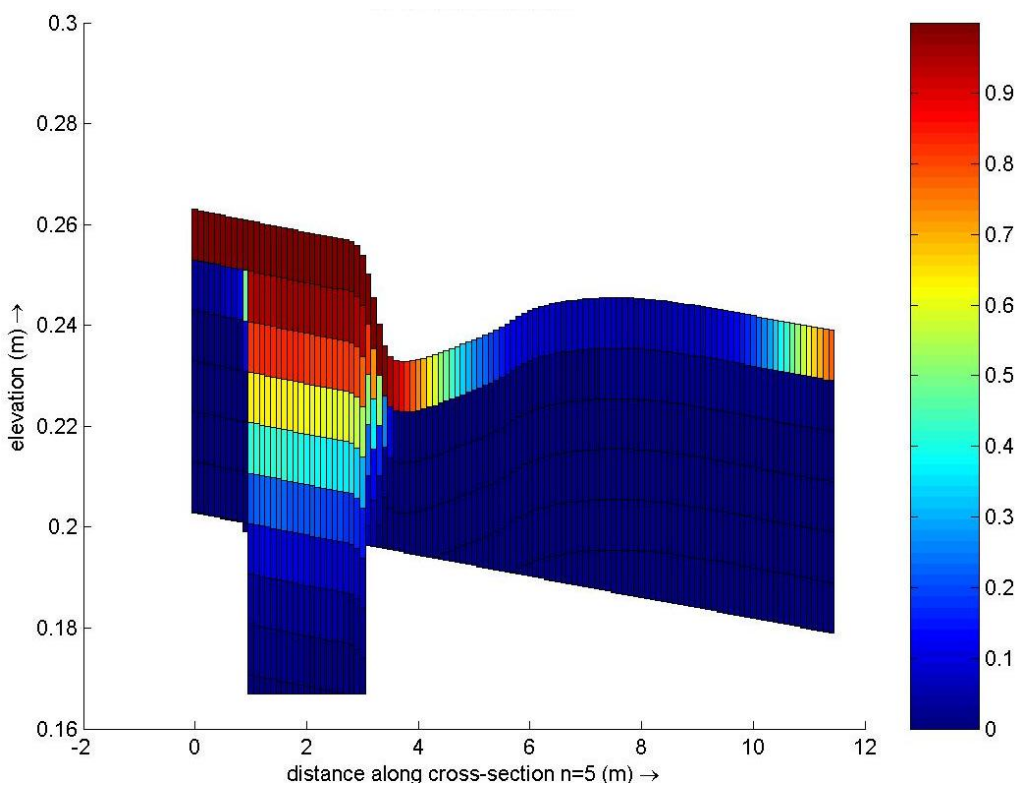


Figure 3.7 Final situation - Lagrangian framework

### 3.2.2.3 Mixed framework

There are two Lagrangian layers (beneath the fixed top layer) and the other layers are Eulerian.

```
[Underlayer]
  IUnderLyr      = 2           [ - ]
  ExchLyr       = false       [T/F]
  TTLForm       = 1           [ - ]
  ThTrLyr       = 0.01        [ m ]
  NLaLyr        = 2           [ - ]
  NEuLyr        = 8           [ - ]
  ThUnLyr       = 0.01        [ m ]
  IniComp       = morlyr.inb
```

Figure 3.8 Definition of the Underlayer chapter in the <\*.mor> file.

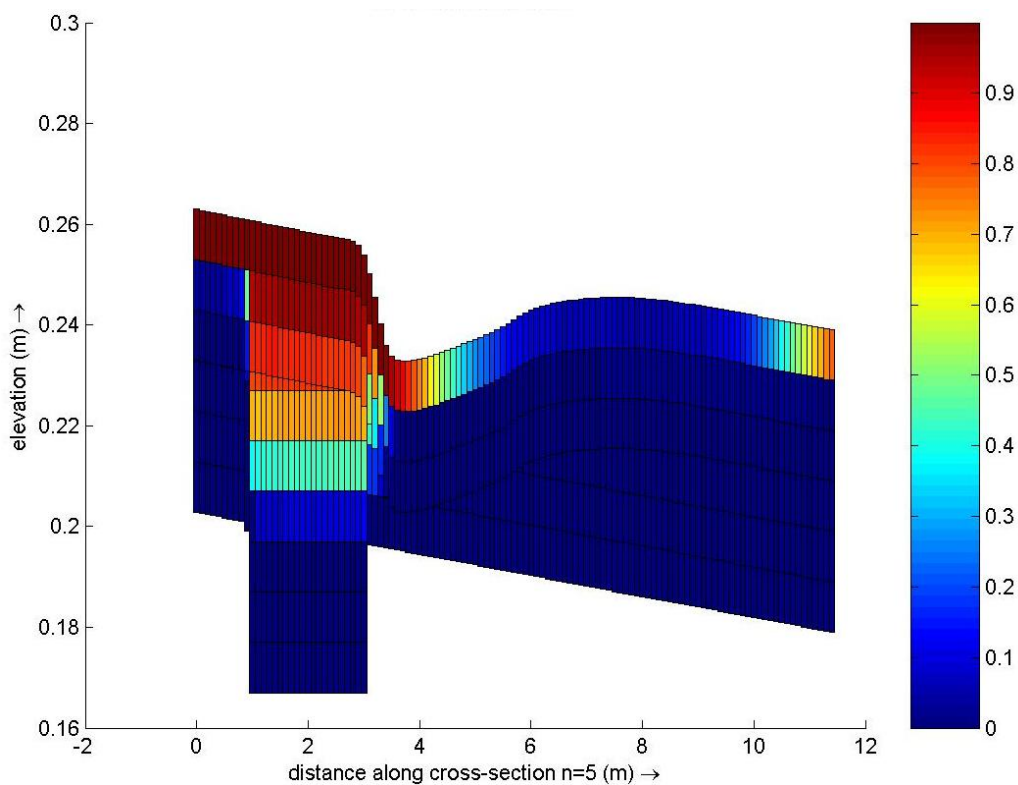


Figure 3.9 Final situation - Mixed framework

### 3.3 Mixing between layers

In reality there is not only interaction between the layers due to erosion and deposition, but also physical and biological mixing can play a role. In principle these can be non-diffusive processes, but only diffusive interaction is implemented. The following central difference scheme in vertical direction is used for each grid cell:

$$m_{k,l}^{n+1} = m_{k,l}^n + F_{k+\frac{1}{2},l} \Delta t - F_{k-\frac{1}{2},l} \Delta t, \quad (3.1)$$

with

$$F_{k+\frac{1}{2},l} = \rho_l \phi_{k+\frac{1}{2}}^n K_{k+\frac{1}{2}} \frac{p_{k+1,l}^n - p_{k,l}^n}{\Delta z^n} \quad (3.2)$$

and

$$\phi_{k+\frac{1}{2}}^n = \frac{\phi_k^n + \phi_{k+1}^n}{2}, \quad \Delta z^n = \frac{\Delta_k^n + \Delta_{k+1}^n}{2} \quad (3.3)$$

where

- $m_{k,l}^n$  : mass of sediment fraction  $l$  in layer  $k$  at time level  $n$  [kg]
- $F_{k+\frac{1}{2},l}$  : diffusive flux of sediment fraction  $l$  between layer  $k$  and  $k+1$  [kg/s]
- $\Delta t$  : (morphological) time step [s]
- $\rho_l$  : density of sediment fraction  $l$  [kg/m<sup>3</sup>]
- $\phi_k^n$  : solid volume fraction of layer  $k$  [-]
- $K_{k+\frac{1}{2}}$  : diffusion coefficient at the interface between layer  $k$  and  $k+1$  [m<sup>2</sup>/s]
- $p_{k,l}^n$  : mass or volume fraction of sediment fraction  $l$  in layer  $k$  at time level  $n$  [-]
- $\Delta z^n$  : vertical distance between centre of layer  $k$  and  $k+1$  [m]
- $\Delta_k^n$  : thickness of layer  $k$  [m]

The mass flux  $F_{k+\frac{1}{2},l} \Delta t$  between two layers within a (morphological) time step  $\Delta t$  is limited to half of the available sediment of fraction  $l$  in a layer, to avoid shortage of sediment.

As diffusion is a very slow process ( $K \approx \text{cm}^2/\text{year}$ ) compared to erosion and deposition it is treated in an explicit way. Diffusion between the layers is applied after the update of the bed composition for erosion and deposition.

The value of the diffusion coefficient  $K$  can be spatially varying in horizontal as well as in vertical direction (but is at the moment constant in time). The horizontal variation is easily implemented by allowing a different value for the diffusion coefficient for each grid cell. The vertical variation is implemented by allowing different (horizontal varying) values at different levels below the bed level. The value of  $K$  at the interface between two layers is then deduced by linear interpolation. Extrapolation is performed by assuming constant values outside the range of given levels. An example for a given gridcell is given in Figure 3.10. The diffusion coefficient is given at four levels below the bed level (indicated with the black dots). The interpolated (and extrapolated) values that are used are depicted with the red line.

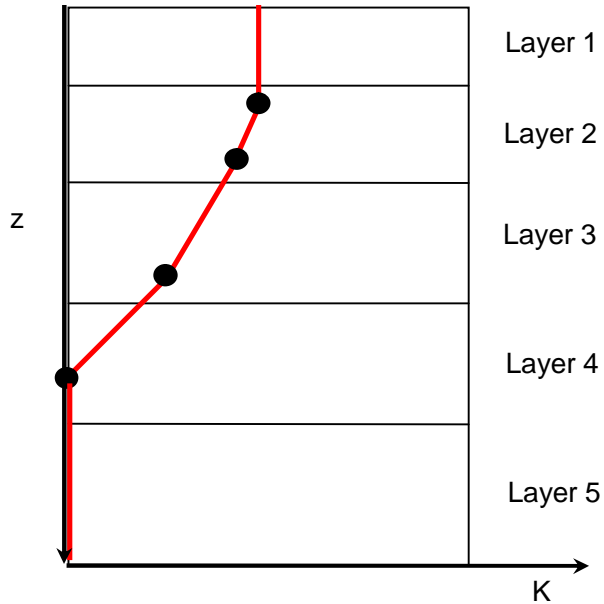


Figure 3.10 Interpolation of diffusion coefficient in vertical direction

NOTE: The porosity (or solid volume fraction) of the layers is not updated (yet) when there is mixing between the layers.

## 3.3.1 Delft3D input files

### 3.3.1.1 Extra keywords in <\*.mor> file

Table 3.2 Overview of possible keywords and values for the computation of mixing between layers in the <.mor> file.

Keyword	Value	Description
<b>Underlayer</b>		
Ndiff	Integer (Default 0)	Number of diffusion coefficients in z-direction
Diffusion	Real(fp) or String (Default 0.0)	Uniform diffusion coefficient (1 real) or diffusion file <*.ind> with spatially varying values and depth below bed level (1 string)
IDiffusion	Integer (Default 0)	0: no diffusion Diffusion based on 1 : diffusion based on mass fractions 2 : diffusion based on volume fractions

An example of the `Underlayer` chapter in the <.mor> file is given in Figure 3.2. Diffusion between layers is only possible if more than one layer is defined (`IUnderLyr=2`).

The number of defined levels for diffusion is equal to 5 and the definition of the location of these levels and the corresponding diffusion coefficients are given in the diffusion file `diffcoeff.ind`. The diffusion is based on mass fractions.

```
[Underlayer]
IUnderLyr      = 2           [ - ]
TTLForm        = 1           [ - ]
ThTrLyr        = 0.2         [ m ]
MxNULyr        = 5           [ - ]
ThUnLyr        = 0.5         [ m ]
IniComp        = morlyr_wl2a.inb
UpdBaseLyr     = 1           [ - ]
Ndiff          = 5           [ - ]
Diffusion      = diffcoeff.ind
IDiffusion     = 1           [ - ]
```

Figure 3.11 Example of extra and changed keywords in the <.mor> file.

### 3.3.1.2 Diffusion file

The diffusion file allows you to specify the values for the diffusion coefficient at different levels below the bed level. If the diffusion coefficient is homogeneous, you can directly specify its value by using the `Diffusion` keyword in the `<*.mor>` file. If the diffusion coefficient is not homogeneous in the vertical or horizontal direction you should use this diffusion file. This `<*.ind>` is keywords based. The only restriction on the diffusion file is that the levels should be defined in such a way that the values for `zdiff` are in ascending order.

Table 3.3 Diffusion file keywords

Keyword	Value	Description
<b>PorosityFileInformation</b>		
FileCreatedBy		contains version number of FLOW-GUI
FileCreationDate		creation date and time of the <code>&lt;*.ind&gt;</code> file
FileVersion		version number
<b>Level</b>		
Kdiff	Real(fp) or <filename> (Default 0.0)	diffusion coefficient at level <code>zdiff</code> : uniform value (1 real) or filename <code>&lt;*.dif&gt;</code> with non-uniform values (1 string) with same setup as a <code>&lt;*.dep&gt;</code> file.
zdiff	Real(fp) (Default 0.0)	depth below bed level

The example file contains three levels. At the first level (same as the bed level, because `zdiff=0`) a space varying diffusion coefficient as given by the Delft3D-QUIKIN file `diffusin1.dif` is defined. At 0.01 m below the bed level the diffusion coefficient is uniform equal to  $1.0e-9$  and below 1.0 m below the bed level there is no diffusion between the layers anymore.

```
[DiffusionFileInformation]
  FileCreationDate    = Fr Feb 11 2011, 12:59:21
  FileVersion         = 01.00
[Level]
  Kdiff               = diffusion1.dif
  zdiff               = 0.0
[Level]
  Kdiff               = 1.0e-9
  zdiff               = 0.01
[Level]
  Kdiff               = 0.0
  zdiff               = 1.0
```

Figure 3.12 Example of a diffusion file `<*.ind>`

### 3.3.2 Examples

In the following two examples, the mixing of sediment between layers due to diffusion is shown. The simulation involves a quasi-1D straight and flat channel with no flow, so the only way the bed composition can change is due to diffusion between the layers. In Figure 3.13, Figure 3.14 and Figure 3.15 the settings for the <\*.mor> file, initial bed composition and diffusion coefficient are shown, respectively. The two examples differ in the used sediment fractions.

```
[Underlayer]
  IUnderLyr      = 2           [ - ]
  TTLForm       = 1           [ - ]
  ThTrLyr       = 0.005       [ m ]
  MxNULyr       = 10          [ - ]
  ThUnLyr       = 0.005       [ m ]
  IniComp       = morlyr.ini
  Ndiff         = 5           [ - ]
  Diffusion     = diffcoeff.ini
  IDiffusion    = 0           [ - ]
```

Figure 3.13 Definition of the Underlayer chapter in the <\*.mor> file.

```
[BedCompositionFileInformation]
  FileVersion    = 01.00
[Layer]
  Type           = mass fraction
  Fraction1      = 1.0
  Fraction2      = 0.0
  Thick         = 0.01
[Layer]
  Type           = mass fraction
  Fraction1      = 0.0
  Fraction2      = 1.0
  Thick         = 0.01
[Layer]
  Type           = mass fraction
  Fraction1      = 0.5
  Fraction2      = 0.5
  Thick         = 0.01
```

Figure 3.14 Definition of morlyr.ini

```
[DiffusionFileInformation]
  FileVersion    = 01.00
[Level]
  Kdiff         = 1.0e-9
  Zdiff        = 0.0
[Level]
  Kdiff         = 1.0e-9
  Zdiff        = 1.0
```

Figure 3.15 Definition of *diffcoeff.ini*

### 3.3.2.1 Sand-mud mixture

In this example the sediment mixture consists of a mud fraction and a sand fraction, with both the same density and value for *Cdryb* as shown in Figure 3.16. In Figure 3.17 the distribution of the mud fraction over the vertical is shown in time. It can be seen that finally the mud fraction is evenly distributed and the thickness of the layers remains constant (after the first adaptation of the thickness of the top layer). The sand fraction shows similar behaviour.

```
[Sediment]
Name           = #Sediment 1#           Name of sediment fraction
SedTyp         = mud                    Must be "sand", "mud" or "bedload"
RhoSol         = 2650 [kg/m3]           Specific density
SalMax         = 0.0 [ppt]              Salinity for saline settling velocity
WS0            = 2.5e-4 [m/s]           Settling velocity fresh water
WSM            = 2.5e-4 [m/s]           Settling velocity saline water
TcrSed         = 1000 [N/m2]            Critical bed shear stress for sedimentation
TcrEro         = 0.5 [N/m2]             Critical bed shear stress for erosion
EroPar         = 1.0e-4 [kg/m2/s]       Erosion parameter
CDryB          = 1600 [kg/m3]           Dry bed density
IniSedThick    = 0.5 [m]                Initial sediment layer thickness at bed
FacDSS         = 1.0 [-]                Initial suspended sediment diameter

[Sediment]
Name           = #Sediment 2#           Name of sediment fraction
SedTyp         = sand                    Must be "sand", "mud" or "bedload"
RhoSol         = 2650 [kg/m3]           Specific density
SedDia         = 1.0e-4 [m]              Median sediment diameter (D50)
CDryB          = 1600 [kg/m3]           Dry bed density
IniSedThick    = 0.0 [m]                Initial sediment layer thickness at bed
FacDSS         = 1.0 [-]                Initial suspended sediment diameter
```

Figure 3.16 Definition of the *<\*.sed>* file

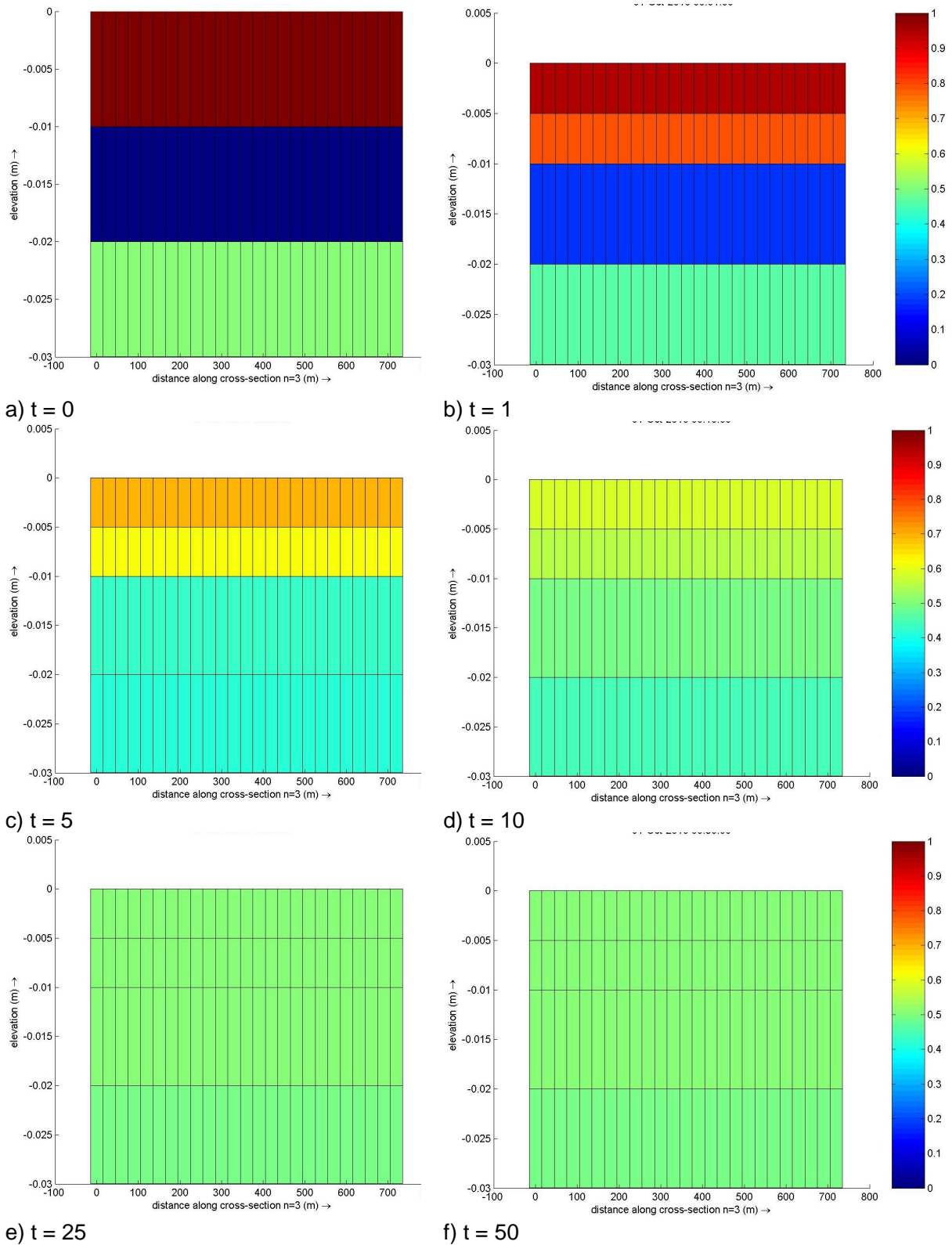


Figure 3.17 Sediment fraction mud at different times.

### 3.3.2.2 Sand mixture with different properties

In this example the sediment mixture consists of two sand fractions, with different values for the density and  $C_{dryb}$  as shown in Figure 3.18. In Figure 3.19 the distribution of the first fraction over the vertical is shown in time. It can be seen that finally the fraction is evenly distributed, and the thickness of all layers is changed. This is due to the fact that diffusion between layers is based on difference in mass fraction and not volume fraction. The other sand fraction shows similar behaviour.

```
[Sediment]
Name          = #Sediment 1#           Name of sediment fraction
SedTyp        = sand                   Must be "sand", "mud" or "bedload"
RhoSol        = 2000 [kg/m3]           Specific density
SedDia        = 2.0e-4 [m]             Median sediment diameter (D50)
CDryB         = 1000 [kg/m3]          Dry bed density
IniSedThick   = 0.0 [m]               Initial sediment layer thickness at bed
FacDSS        = 1.0 [-]               Initial suspended sediment diameter
[Sediment]
Name          = #Sediment 2#           Name of sediment fraction
SedTyp        = sand                   Must be "sand", "mud" or "bedload"
RhoSol        = 3000 [kg/m3]           Specific density
SedDia        = 2.0e-4 [m]             Median sediment diameter (D50)
CDryB         = 2000 [kg/m3]          Dry bed density
IniSedThick   = 0.0 [m]               Initial sediment layer thickness at bed
FacDSS        = 1.0 [-]               Initial suspended sediment diameter
```

Figure 3.18 Definition of the `<*.sed>` file

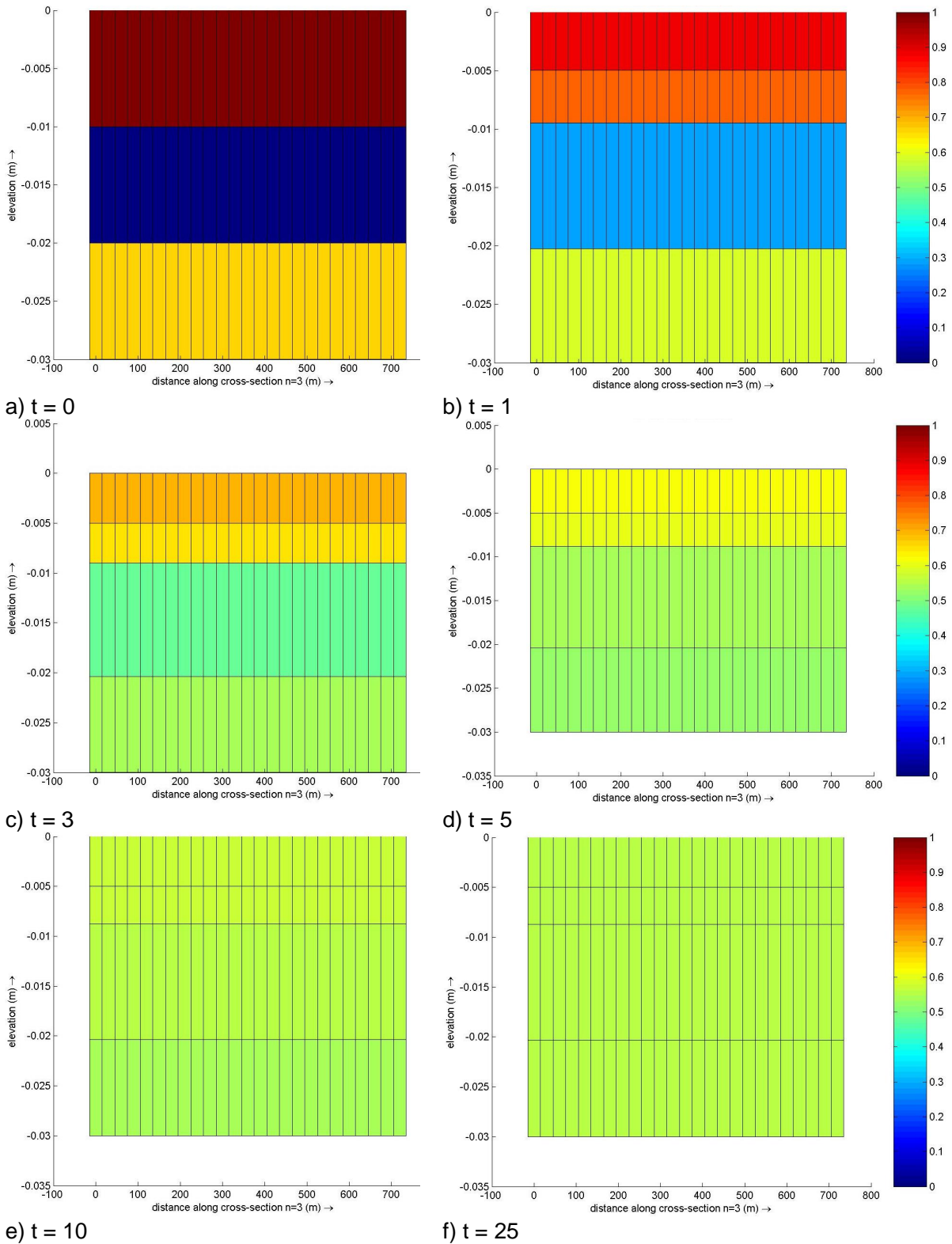


Figure 3.19 Sediment fraction at different times.

## 3.3.3 Changes in the source code

3.3.3.1 *Bedcomposition module:***New**

lyrdiffusion	Bed composition (msed and thlyr) is updated for diffusion between layers. No update of 'svfrac' (yet).
--------------	--

**Changed**

type bedcomp_settings	Added 'idiffusion', 'ndiff', 'kdiff' and 'zdiff'
updmorlyr	In case of 'mixing' call to 'lyrdiffusion' at end of routine (only for 'iunderlyr=2') and added extra input parameters 'rholol' and 'dt'.
initmorlyr	Initialization of 'idiffusion', 'ndiff', 'kdiff' and 'zdiff'. Nullifying 'kdiff' and 'zdiff'.
allocmorlyr	In case of 'idiffusion>0' allocation of 'kdiff' and 'zdiff'.
clrmorlyr	Deallocation of 'kdiff' and 'zdiff'
bedcomp_getpointer_integer_scalar	Adding 'idiffusion' and 'ndiff'
bedcomp_getpointer_fp_1darray	Adding 'zdiff'.
bedcomp_getpointer_fp_2darray	Adding 'kdiff'

3.3.3.2 *Other subroutines:***New**

rdinidiff.f90	(Called in inimorlyr.f90 ) Analogue to rdinimorlyr.f90 Extra keyword "Diffusion= <*.ind>" in chapter [Underlayer] of the <*.mor> file. The <*.ind> file contains either constant diffusion coefficients or a <*.dep> file prescribed for each level.. Values for 'zdiff' should be in ascending order. Values for levels that are not defined are set equal to that of the last defined level.
---------------	--

**Changed**

dredge.f90	Changed call to 'updmorlyr' (line 1575) and add variable 'rholol'
bott3d.f90	Changed call to 'updmorlyr' (line 978)
rdmorlyr.f90	Reading 'idiffusion', 'ndiff', 'kdiff' and 'zdiff' from Underlayer chapter of the .mor file and calling rdinidiff.f90.

### 3.4 Fluff layer concept

The main advantage of the two-layer model is the presence of a fast-responding fluff layer and a slow responding bed layer. As the fluff layer is very thin, it does hardly contribute to the bed level. The amount of sediment in the fluff layer should be in the order of magnitude of the amount of sediment in the water during spring tide ( $O(0.1-1 \text{ g/m}^2)$ , depending on the location). The mass in the fluff layer changes significantly during the tide. Roughly speaking, the sediment is in the water column during high velocities and in the fluff layer during low velocities (of course with a phase lag). This is a significantly shorter timescale than for the bed layers below! It is therefore better to keep this layer out of the 'normal' bed layers in Delft3D. Therefore the fluff layer is treated separately.

The bed module is used as it is for the bed and one single layer, representing the fluff layer, is added. This fluff layer does not contribute to the bed level. The properties of the fluff layer are different from the ones in the bed. For example, the critical shear stress will be much smaller. There are two different possibilities to define the fluxes (see Figure 3.20) and they are described in the next two sections.

For both methods holds:

- The fluff layer contains no sand. The sand fluxes are only between bed and water.
- The fluff layer is in between the bed and the water column, but has no contribution to the water depth or bed level.

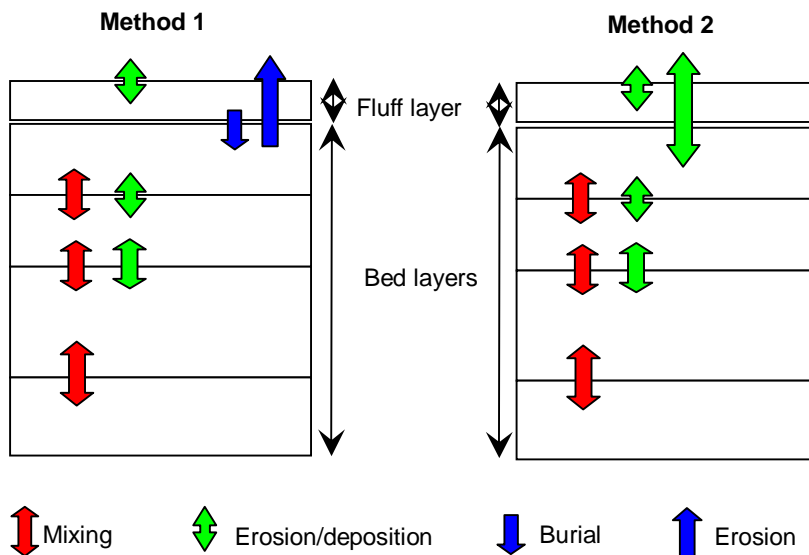


Figure 3.20 Fluff layer

### 3.4.1 Method 1

Erosion fluxes from the bed layer and from the fluff layer. Deposition flux is only to the fluff layer and a burial flux from the fluff layer to the first bed layer.

Fines from the water column deposit only towards the fluff layer and may subsequently be buried in the bed. Fines may resuspend concurrently from the fluff layer and the first bed layer.

#### 3.4.1.1 Deposition

For the deposition of mud fraction  $l$  to the fluff layer yields:

$$D_f = e_d w_s C,$$

with:

$D_f$  : deposition flux of mud fraction  $l$  to fluff layer [kg/m<sup>2</sup>/s]

$e_d$  : deposition efficiency [-]

$w_s$  : settling velocity [m/s]

$C$  : concentration of mud fraction  $l$  in water column [kg/m<sup>3</sup>]

The deposition efficiency  $e_d$  is added for calibration purposes (parameterization of near-bed processes such as floc break-up, shear stress distribution). Since there is no deposition of mud fractions directly to the bed, the deposition flux of mud fraction  $l$  to the bed is:  $D_b = 0$ .

#### 3.4.1.2 Erosion

For the erosion of mud fraction  $l$  from the fluff layer yields:

$$E_f = pM(\tau - \tau_{crit}),$$

with:

$E_f$  : erosion flux of mud fraction  $l$  from fluff layer [kg/m<sup>2</sup>/s]

$p$  : mass fraction of mud fraction  $l$  in the fluff layer [-]

$M$  : erosion parameter [s/m]

$\tau$  : bed shear stress [N/m<sup>2</sup>]

$\tau_{crit}$  : critical bed shear stress [N/m<sup>2</sup>]

The erosion parameter  $M$  is defined as follows:

$$M = \min(mM_1, M_0)$$

with:

$m$  : total mass of the fluff layer per unit area [kg/m<sup>2</sup>]

$M_0$  : erosion coefficient 1 [s/m]

$M_1$  : erosion coefficient 2 [ms/kg]

This means that the erosion parameter  $M$  is linearly dependent on the available mass in the fluff layer, but is limited by the value of  $M_0$ .

The erosion flux from the bed layers remains unchanged. The values of the erosion coefficients and the critical bed shear stress of the fluff layer may be different from those of the bed layers.

NOTE: The erosion from the bed layers is defined as:

$$E_b = pM_b \left( \frac{\tau}{\tau_{crit}} - 1 \right),$$

so the units of the erosion coefficient are different as well ( $M_b$  [kg/m<sup>2</sup>/s])

### 3.4.1.3 Exchange between fluff layer and bed layers

Exchange between the fluff layer and the first bed layer is handled by a burial term that is defined as follows for each mud fraction  $l$ :

$$B_f = p \min(mB_1, B_0),$$

with:

- $B_f$  : burial flux for mud fraction  $l$  from the fluff layer to the first bed layer [kg/m<sup>2</sup>/s]
- $p$  : mass fraction of mud fraction  $l$  in the fluff layer [-]
- $m$  : total mass of the fluff layer per unit area [kg/m<sup>2</sup>]
- $B_0$  : burial coefficient 1 [kg/m<sup>2</sup>/s]
- $B_1$  : burial coefficient 2 [1/s]

This means that the burial rate is linearly dependent on the available mass in the fluff layer, but is limited by the value of  $B_0$ .

At a later stage, the burial rate parameters may be linked to biological mixing or bed forms. It is not possible to have sediment transport from the bed layers to the fluff layer. That is only possible through the water column.

### 3.4.2 Method 2

Use the 2-layer model: Erosion fluxes from the first bed layer and from the fluff layer and deposition fluxes from the water column to the fluff layer and to the first bed layer.

Fines from the water column deposit concurrently partly towards the fluff layer and partly towards the first bed layer. There is no direct sediment exchange between the fluff layer and the bed. Fines may resuspend concurrently from the fluff layer and the first bed layer.

#### 3.4.2.1 Deposition

For the deposition of mud fraction  $l$  to the fluff layer and the bed layers yields respectively:

$$D_f = e_d(1-\alpha)w_sC,$$

$$D_b = e_d\alpha w_sC,$$

with:

$\alpha$  : deposition fraction to the bed layers [-]

The value of  $\alpha$  should be between zero and one and is typically much smaller than one.

#### 3.4.2.2 Erosion

Equal to Method 1.

#### 3.4.2.3 Exchange between fluff layer and bed layers

There is no exchange between the fluff layer and the first bed layer.

### 3.4.3 Delft3D input files

#### 3.4.3.1 Extra keywords in <\*.mor> file

Table 3.4 Overview of possible keywords and values for the simulation of a fluff layer in the <.mor> file.

Keyword	Value	Description
<b>Underlayer</b>		
Flufflyr	Integer (Default 0)	Switch for fluff layer mechanism 0: no fluff layer 1: all mud to fluff layer, burial to bed layers 2: part mud to fluff layer, other part to bed layer (no burial)
DepEff	Real(fp) or String (Default 0.0)	Deposition efficiency. Uniform (1 real) or file <*.dff> with spatially varying values (1 string)
ParFluff0	Real(fp) or String (Default 0.0)	Erosion parameter 1 of fluff layer. Uniform (1 real) or file <*.pf0> with spatially varying values (1 string)
ParFluff1	Real(fp) or String (Default 0.0)	Erosion parameter 2 of fluff layer. Uniform (1 real) or file <*.pf1> with spatially varying values (1 string)
TCrFluff	Real(fp) or String (Default 0.0)	Critical bed shear stress of fluff layer. Uniform (1 real) or file <*.tcf> with spatially varying values (1 string)
BurFluff0	Real(fp) or String (Default 0.0)	Burial coefficient 1 (only when Flufflyr=1) . Uniform (1 real) or file <*.bf0> with spatially varying values (1 string)
BurFluff1	Real(fp) or String (Default 0.0)	Burial coefficient 2 (only when Flufflyr=1) . Uniform (1 real) or file <*.bf1> with spatially varying values (1 string)
DepFac	Real(fp) or String (Default 0.0)	Deposition factor (only when Flufflyr=2) . Uniform (1 real) or file <*.dfc> with spatially varying values (1 string)

An example of the `Underlayer` chapter in the <.mor> file is given in Figure 3.2. Fluff layer mechanism A is used with a deposition efficiency of 95% ( $e_d = 0.95$ ). The values for the erosion parameters of the fluff layer are  $M_0 = 2 \cdot 10^{-4}$  s/m and  $M_1 = 0.1$  ms/kg. The critical bed shear stress of the fluff layer is  $\tau_{crit} = 0.05$  N/m<sup>2</sup>. The maximum burial rate is  $B_0 = 1 \cdot 10^{-5}$  kg/m<sup>2</sup>/s and the other burial coefficient is  $B_1 = 0.02$  1/s.

If fluff layer mechanism B was chosen (`Flufflyr=2`), 15% of the mud would be deposited to the bed layers and 85% to the fluff layer ( $\alpha = 0.15$ ).

```
[Underlayer]
  IUnderLyr      = 2           [ - ]
  ExchLyr       = false      [ T/F ]
  TTLForm       = 1           [ - ]
  ThTrLyr       = 0.02       [ m ]
  MxNULyr       = 5           [ - ]
  ThUnLyr       = 0.05       [ m ]
  IniComp       = morlyr_wl2a.inb
  UpdBaseLyr    = 1           [ - ]
  Flufflyr      = 1           [ - ]
  DepEff        = 0.95       [ - ]
  ParFluff0     = 2e-4       [ s/m ]
  ParFluff1     = 0.1        [ ms/kg ]
  TCrFluff     = 0.05       [ N/m2 ]
  BurFluff0     = 1e-5       [ kg/m2/s ]
  BurFluff1     = 2e-2       [ 1/s ]
  DepFac       = 0.15       [ - ]
```

Figure 3.21 Example of extra keywords in the <.mor> file.

### 3.4.4 Changes in the source code

#### 3.4.4.1 Bedcomposition module:

##### Changed

type bedcomp_settings	Added 'flufflyr', 'bfluff0' and 'bfluff1'
type bedcomp_settings	Added 'fluffshort' and 'mfluff'
updmorlyr	In case of 'flufflyr'>0 upating fluff layer and exchange to bed layers(s) in case of 'flufflyr=1' (both for 'iunderlyr=1/2'). Added extra input parameters 'dfluff' and 'morfac'.
gettoplyr	(should also be adapted possibly)
initmorlyr	Initialization of 'flufflyr'. Nullifying 'bfluff0', 'bfluff1','fluffshort' and 'mfluff'.
allocmorlyr	In case of 'flufflyr>0' allocation of 'fluffshort' and 'mfluff'. In case of 'flufflyr==1' allocation of 'bfluff0' and 'bfluff1'.
clrmorlyr	Deallocation of 'bfluff0', 'bfluff1','fluffshort' and 'mfluff'.
bedcomp_getpointer_logical_integer	Adding 'flufflyr'
bedcomp_getpointer_fp_2darray	Adding 'bfluff0', 'bfluff1' and 'mfluff'.

## 3.4.4.2 Other subroutines:

### New

rdflufflyr.f90	(Called in rdmorlyr.f90 ) Reading 'bfluff0', 'bfluff1', 'depeff', 'depfac', 'parfluff0', 'parfluff1' and 'tcrfluff' from Underlayer chapter of the <.mor> file. (To be able to define the values per fraction, it should also be possible to define these values in the <.sed> file)
restart_flufflyr.f90	(Called in inimorlyr.f90) Reading 'mfluff' from trim-file.

### Changed

eroded.igs	Added 'dfluff', 'sinkf' and 'sourf'.
sedpar.igs	Added 'depeff', 'depfac', 'parfluff0', 'parfluff1' and 'tcrfluff'.
bott3d.f90	Changed call to 'updmorlyr' (line 978) Calculate variable 'dfluff' from 'sourf' and 'sinkf' (analogue to 'dbodsd')
cleroded.f90	Clearing 'dfluff', 'sinkf' and 'sourf'.
clrsedpar.f90	Clearing 'depeff', 'depfac', 'parfluff0', 'parfluff1' and 'tcrfluff'.
dfwrmorm1.f90	Write 'mfluff' to trim-file.
dfwrmorm2.f90	Write 'mfluff' to trim-file.
dredge.f90	Changed call to 'updmorlyr' (line 1575) and add variable 'dfluff' (=0)
eroded.f90	Allocating 'dfluff', 'sinkf' and 'sourf'. Changed call to erosilt.f90. Adding 'sourf' to 'sour' and 'sinkf' to 'sink'
erosilt.f90	Calculating 'sourf' and 'sinkf'. Modifying calculation of 'sinkf'.
inimorlyr.f90	Initialization of 'mfluff' and call to restart_flufflyr.f90
initeroded.f90	Nullify 'dfluff', 'sinkf' and 'sourf'.
initsedpar.f90	Nullify 'depeff', 'depfac', 'parfluff0', 'parfluff1' and 'tcrfluff'.
rdmorlyr.f90	Reading 'flufflyr', from Underlayer chapter of the <.mor> file. Calling rdflufflyr.f90
wrmorm.f90	Change calls to wrmorm1.f90, dfwrmorm1.f90, wrmorm2.f90 and dfwrmorm2.f90
wrmorm1.f90	Write 'mfluff' to trim-file.
wrmorm2.f90	Write 'mfluff' to trim-file.

### 3.5 Formulations for sand-mud interaction

This section describes the erosion formulations taking into account the interaction between sand and mud. According to Van Ledden (2003) and Van Kessel (2002) the erosion of mud and sand is in this case related to each other, and the type of relation depends on the mud content. There can be made a distinction between a cohesive and non-cohesive regime, as described in the following sections.

Table 3.5 Nomenclature

$\beta$	empirical constant for critical bottom shear stress for erosion [-]
$\tau_b$	bottom shear stress [Pa]
$\tau_{e,cr}$	critical bottom shear stress for erosion [Pa]
$\tau_{m,cr}$	critical bottom shear stress for mud [Pa]
$\tau_{s,cr}$	critical bottom shear stress for sand [Pa]
$E_{fm,i}$	erosion velocity in fully mud regime of mud fraction $i$ [m/s]
$E_{m,i}$	erosion velocity of mud fraction $i$ [m/s]
$E_{s,i}$	erosion velocity of sand fraction $i$ [m/s]
$m_{m,i}$	mass of mud fraction $i$ [kg]
$m_{s,i}$	mass of sand fraction $i$ [kg]
$m_m$	total mass of mud [kg]
$m_s$	total mass of sand [kg]
$m_{tot}$	total mass of sediment [kg]
$M_c$	erosion parameter cohesive regime [m/s]
$M_{e,i}$	erosion parameter fully mud regime for mud fraction $i$ [m/s]
$M_{nc,i}$	erosion parameter non-cohesive regime for sand fraction $i$ [m/s]
$n_{mud}$	number of mud fractions [-]
$n_{sand}$	number of sand fractions [-]
$p_{m,cr}$	critical mud fraction [-]
$p_m$	mud content: total fraction of mud (grain size < 63 $\mu\text{m}$ ) [-]
$p_{m,i}$	fraction of mud fraction $i$ [-]
$p_s$	sand content: total fraction of sand (grain size > 63 $\mu\text{m}$ ) [-]
$p_{s,i}$	fraction of sand fraction $i$ [-]

The following relations hold between the mass per fraction, total mass and mass fractions for sand and mud:

$$m_m = \sum_{i=1}^{n_{mud}} m_{m,i}, \quad m_s = \sum_{i=1}^{n_{sand}} m_{s,i}, \quad p_m = \frac{m_m}{m_{tot}}, \quad p_s = \frac{m_s}{m_{tot}},$$

$$p_{m,i} = \frac{m_{m,i}}{m_m} = \frac{p_i}{p_m}, \quad p_{s,i} = \frac{m_{s,i}}{m_s} = \frac{p_i}{p_s}, \quad p_m + p_s = 1$$

## 3.5.1 Non-cohesive regime ( $p_m < p_{m,cr}$ )

It is assumed that, in this regime, mud is proportionally eroded with sand and the presence of mud only influences the erosion velocity of sand, due to a change in the critical bottom shear stress. This means that the erosion flux of each sand fraction,  $E_{s,i}$ , can be computed using a standard erosion formula. However, if a critical bottom shear stress  $\tau_{s,cr}$  is used in the erosion formula this shear stress should be replaced by :

$$\tau_{e,cr} = \tau_{s,cr} (1 + p_m)^\beta \quad (3.4)$$

(This is already the case for the Van Rijn (1993) and Van Rijn (2004) erosion formulas implemented in Delt3D, with  $\beta = 3$ .)

The relation between the erosion flux  $S_i$  and erosion velocity  $E_i$  is as follows:

$$S_i = \rho_i p_i E_i$$

Since mud is proportionally eroded with sand, the following relation hold:

$$E_{m,i} = \overline{E_s}$$

With  $E_{m,i}$  the erosion velocity of each mud fraction and  $\overline{E_s}$  the weighted average of the erosion velocities of the sand fractions. The erosion velocity for each mud fraction is then given by:

$$E_{m,i} = \overline{E_s} = \frac{1}{p_s} \sum_{j=1}^{n_{sand}} p_j E_{s,j} \quad (3.5)$$

## 3.5.2 Cohesive regime ( $p_m > p_{m,cr}$ )

In this regime, the sediment is cohesive and considered to be homogeneous. The erosion fluxes of mud and sand are proportional to the mud and sand fraction, respectively.

When the erosion velocity for the mud fractions is known, the erosion velocity for each sand fraction is given by:

$$E_{s,i} = \frac{1}{p_m} \sum_{j=1}^{n_{mud}} E_{m,j}$$

When there is only mud available ( $p_m = 1$ ), the erosion velocity for each mud fraction is calculated using the standard Partheniades-Krone formula:

$$E_{m,i} = E_{fm,i} = M_{e,i} T_c \quad (3.6)$$

with  $M_{e,i}$  a given constant and

$$T_c = \max \left( \frac{\tau_b}{\tau_{e,cr}} - 1, 0 \right)$$

where  $\tau_{e,cr} = \tau_{m,cr}$ , the critical bottom shear stress for mud.

For the region  $p_{m,cr} < p_m < 1$  there is a transition between the non-cohesive regime and the fully-mud regime. This transition can be treated in various ways and in the next sections, two of them are described.

### 3.5.2.1 Interpolation of $M_c$ and $\tau_{e,cr}$

In Van Ledden (2003) the erosion formula for sand is assumed to be of the form:

$$E_s = M_{nc} T_c^\alpha$$

where the relation for  $\tau_{e,cr}$  used in  $T_c$  is given in equation (1.1).

Since there is only one sand fraction and one mud fraction modeled in Van Ledden (2003), the transition from the non-cohesive to the fully mud regime is obtained by interpolating the erosion parameter  $M_c$  for the cohesive regime between the erosion parameter for the non-cohesive regime  $M_{nc}$  and the erosion parameter for the fully mud regime  $M_e$  by

$$M_c = M_e \left( \frac{M_{nc}}{1 - p_{m,cr}} \frac{1}{M_e} \right)^{\frac{1-p_m}{1-p_{m,cr}}} \quad (3.7)$$

Also the critical bottom shear stress for erosion is linearly interpolated between the critical bottom shear stress for the non-cohesive regime and the fully mud regime according to:

$$\tau_{e,cr} = \left[ \frac{\tau_{s,cr}(1-p_{m,cr})^\beta - \tau_{m,cr}}{1-p_{m,cr}} \right] (1-p_m) + \tau_{m,cr}$$

The erosion velocity for mud is then given by:

$$E_m = p_m M_c T_c$$

### 3.5.2.2 Interpolation of $E_m$

For multiple sand and mud fractions, the approach of van Ledden (2003) is not possible, since each mud and sand fraction can have its own value for  $M_e$  and  $M_{nc}$ , respectively. Therefore it is proposed to interpolate the erosion velocity itself, instead of the erosion parameter and critical bottom shear stress separately, according to:

$$E_{m,i} = E_{fm,i} \left( \frac{E_{sm,i}}{E_{fm,i}} \right)^{\frac{1-p_m}{1-p_{m,cr}}},$$

where  $E_{fm,i}$  the erosion velocity of the mud fraction in the fully mud regime as given in equation (1.3) and  $E_{sm,i}$  the erosion velocity for mud in the non-cohesive regime as given in equation (1.2).  $E_{sm,i}$  can be computed either with the current value of  $p_m$  or with  $p_m = p_{m,cr}$ .

### 3.5.3 Results

In this section we investigate the difference in erosion velocity for mud for the three approaches: 1) interpolating  $M_{nc}$  and  $\tau_e$ , 2) interpolating  $E_m$  based on  $p_m$  and 3) interpolating  $E_m$  based on  $p_{m,cr}$ . This is performed for the case with only one sand and one mud fraction, since the first approach is only valid for this case.

The settings for the first test case are given in Table 3.6. The results for the erosion coefficient,  $M_c$ , critical bottom shear stress for erosion,  $\tau_e$ , and the erosion velocity  $E_s$  are shown in Figure 3.22. It can be seen that in this case the behavior of the erosion velocity is very similar for the three approaches.

Table 3.6 Settings of the first test case

Parameter	Value	dimension
$\beta$	1.0	-
$\tau_b$	2.0	Pa
$\tau_{m,cr}$	1.0	Pa
$\tau_{s,cr}$	0.4	Pa
$M_e$	$1 \cdot 10^{-8}$	m/s
$M_{nc}$	$2.3 \cdot 10^{-4}$	m/s
$p_{m,cr}$	0.3	-

The settings for the second test case are the same as for the first test case, only the value for  $M_e$  is changed and given in Table 3.6. In this case there is quite some difference in the erosion velocity in the cohesive regime computed with the three approaches as can be seen in Figure 3.23

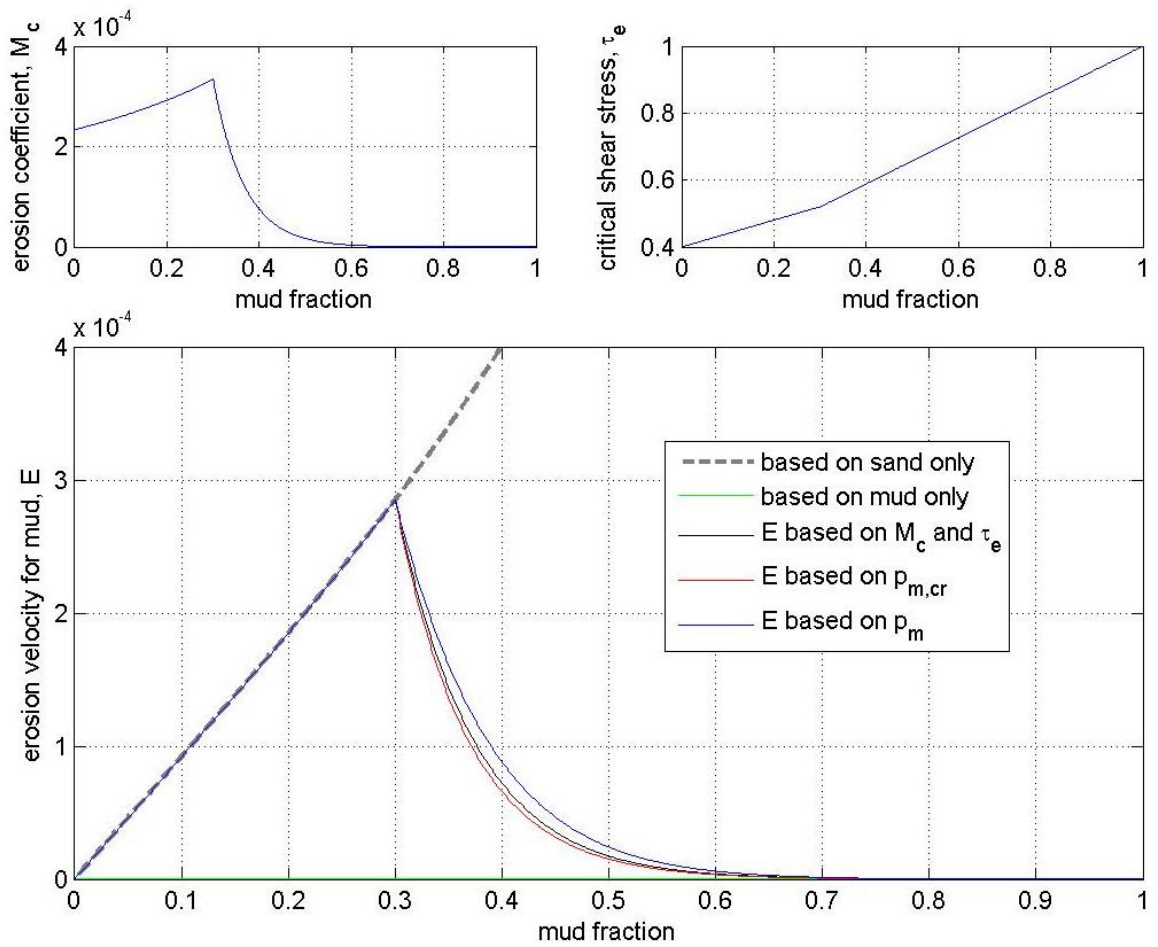


Figure 3.22 Results of the first test case

Table 3.7 Settings for the second test case

Parameter	Value	dimension
$M_e$	$1 \cdot 10^{-4}$	m/s

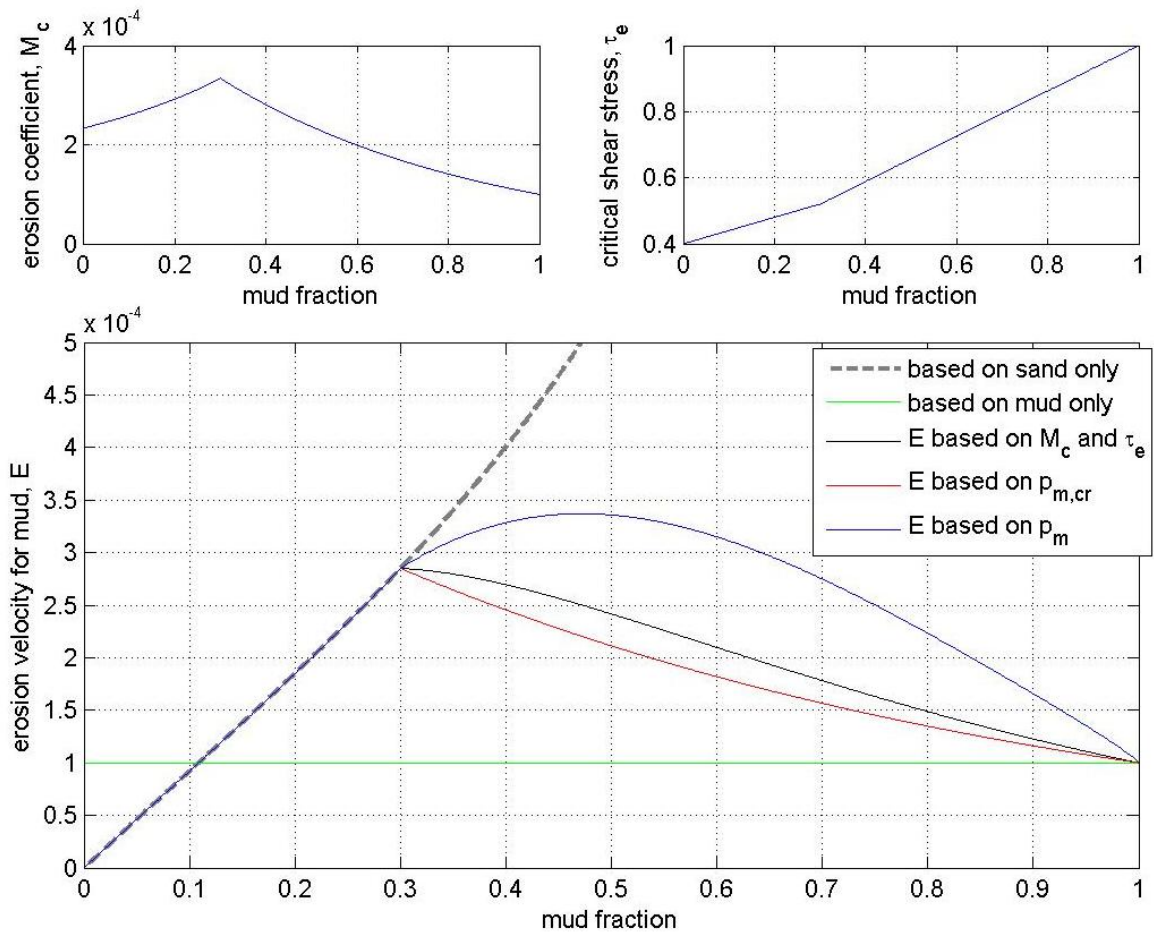


Figure 3.23 Results of the second test case

### 3.5.4 Implementation in Delft3D

The erosion flux for cohesive sediment is within Delft3D defined for each mud fraction as:

$$E_{m,i} = M_i \left( \frac{\tau}{\tau_{cr,i}} - 1 \right)$$

if  $\tau > \tau_{cr,i}$  and zero otherwise.  $M_i$  is a user defined erosion parameter (EROUNI in the <\*.sed> file) and  $\tau_{cr,i}$  a user defined critical erosion shear stress (TCEUNI in the <\*.sed> file).

For non-cohesive sediment there is a distinction between bedload transport and suspended transport. For the interaction between sand and mud we only consider the erosion fluxes due to suspended sediment. In Delft3D the erosion flux due to upward diffusion (suspended sediment) is split in a source and a sink term:

$$E_{s,i} = \underbrace{\frac{\alpha_{2,i} \epsilon_{s,i} c_{a,i}}{\Delta z}}_{source} - \underbrace{\frac{\alpha_{2,i} \epsilon_{s,i} c_{kmx,i}}{\Delta z}}_{sink}$$

with

- $\alpha_{2,i}$  : correction factor for sediment concentration [-],
- $\epsilon_{s,i}$  : sediment diff. coeff. evaluated at bottom of *kmx* cell of sediment fraction *i* [ $m^2/s$ ],
- $c_{a,i}$  : reference concentration of sediment fraction *i* [ $kg/m^3$ ],
- $c_{kmx,i}$  : average concentration of the *kmx* cell of sediment fraction *i* [ $kg/m^3$ ],
- $\Delta z$  : difference in elevation between centre of the *kmx* cell and Van Rijn's ref. height [m]:  
 $\Delta z = z_{kmx} - a$ .

The first term is evaluated explicitly and is implemented as a sediment source term. The second term can only be evaluated implicitly and is implemented as a positive sink term. Normally the sink term is added to the deposition flux directly. However, since we want to implement the interaction between sand and mud and therefore want to adapt the total erosion flux, we first store the erosion and deposition sink terms separately.

When we are in the cohesive regime, the erosion flux for sand is computed proportionally to that of mud (see section 1.2). We assume that the adaptation of the erosion flux is due to a change in reference concentration and therefore only the source term of the erosion flux is updated.

In the non-cohesive regime, the critical bottom shear stress, computed in different erosion formula's should be adapted (see section 1.1). This has its influence on the value of the reference concentration (computed in the same transport formula's) and therefore on the erosion flux. At the moment this is done for the van Rijn (1993) and van Rijn (2004) erosion formula's with standard  $\beta = 3$ . For van Rijn (1984) it is possible to choose the value of  $\beta$  through the keyword `BETAM` in the <\*.mdf> file.

## 3.5.5 Delft3D input files

Extra keywords in <\*.mdf> file

Table 3.8 Overview of possible keywords and values for the simulation of sand-mud interaction in the <.mdf> file.

Keyword	Value	Description
PmCrit	Real(fp) or String (Default -1.0)	Critical mud fraction. Uniform (1 real) or file <*.pmc> with spatially varying values (1 string) Negative value: no sand-mud interaction.
Betam	Real(fp) (Default 0.0)	Power factor for adaptation of critical bottom shear stress for sand-mud interaction

## 3.5.6 Examples

The geometry consists of a simple straight channel with a width of B=10m, length L=300m, water depth of h=1 m and a slope of  $i=2.5e-4$ . The imposed flow velocity at the inflow is  $v=0.71$  m/s and a Chezy value of  $C=50$  is used. The grid consist of 10x150 cells, a time step of 30 s for a period of 50 min is used.

There is no update of bed level or bed composition during the computation.

The composition of the bed consist of a mud and a sand fraction. The thickness of the bed is constant, but the composition varies between the simulations. The sediment transport formula of van Rijn (1984) is used, with  $\beta = 0.0$  (so original setting).

Computations are performed with and without sand-mud interaction for 2D as well as 3D flow, different values of the critical mud fraction and different values for the dry bed density of the sand and mud fractions. In the Figures the erosion velocity  $E$  [m/s] is compared. The erosion velocity  $E_i$  for fraction  $i$  is computed from the erosion flux  $F_i$  [ $kg/m^3/s$ ] (as is used within Delft3D) by:

$$E_i = \frac{F_i}{\rho_i c_{dry} b_i}$$

With  $c_{dry} b_i$  the dry bed density of fraction  $i$ .

### 3.5.6.1 Example 1

In this simulation a 2D computation with a uniform bed is carried out. The dry bed density for mud is  $500 \text{ kg/m}^3$  en for sand  $1600 \text{ kg/m}^3$ . For the computation with sand-mud interaction a critical mud fraction of  $p_{\text{mcrit}}=0.3$  is used.

In Figure 3.22 the results are shown. First a computation without sand-mud interaction is performed. The green line is the erosion velocity for mud without sand-mud interaction. The solid black line is the erosion velocity for mud if it would proportionally erode with the sand for all mud fractions ( $E_m = p_m / (1 - p_m) E_s$ ). The dashed black line is the expected erosion velocity for mud if sand-mud interaction is imposed.

Secondly, a computation with sand-mud interaction is performed. The erosion velocity for mud (red line) and for mud proportionally eroding with sand (blue line) are shown and are the same (as it should be). However, this erosion velocity is slightly higher than expected based on the computation without interaction (black dashed line) when the mud fraction is higher than the critical mud fraction. This can be explained by the fact that in case of sand-mud interaction the density of sand in the flow is lower, leading to slightly more erosion.

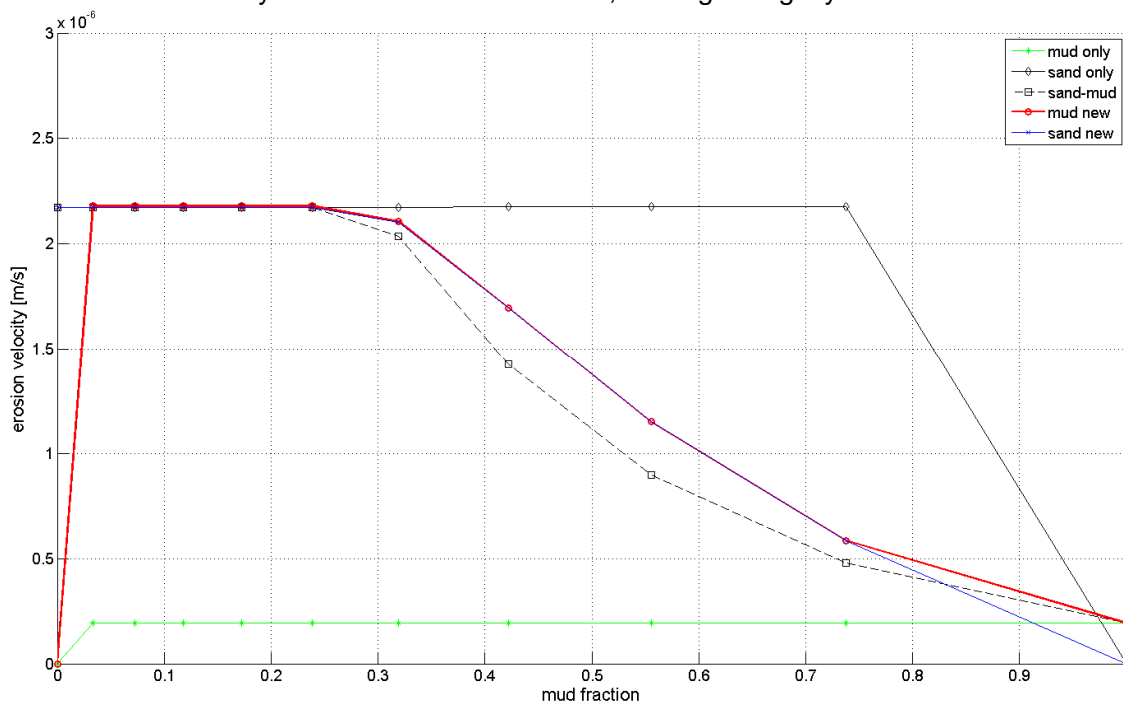


Figure 3.24 2D, single bed layer, different  $c_{dry}$ ,  $p_{mcrit}=0.3$

### 3.5.6.2 Example 2

In this simulation a 3D computation with a uniform bed is carried out. The dry bed density for both mud and sand is  $1600 \text{ kg/m}^3$ . For the computation with sand-mud interaction a critical mud fraction of  $p_{\text{mudcrit}}=0.3$  is used. In Figure 3.25 the erosion velocity  $E$  [m/s] is shown for different values of the mud fraction.

In Figure 3.22 the results are shown. First a computation without sand-mud interaction is performed. The green line is the erosion velocity for mud without sand-mud interaction. The solid black line is the erosion velocity for mud if it would proportionally erode with the sand for all mud fractions ( $E_m = p_m / (1 - p_m) E_s$ ). The dashed black line is the expected erosion velocity for mud if sand-mud interaction is imposed.

Secondly, a computation with sand-mud interaction is performed. The erosion velocity for mud (red line) and for mud proportionally eroding with sand (blue line) are shown and are again the same (as it should be). However, this erosion velocity is slightly lower than expected based on the computation without interaction (black dashed line) when the mud fraction is higher than the critical mud fraction. This can be explained by the fact that in case of sand-mud interaction the density of sand in the flow is lower, leading to

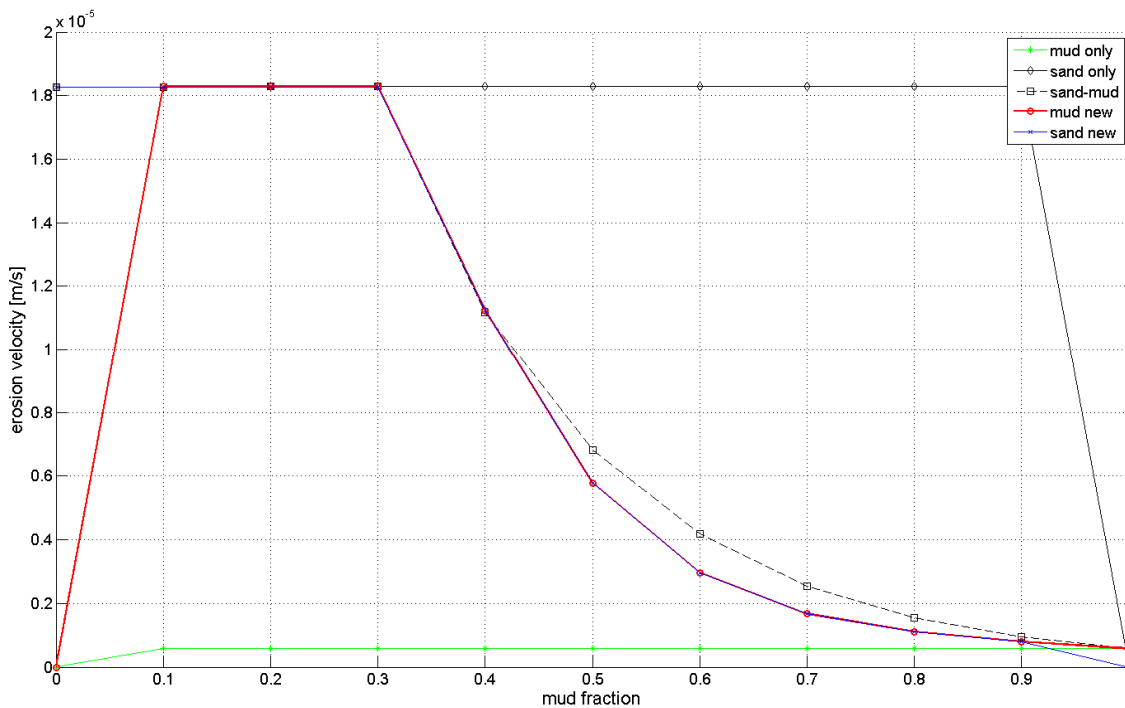


Figure 3.25 3D, single bed layer, same  $c_{dryb}$ ,  $p_{mudcrit}=0.3$

### 3.5.6.3 Example 3

In this simulation a 2D computation with a bed consisting of 5 layers is carried out. The initial composition of the layers is imposed with a separate morlyr.ini file. The dry bed density for both mud and sand is  $1600 \text{ kg/m}^3$ . For the computation with sand-mud interaction a critical mud fraction of  $p_{\text{mcrit}}=0.6$  is used. Figure 3.26

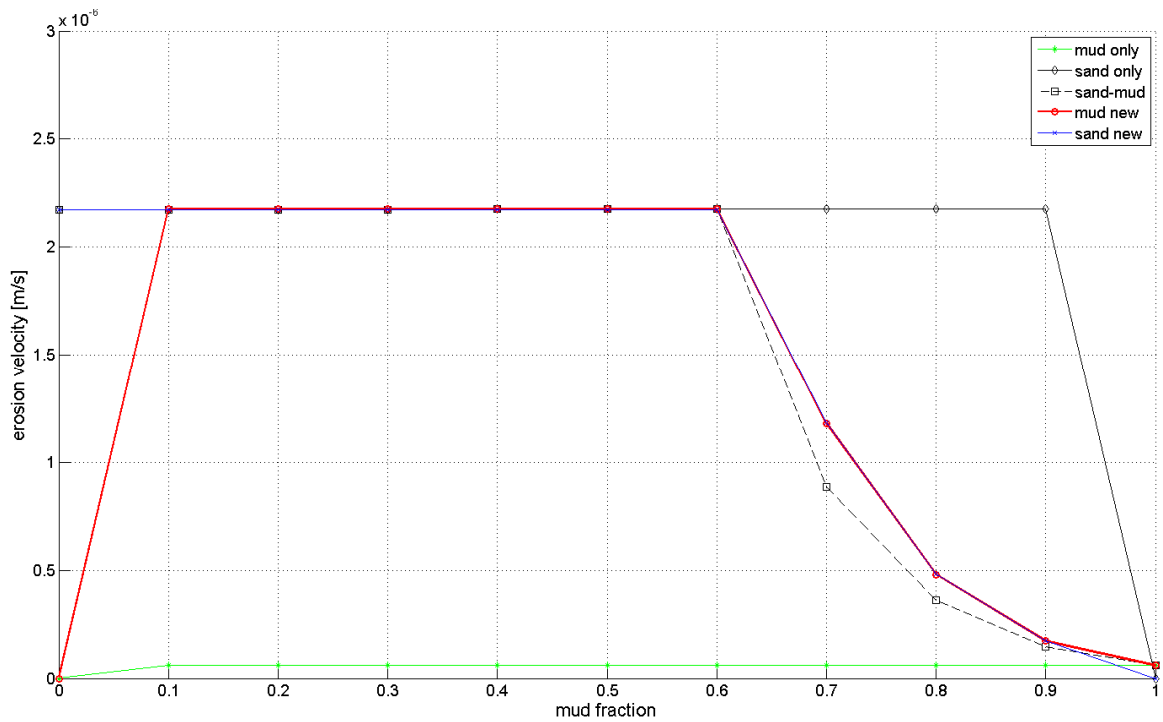


Figure 3.26 2D, 5 bed layers, same  $c_{dryb}$ ,  $p_{mcrit} = 0.6$

## 3.5.7 Changes in the source code

### New

sand_mud.f90	(Called in erosed.f90 ) Computes erosion fluxes at the bed based on sand-mud interaction.
--------------	--

### Changed

eqtran.igs	Added 'pmcrit' and 'betam'
erosed.igs	Added 'sour_im'
clreqtran.f90	Clearing 'pmcrit'
clrerosed.f90	Clearing 'sour_im'
eqtran.f90	Added 'smfac' and changed call to 'tranb7.f90'
erosed.f90	Allocating and initializing 'sour_im'. Changed call to soursin_3d.f90 and soursin_2d.f90. 'sinkse' temporarily only contains real sink term, 'sour_im' contains implicit part of source term. Added call to sand_mud.f90. Adding 'sour_im' to 'sinkse' at the end. Computing 'smfac' and add it to eqtran.f90
initeqtran.f90	Nullify 'pmcrit'
initerosed.f90	Nullify 'sour_im'
rdtrafrm.f90	Allocating 'pmcrit' and reading 'pmcrit' and 'betam' from mdf-file
red_soursin.f90	Also reducing 'sour_im'.
readmd.f90	Changed call to rdtrafrm.f90
soursin_2d.f90	Splitting source term in implicit and explicit part.
soursin_3d.f90	Splitting source term in implicit and explicit part.
tranb7.f90	Multiplying critical bed shear stress with 'smfac'.

## 4 Idealised Tests

### 4.1 Introduction

This chapter describes the academic testing of the MATLAB version of the stand-alone (1DV) sand-mud-bed module (Revision 3402, MATLAB version R2010a). This means that bed load effects on bed composition are not accounted for. We aim to test the bed module in the most basic way (e.g. continuity of mass) and to show its behavior as function of parameter settings in order to better understand the application of the bed module within the framework of a morphological modeling system like Delft3D. In order to do so, four tests were carried out:

1. general test
2. testing vertical diffusion
3. testing the fluff layer
4. testing sand-mud interaction

### 4.2 Test 1: General test

In this first test we switched off vertical diffusion, fluff layer and sand-mud interaction. Further settings were:

- maximum thickness transport layer 0.1 m
- only Eulerian underlayers with a maximum number of 10 and a maximum thickness of 0.3 m
- two sediment fractions with a (dry bed) density  $\rho_s$  ( $\rho_{s, dry}$ ) of (1600) 2650 kg/m<sup>3</sup>, of which 1 non-cohesive (sedfrac1) with a median grain size  $D_{50} = 0.2$  m and 1 cohesive (sedfrac2) with  $D_{50} = 0.05$  m

We impose a net sediment exchange between the water column and the bed, see Figure 4.1, with positive values indicating deposition and negative values erosion. The total sediment flux is 32 kg/m<sup>2</sup> per time step the first 100 time steps and -32 kg/m<sup>2</sup> the second 100 time steps. For  $t = 1-100$  the sediment flux of fraction 1 decreases from 24 kg/m<sup>2</sup> (75% of total) to 8 kg/m<sup>2</sup> (25%), where the net flux of fraction 2 into the bed increase from 8 kg/m<sup>2</sup> to 24 kg/m<sup>2</sup>. For  $t = 101-200$  the erosion flux of sediment fraction 1 (2) increases (decreases) from -8 (-24) kg/m<sup>2</sup> to -24 (-8) kg/m<sup>2</sup>. It is important to note that there is no feedback between the bed composition and the sediment fluxes from the water column into the bed. Furthermore, we start with an “empty” bed.

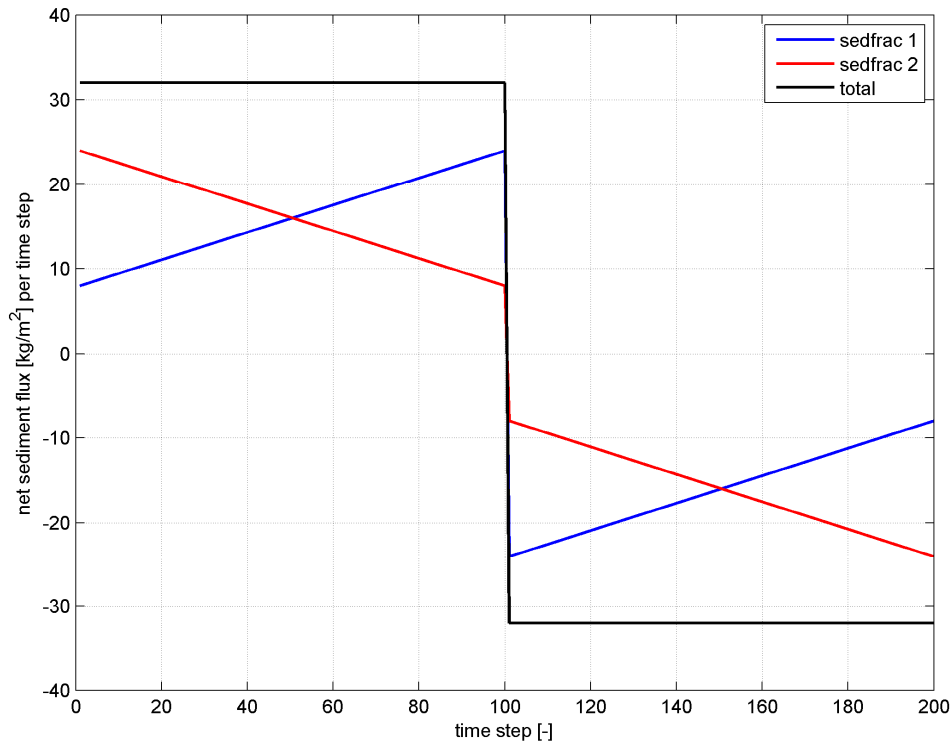


Figure 4.1 Imposed net sediment fluxes from the water column into the bed.

Figure 4.2 shows the cumulative masses of sediment fraction 1 and 2, both the supplied ones and those stored in the bed. This figure shows that mass is conserved (solid and dashed lines on top of each other). Reflecting the imposed net flux, the masses of the two sediment fractions in the bed deviate for  $t = 1-50$ , converge for  $t = 51-100$ , deviate again for  $t = 101-150$ , and converge again for  $t = 151-200$ . The mass of sediment fraction 2 is always greater than or equal to sediment fraction 1.

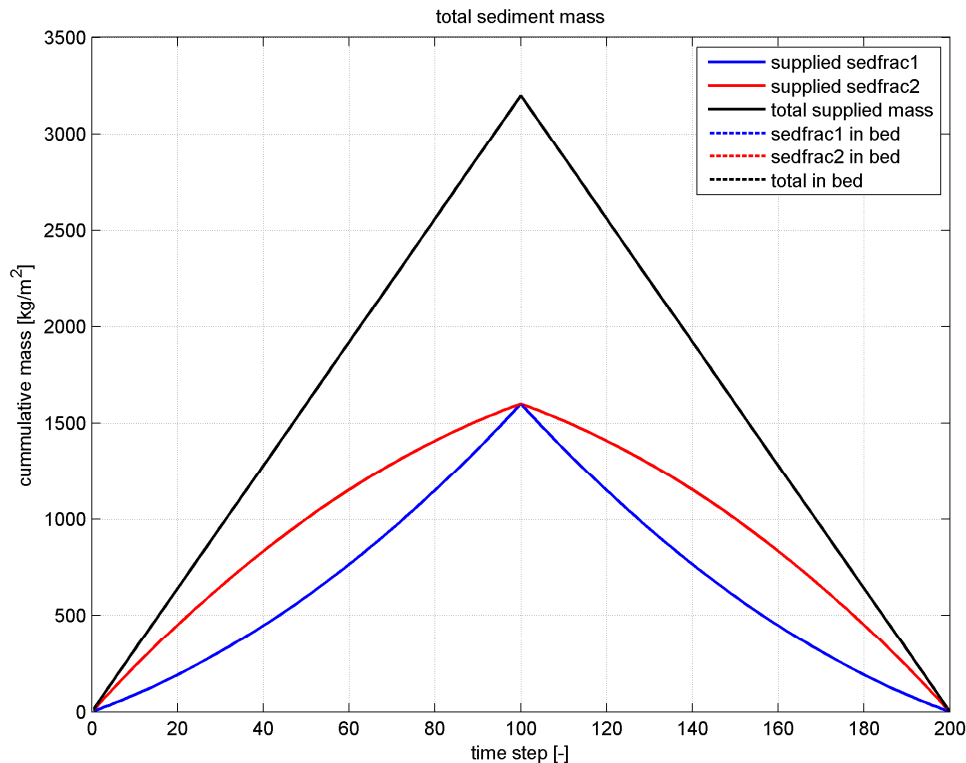


Figure 4.2 Cumulative supplied and stored sediment masses.

Figure 4.3 shows the mass fractions per layer for both sediment fractions in time. One can see that the transport layer has a maximum thickness of 0.1 m and the Eulerian underlayers a maximum thickness of 0.3 m. The bed level goes 2 m up the first 100 time steps, after which it is completely eroded the 100 time steps there after. The bed level change per time step is thus 0.02 m corresponding to the imposed total sediment flux divided by the dry bed density ( $32 \text{ kg/m}^2/1600 \text{ kg/m}^3$ ). From  $t = 1$  to  $t = 5$  the transport layer is built up, at  $t = 6$  the first underlayer is created and every 15 time steps a new one is added. In the erosive half of the test, every 15 time steps the transport layer incises a new underlayer.

As the composition of the transport layer reflects the net sediment flux over five time steps (next to the influence of the underlayers in the erosion phase), its composition changes in time. In the beginning the transport layers consists mainly of sediment fraction 2 (about 75% by mass), half way it contains approx. 75% sediment fraction 1, and in the end sediment fraction 2 dominates again (~75%).

Each underlayer has a constant composition in time. Due to the increase of mass of sediment fraction 1 into the bed, the highest underlayers contain the highest amount of sediment fraction 1 and consequently the lowest of sediment fraction 2. The composition of the transport layer is controlled by the imposed sediment flux, whereas in the erosive half of the test the incision of the underlayers affects the composition of the transport layer (due to the vertical gradient of the composition of the underlayers). This is shown in Figure 4.4 that shows the masses of the two sediment fractions in the top layer. The incision of the underlayers can clearly be seen as discontinuities; the exponential behavior per underlayer is related to the temporal change in imposed sediment flux in relation to the constant composition of each underlayer.

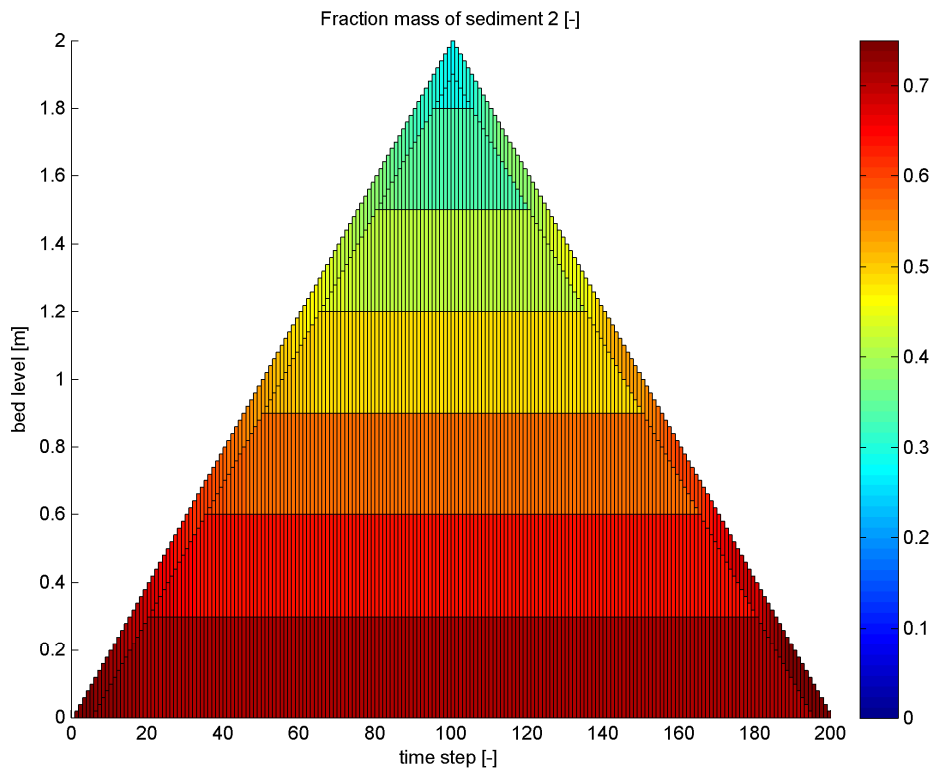
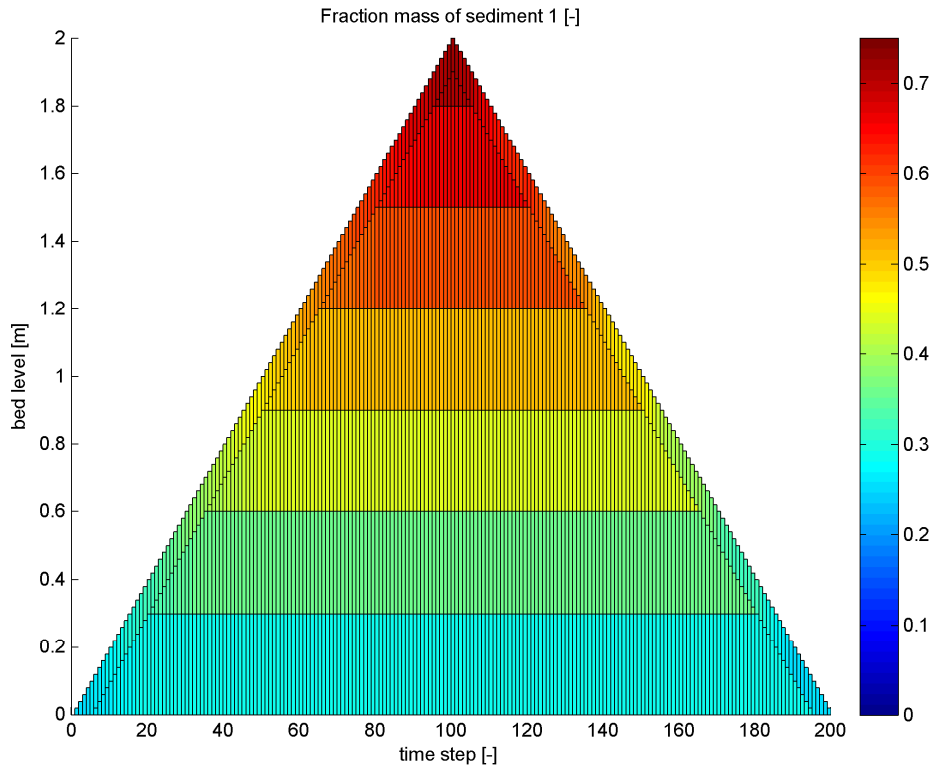


Figure 4.3 Mass fraction sediment 1 and 2 in the transport layer and the underlayers beneath.

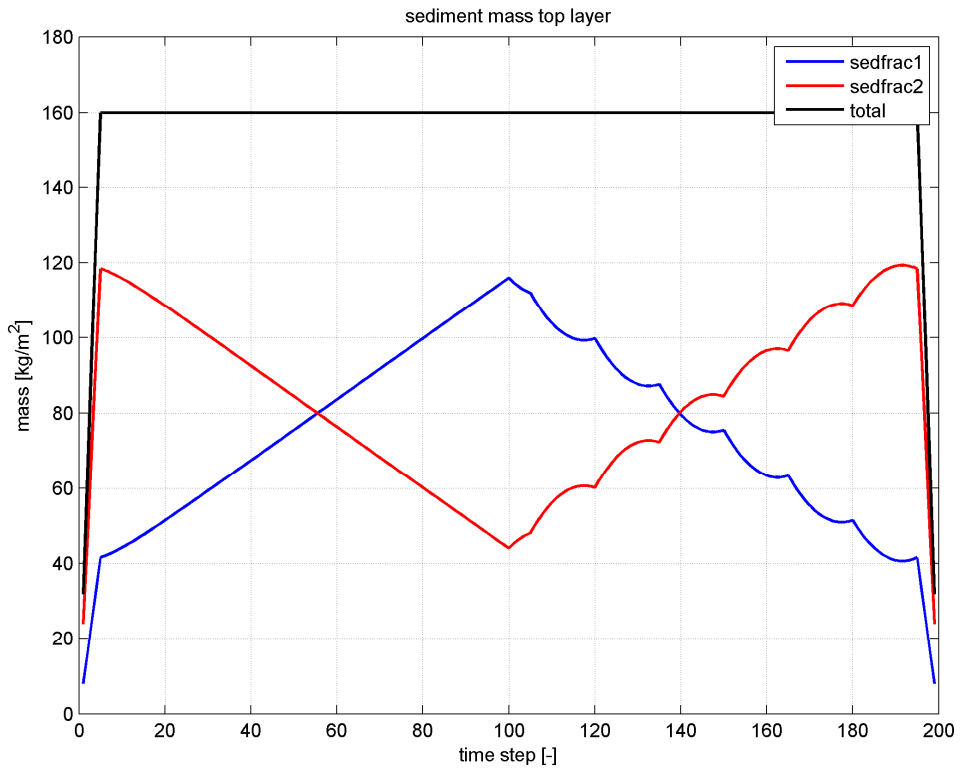


Figure 4.4 Mass sediment fractions 1 and 2 in the top layer.

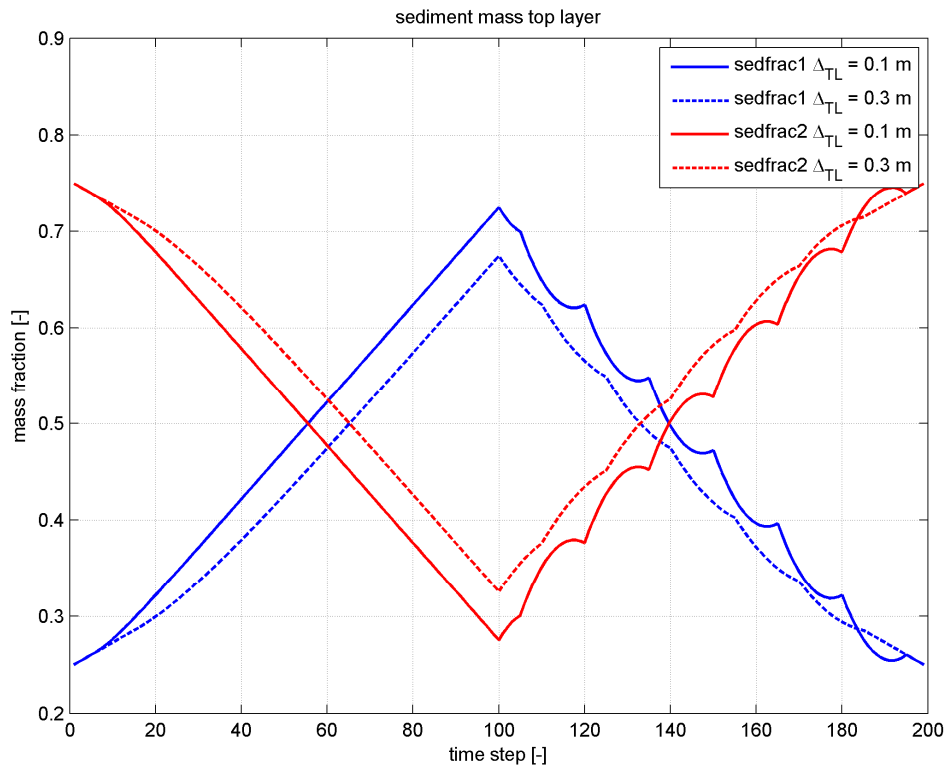


Figure 4.5 Mass fractions sediment 1 and 2 in the top layer with different transport layer thicknesses.

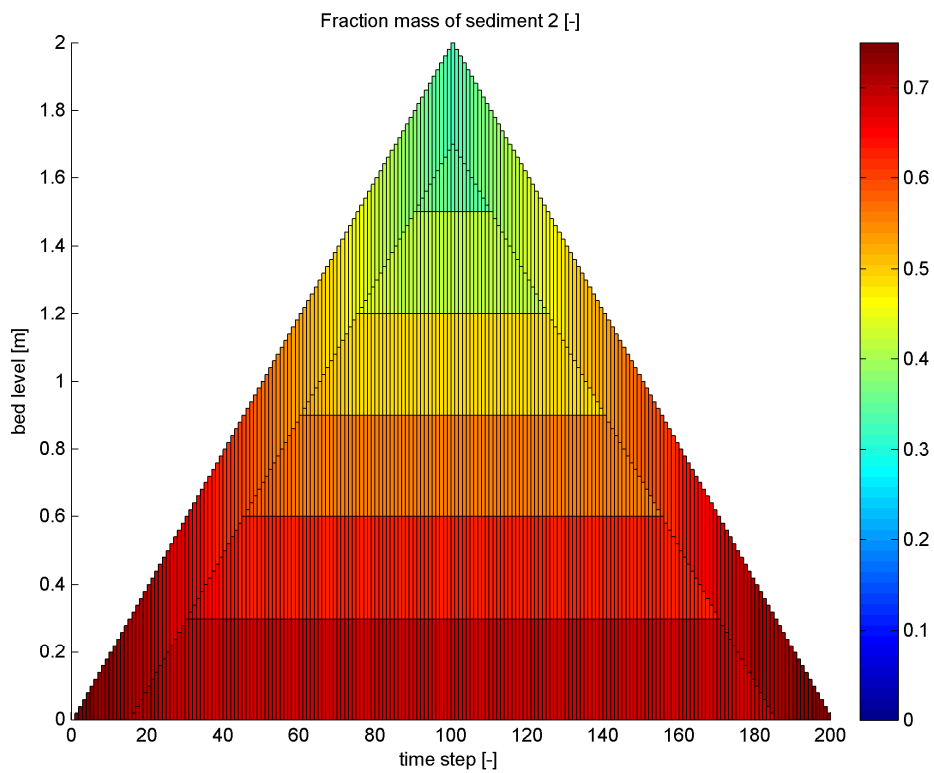
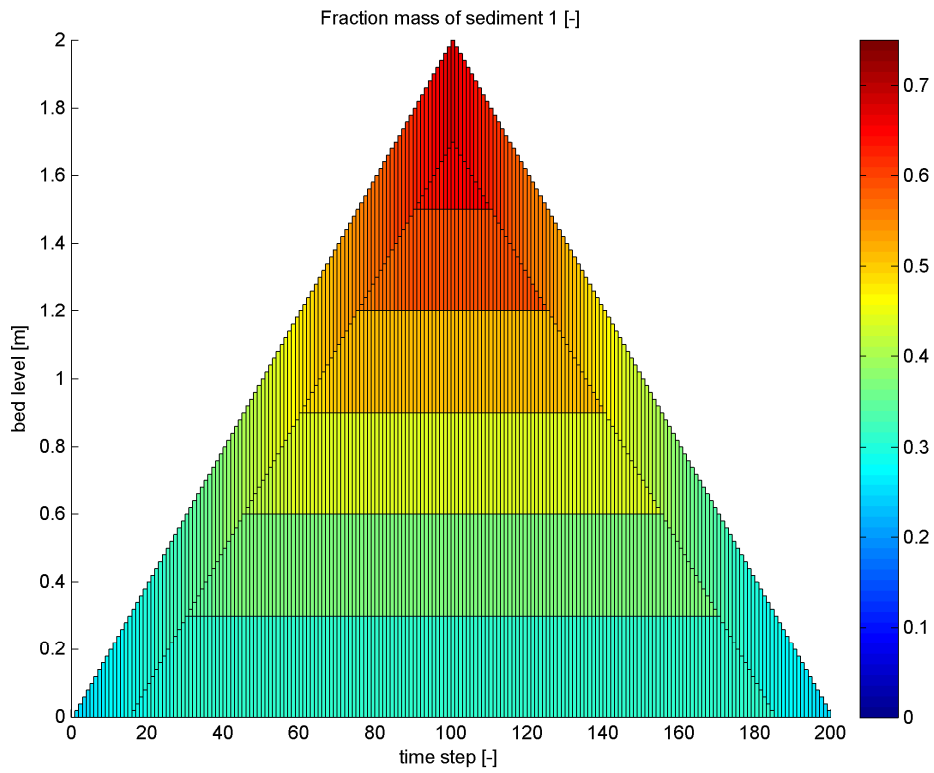


Figure 4.6 Mass fraction sediment 1 and 2 in the transport layer and the underlayers beneath with a maximum transport layer thickness of 0.2 m.

### Effect thickness transport layer

If we increase the maximum thickness of transport layer from 0.1 to 0.3 m, the transport layer contains more mass and responds slower, which is illustrated in Figure 4.5 - Figure 4.6 (compare with Figure 4.4).

### Effect Lagrangian instead of Eulerian underlayers

Next we test how using Lagrangian instead of Eulerian underlayers affects the bed comparison. To avoid sediment shortage in the transport layer we scaled the imposed sediment flux with 0.5. Figure 4.7 shows that mass is conserved.

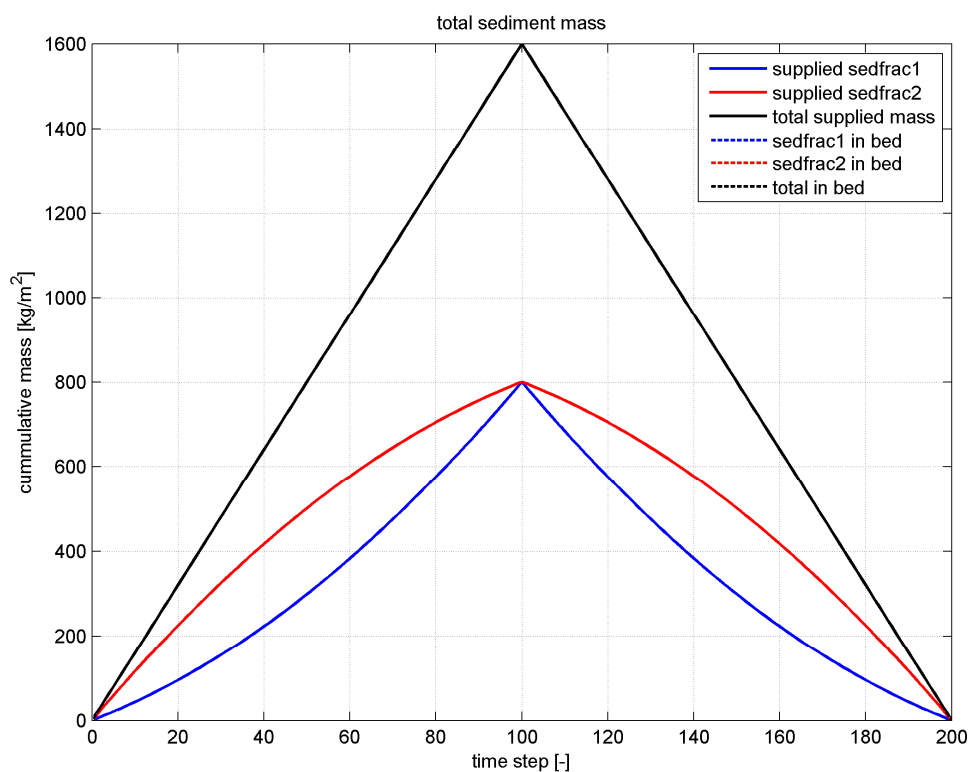


Figure 4.7 Cumulative supplied and stored sediment masses.

In the sedimentation phase the composition of the transport layer is not affected by choosing Lagrangian instead of Eulerian underlayers, as there is no effect at all of the underlayers on the transport layer in case of deposition (and without vertical diffusion). In the erosion half of the test, we see large differences between adopting the Lagrangian underlayer concept: the top layer contains far more sediment 2 and less sediment 1 compared to the Eulerian case. In the Lagrangian case, the composition of the transport layer is only affected from the instant the last underlayer is incised at  $t = 160$ . Before that, the Lagrangian underlayers merge and their positions shift downwards following the eroding bed level and the composition of the top layer is fully controlled by the exchange with the water column. As the cumulative erosive flux of sediment fraction 2 always exceeds the erosive flux of sediment fraction 1, but this exceedance slows down in time, an exponential behavior can be observed until  $t = 160$ . As the Lagrangian underlayers move up and down with the transport layer, mixing takes place in time, and therefore the vertical composition gradient is smaller than in the case of Eulerian underlayers.

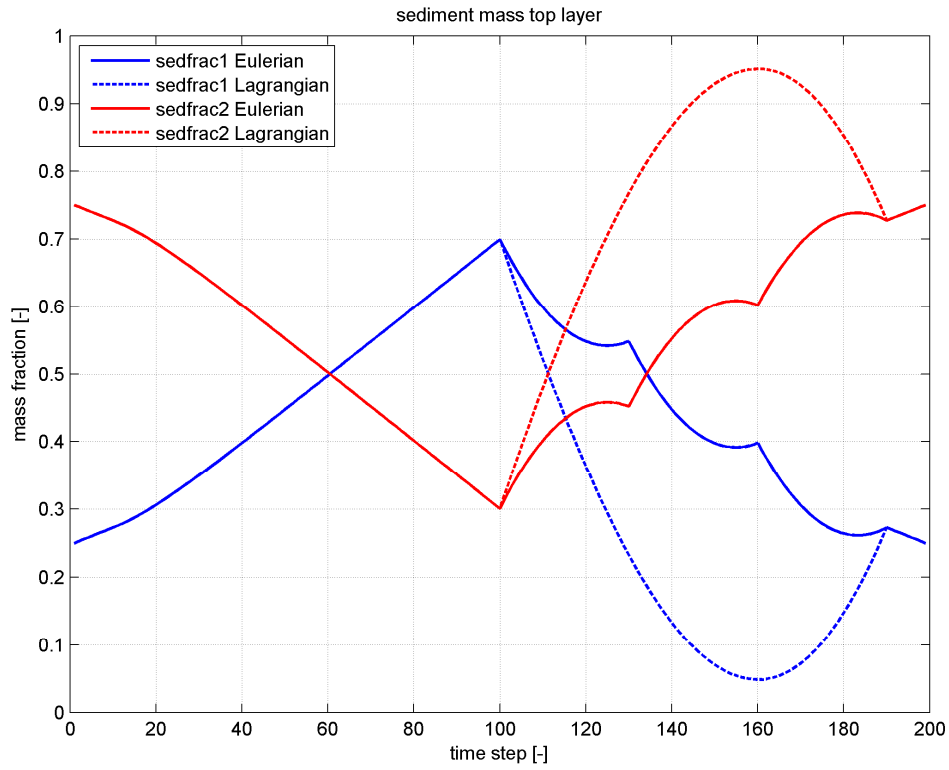


Figure 4.8 Mass fractions sediment 1 and 2 in the top layer with Eulerian and Lagrangian underlayers.

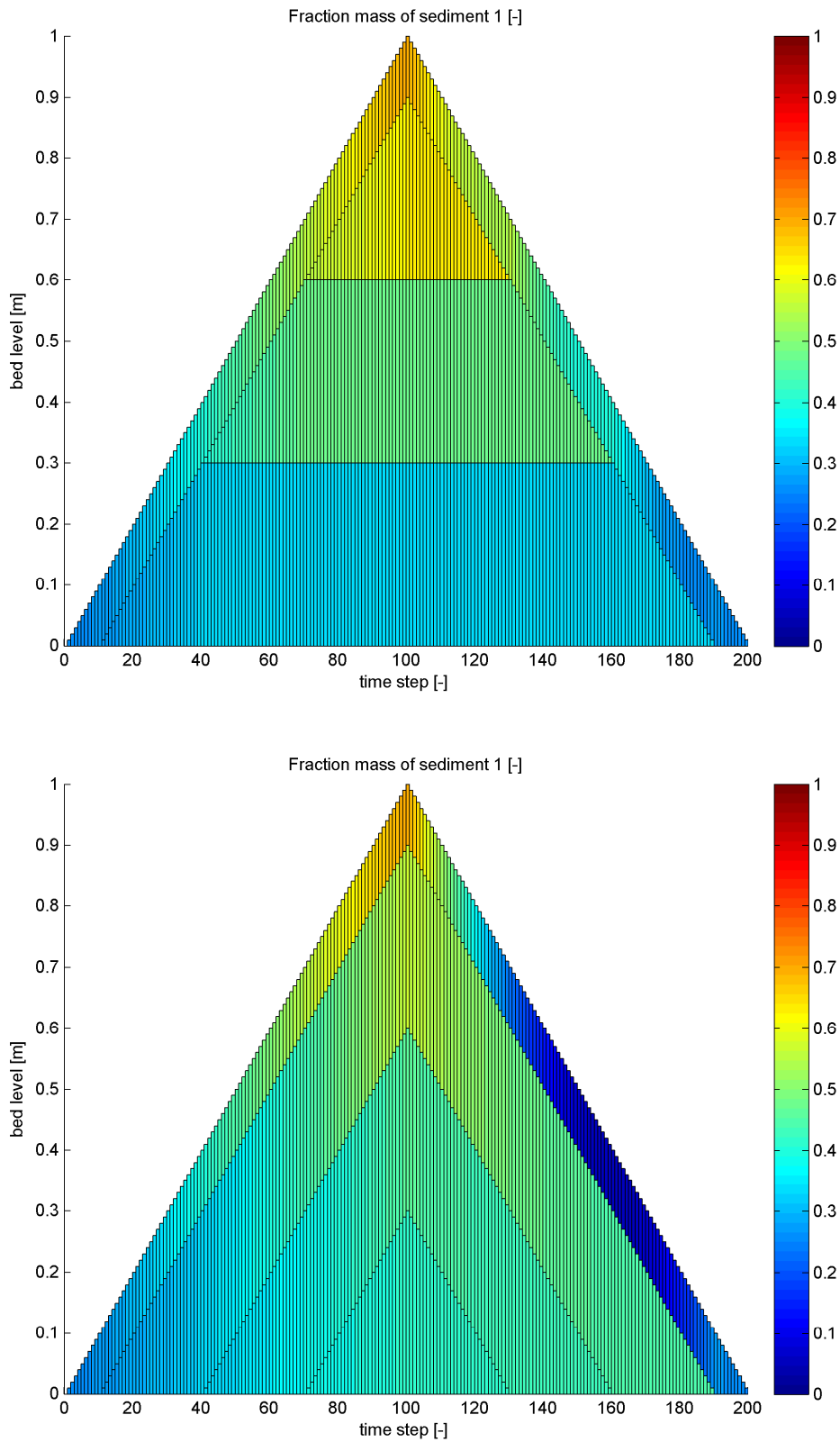


Figure 4.9 Mass fraction sediment 1 in the transport layer and the underlayers in cases of Eulerian underlayers (top panel) and Lagrangian underlayers (lower panel).

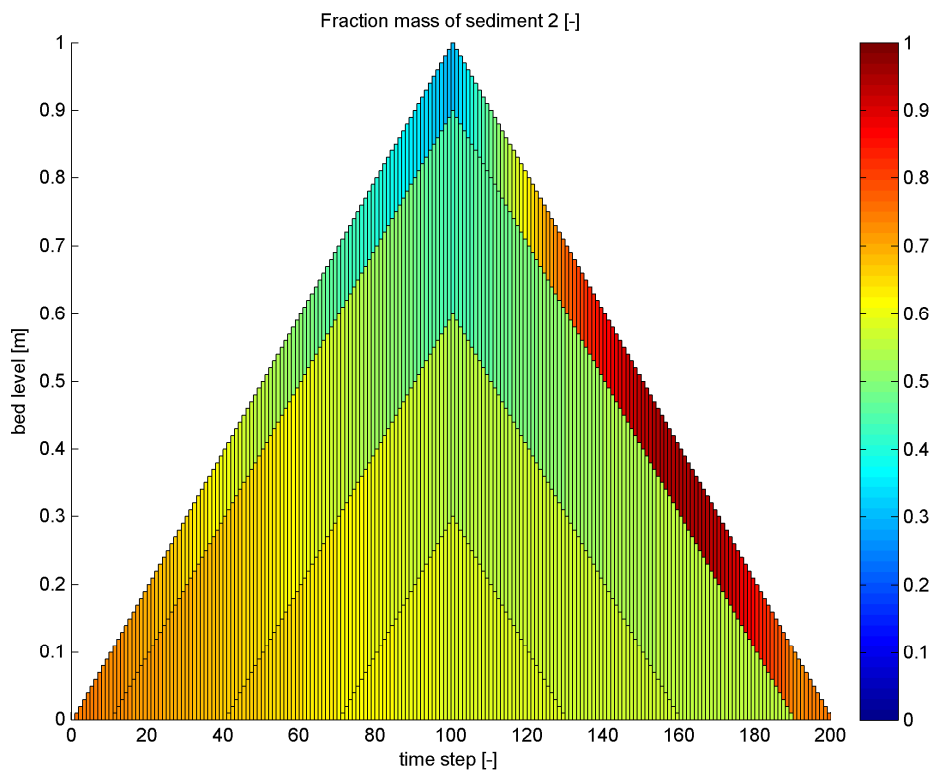
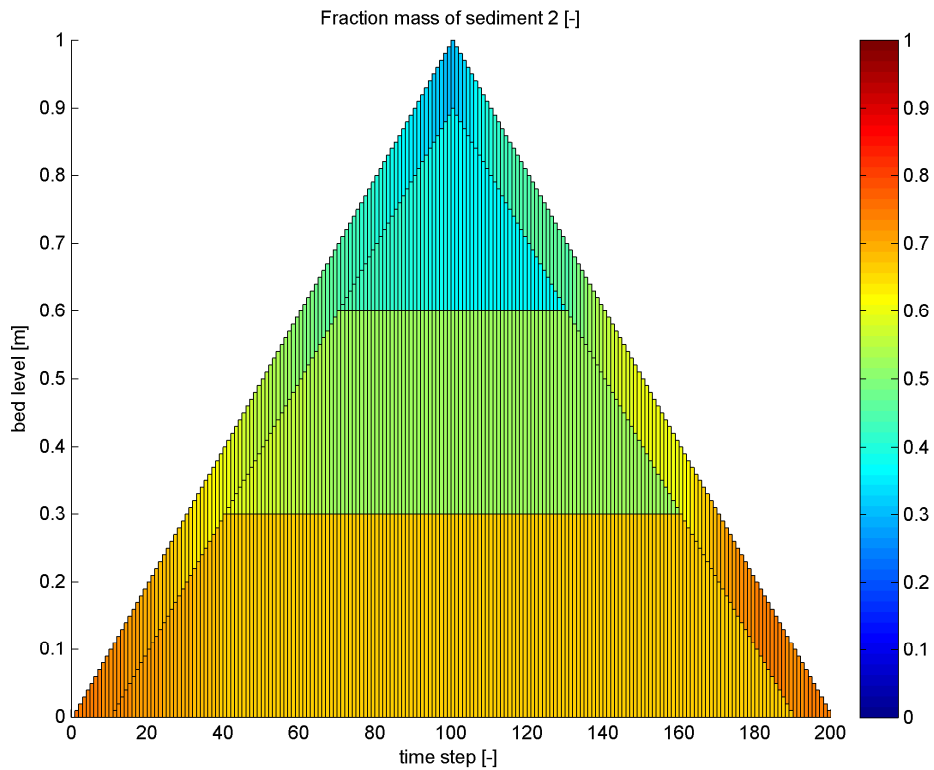


Figure 4.10 Mass fraction sediment 2 in the transport layer and the underlayers in cases of Eulerian underlayers (top panel) and Lagrangian underlayers (lower panel).

### 4.3 Test 2: Vertical diffusion

In this test we have no fluff layer and no sand-mud interaction. The thickness of the transport layer is 0.2 m, and we adopt the Eulerian underlayer concept with a maximum thickness of 0.4 m. We took a very large constant diffusion coefficient  $K_{diff} = 0.02 \text{ m}^2/\text{s}$  for demonstration purposes, with diffusion based on the volume fractions. We used two sediment fractions with the same properties as in Test 1.

The sediment flux is imposed as shown in Figure 4.11, corresponding to a 0.05 m deposition per time step for  $t = 1-100$  followed by no bed level change between  $t = 101-200$ . The supply of sediment fraction 1 to the bed decreases from 100% to 0 %, whereas the sediment supply of fraction 1 increases from 0% to 100%.

Figure 4.12 shows that mass is conserved for the case with diffusion. The same goes for the case without diffusion (not shown here).

Figure 4.13 - Figure 4.15 clearly illustrate how the vertical diffusion affects the bed composition. Especially, from  $t = 100$  (no more sedimentation or erosion) this becomes apparent: the composition is constant if there no diffusion and sediment exchange with the water column, whereas diffusion mixes the bed until it is fully mixed. This goes in an exponential way, as the diffusion fluxes scale with the vertical gradient in mass fractions, which decreases in time due to diffusion. Also, in the deposition phase of the test we can observe an impact of the diffusion. After 4 time steps the first underlayer is created and from hereon the effect of diffusion kicks in related to the concentration gradient as the imposed fluxes for the sediment fractions are not constant. As the imposed flux of sediment 1 increases in time, the vertical gradient of the mass fraction of sediment 1 is positive (mass sediment 1 increases with depth), resulting in a downward diffusion flux lower sedfrac1 in the top and underlayers. The opposite is true for sedfrac2. The addition of new underlayers is visible as discontinuities in the composition of the transport layer as now an additional flux is added between the new underlayer and the underlayer directly above this new underlayer.

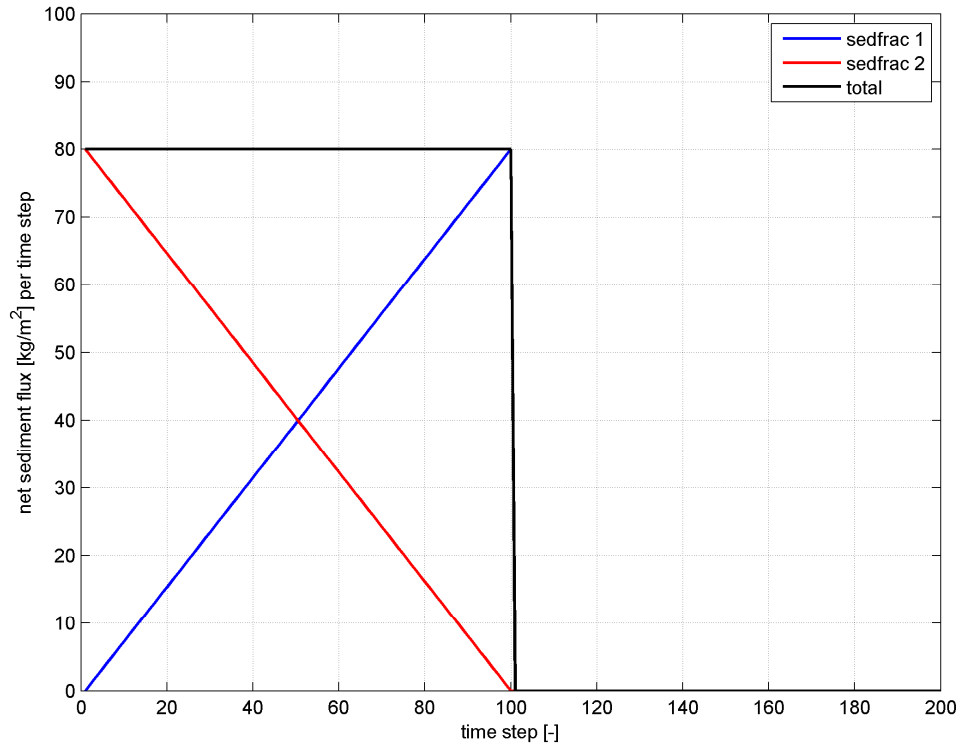


Figure 4.11 Imposed net sediment fluxes from the water column into the bed.

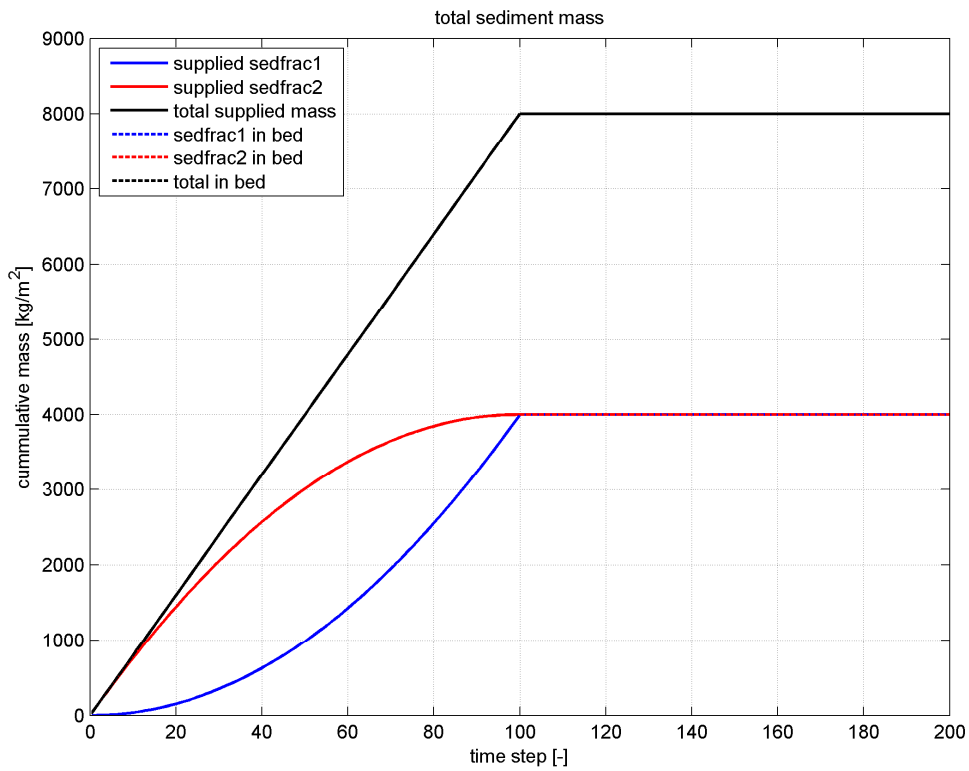


Figure 4.12 Cumulative supplied and stored sediment masses.

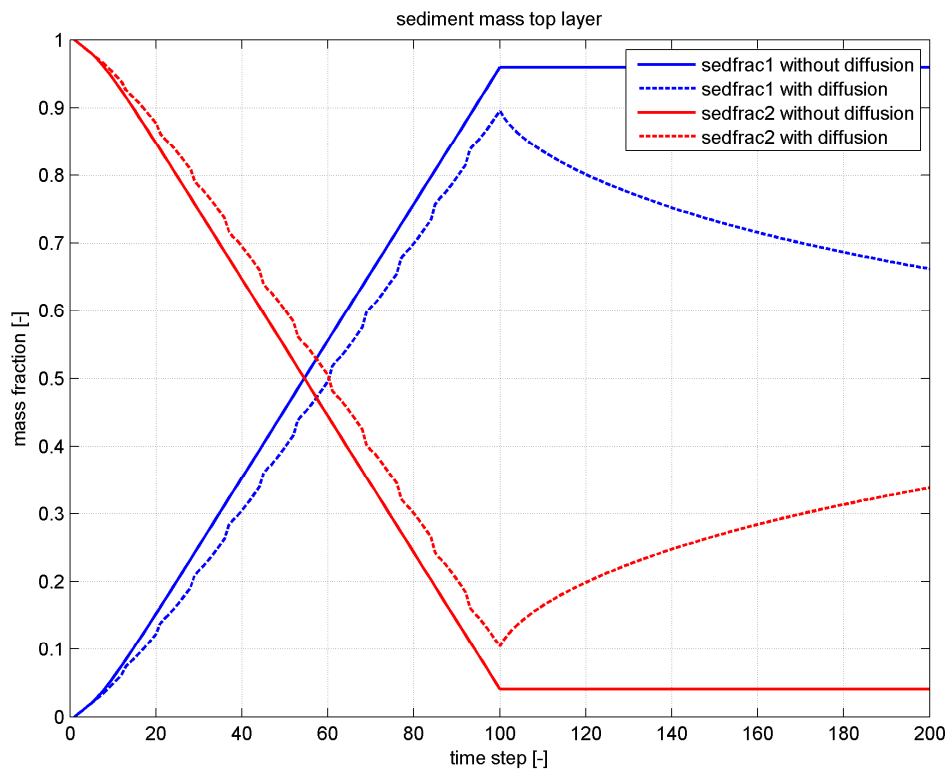


Figure 4.13 Mass fractions sediment 1 and 2 in the top layer with with and without vertical diffusion.

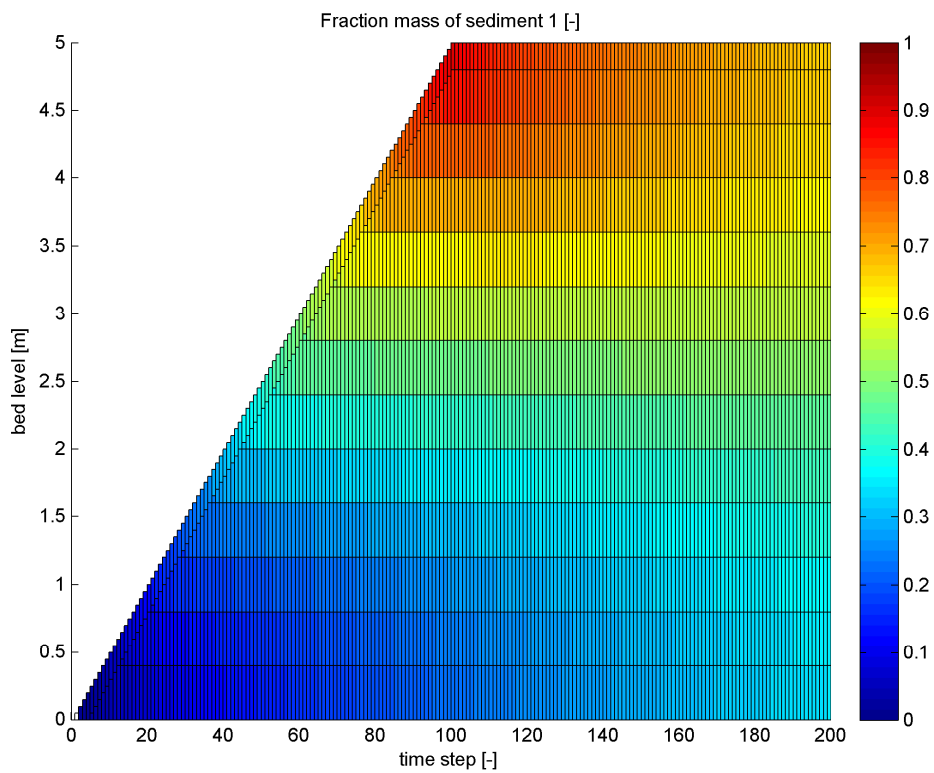
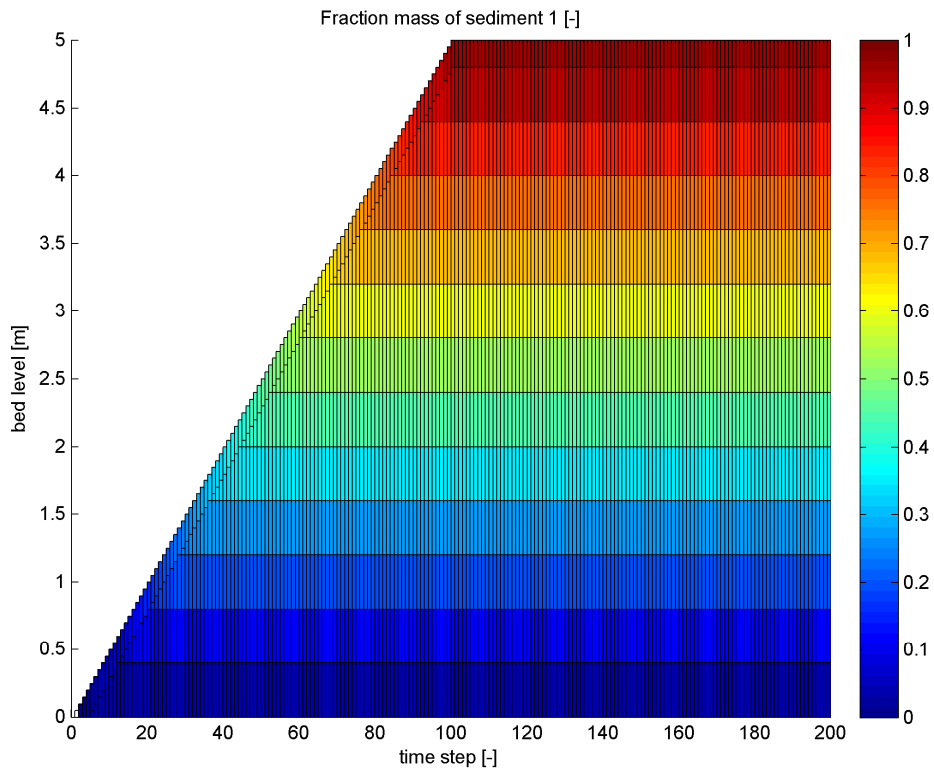


Figure 4.14 Mass fraction sediment 1 in the transport layer and the underlayers in cases without (top panel) and without vertical diffusion (lower panel).

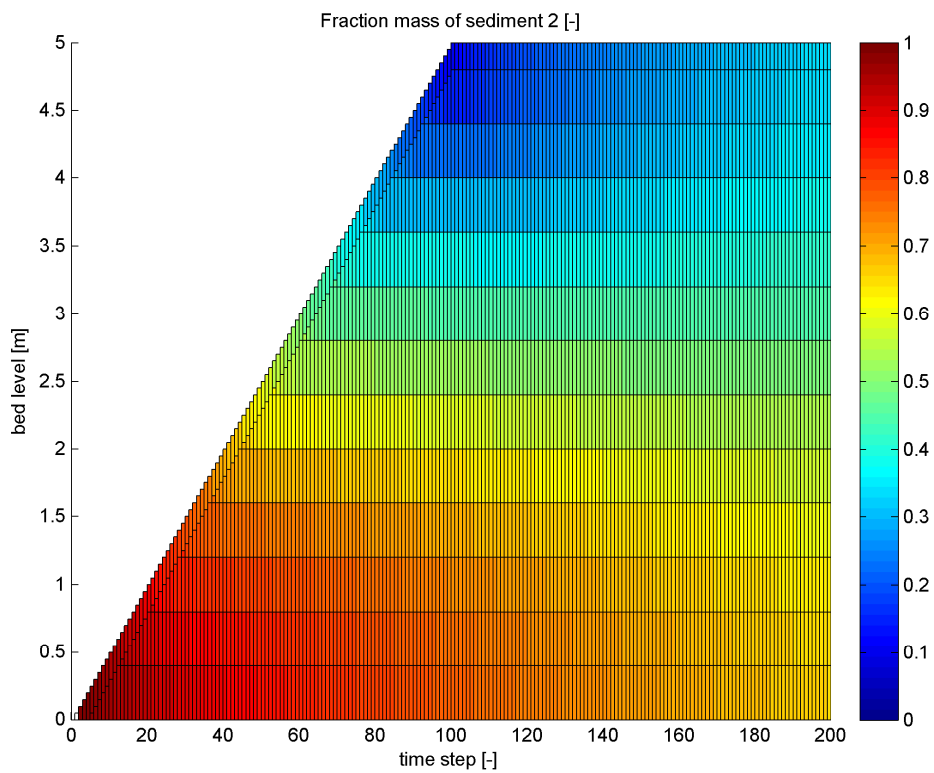
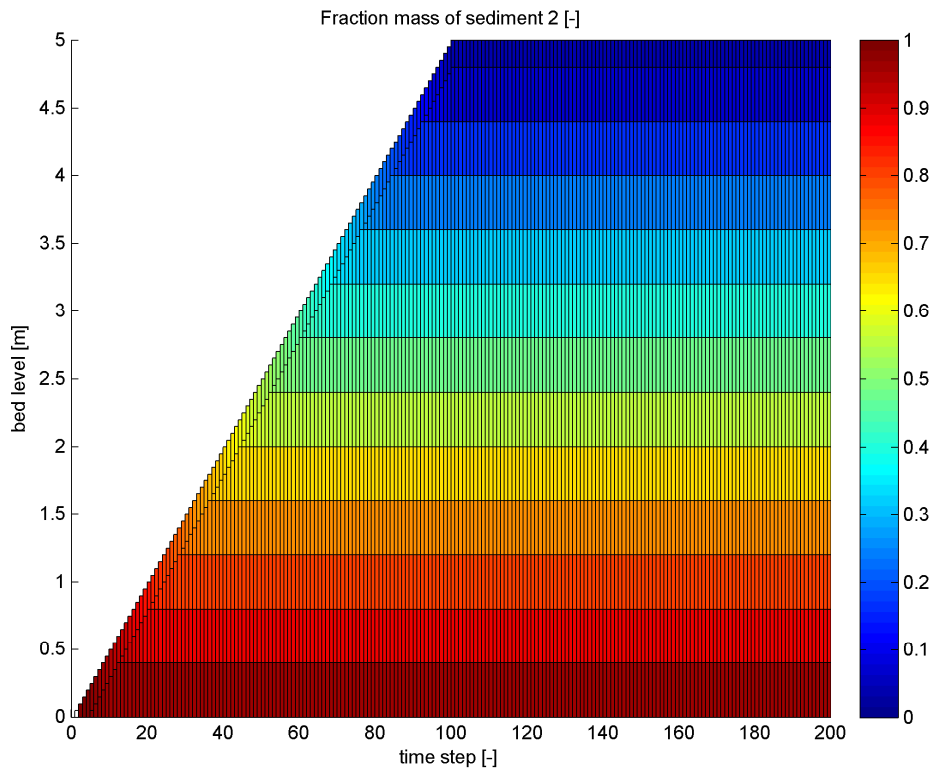


Figure 4.15 Mass fraction sediment 2 in the transport layer and the underlayers in cases without (top panel) and without vertical diffusion (lower panel).

## Vertical profile diffusion coefficient

Next we test the effect of a vertical profile for the diffusion coefficient. In the first test there is only vertical diffusion in up to 1 m below the bed level with a diffusion coefficient of  $0.02 \text{ m}^2/\text{s}$ , and in the other there is no diffusion in the top 1 m of the bed while there is vertical diffusion with  $K_{diff} = 0.02 \text{ m}^2/\text{s}$  below this level.

Figure 4.16 compares the mass fractions of sediment 1 and 2 in the top layer. The blue and cyan lines are on top of each other, which makes sense because in both cases there is no diffusion in the top 1 m of the bed. The same goes for the first time steps for the tests with diffusion (red lines) and the test with only diffusion in the top 1 m (green lines). However, when 1 m sedimentation has occurred and the third underlayer is added the composition of the lowest underlayer (which lies below 1 m) is fixed, mixing is confined to a smaller part of the bed compared to the case with uniform mixing over the complete profile, and therefore the mass fraction of sediment 1 (2) in the top layer will be higher (lower), i.e. closer to the case without diffusion. It also apparent from this figure that the time that diffusion influences the composition of the top layer after there is no longer sediment supply (from  $t = 100$ ) is much shorter, because it takes far less time to mix a bed layer of 1 m compared to a bed layer with a thickness of 5 m.

These observations are reflected in the composition of all layers, see Figure 4.17 and Figure 4.18. The instants when the composition of the underlayer is fixed (upper panels) and when the underlayers start to change distribution (lower panels) can clearly be identified.

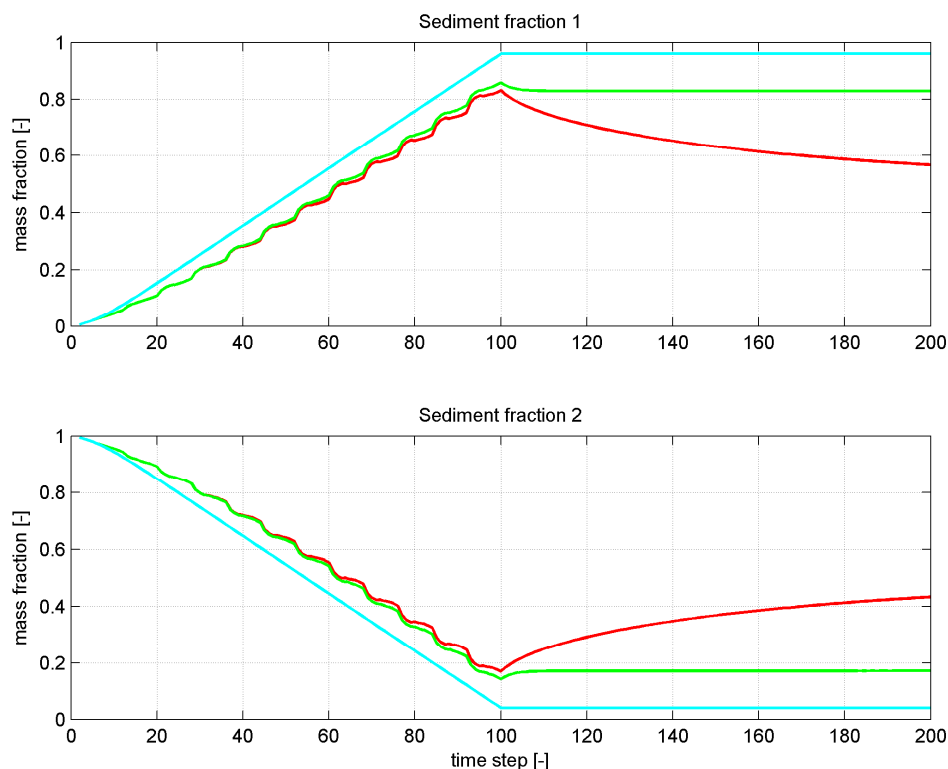


Figure 4.16 Mass fractions of sediment fraction 1 and 2 in the top layer without diffusion (blue lines), with diffusion (red lines), with diffusion in the top 1 m of the bed (green lines) and with only diffusion from 1 m below the bed level downwards (cyan lines).

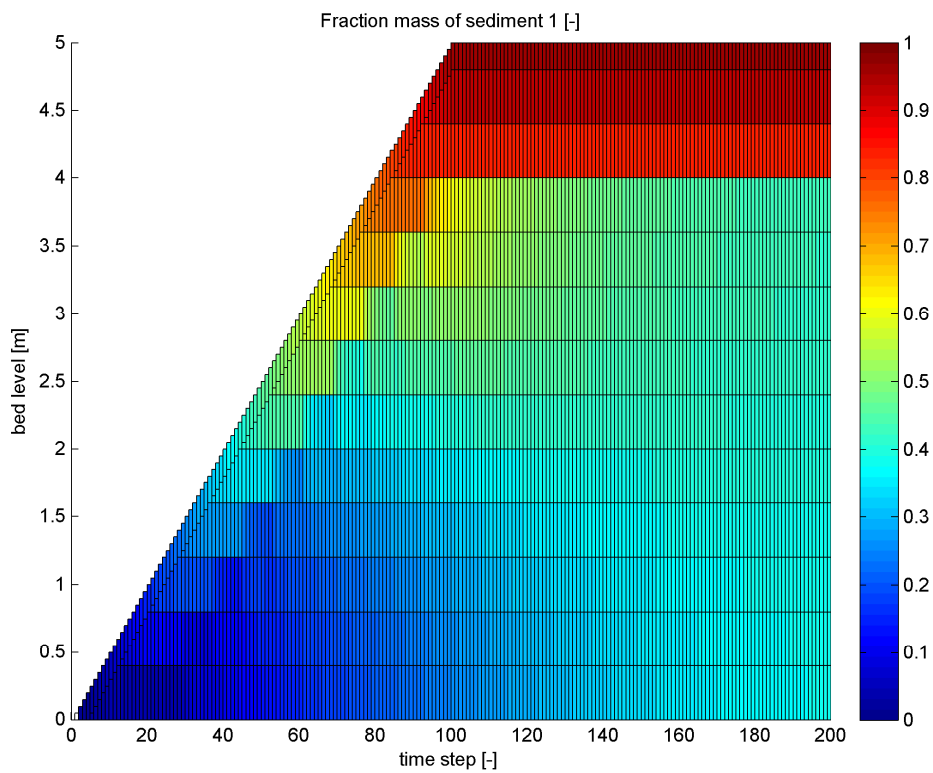
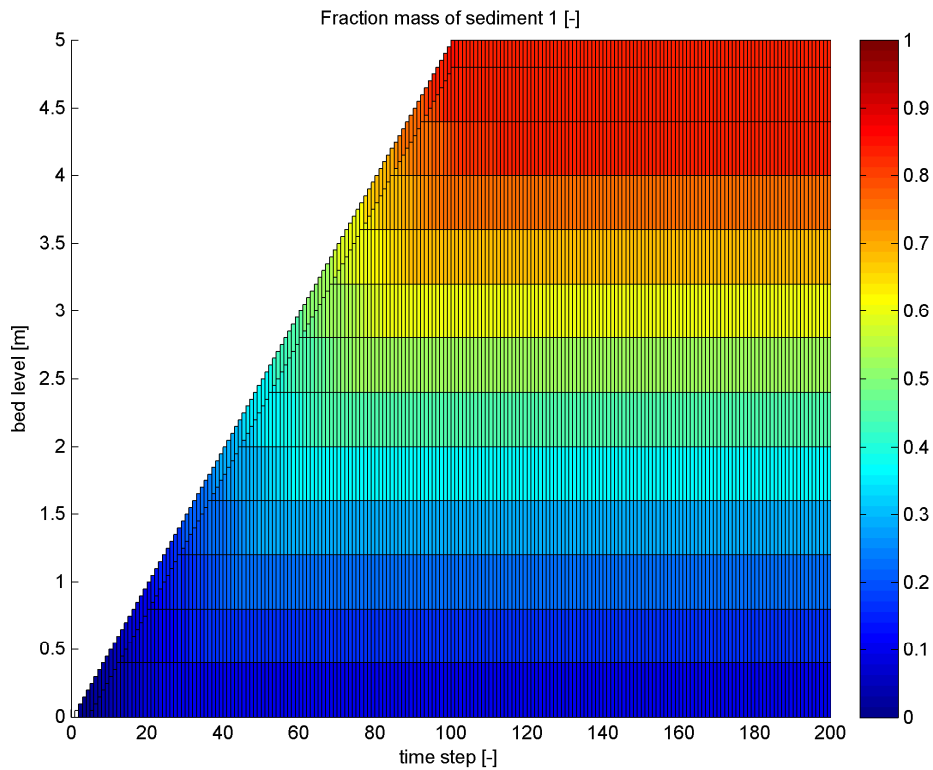


Figure 4.17 Mass fraction sediment 1 in the transport layer and the underlayers in cases with diffusion in the top 1 m of the bed (top panel) and with only diffusion from 1 m below the bed level downwards (lower panel).

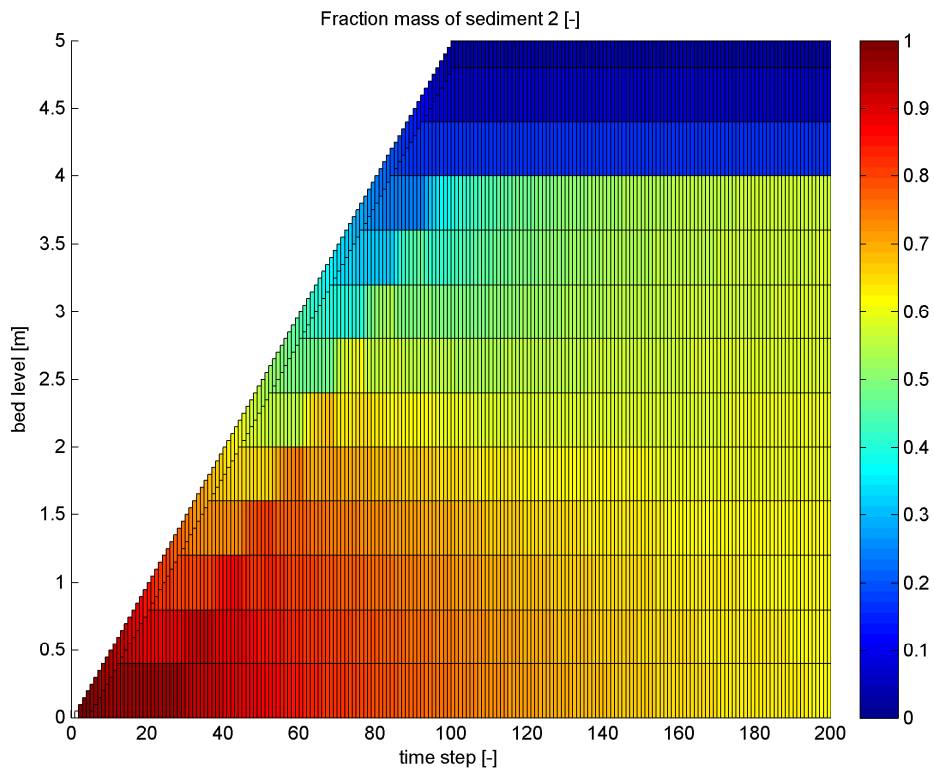
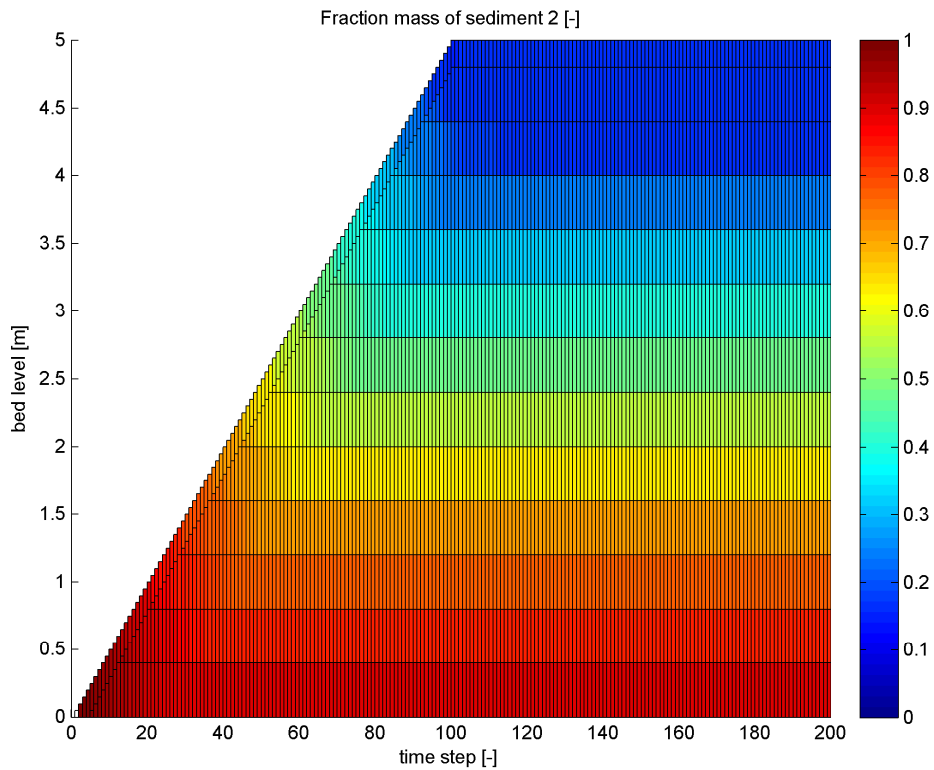


Figure 4.18 Mass fraction sediment 2 in the transport layer and the underlayers in cases with diffusion in the top 1 m of the bed (top panel) and with only diffusion from 1 m below the bed level downwards (lower panel).

#### 4.4 Test 3: Fluff layer

This test focuses on the influence of a fluff layer on the sediment dynamics. In order to isolate this influence, we have switched off vertical diffusion and sand-mud interaction. We have a transport layer with a thickness of 0.01 m, and Eulerian underlayers with the same maximum thickness. Further model settings are:

- Flufflyr = 1 (all mud to fluff layer), no mud burial
- Critical bed shear stress fluff layer,  $\tau_{cr,fluff} = 0.05$  Pa (keyword TCrFluff)
- Deposition efficiency to the fluff layer  $e_d = 0.95$  (keyword DepEff)
- Erosion parameters fluff layer:  $M_0 = 2 \times 10^{-4}$  ms/kg,  $M_1 = 0.1$  s/m (keywords ParFluff0 and ParFluff1)
- Mud erosion parameter from bed layer  $M_b = 0.01$  kg/m<sup>2</sup>/s (keyword Eropar)
- Critical bed shear stress for deposition/erosion mud to/from bed:  $\tau_{cr,dep} = 1000$  Pa,  $\tau_{cr,dep} = 1.0$  Pa (keywords tcrdep and tcrero)

We have two sediment fractions with the same properties as before. We also need now to provide the fall velocities for these sediment fractions and the initial sediment concentration in the water column. For this we took  $w_s = 2.0$  and  $0.05$  cm/s and  $C_0 = 0.05$  and  $0.4$  kg/m<sup>3</sup> for sedfrac1 (sand) and sandfrac2 (mud), respectively. Initially, the bed is uniformly distributed and has a total thickness of  $0.05$  m ( $80$  kg/m<sup>2</sup>). Furthermore, the water depth is  $3$  m.

The sand fluxes follow from the equilibrium suspended sand concentration based on the Van Rijn (1984) formulation accounting for relaxation time following the approach of Galappatti (1983).

Figure 4.19 and Figure 4.20 show the applied bed shear stress, the sediment exchange with the bed and the suspended concentration in the water column. The peak in sediment source for both the sand and mud fraction coincide with the peak bed shear stress. When bed shear stress drop, the downward, settling sand flux increases after which it decreases again as sand concentrations in the water column go down as well. The dip in sand sink is related to the velocity going below a threshold value and the sink flux is no longer computed using the Galappatti method, but simply by assuming that the sand sink is  $w_s \cdot C$ . The phase difference between peak bed shear stress and peak sand concentration is also apparent. As all mud settles to the fluff layer and the bed burial is set to zero, there is not sinking of mud to the bed. The figure shows that the sand concentrations are in dynamic equilibrium with the forcing, whereas mud concentrations need for more time for this; mud concentration has increased from the initial concentration of  $0.4$  to  $0.6$  g/l at  $t = 100$  s.

Figure 4.21 shows the mass of the fluff layer. Mud is eroded at high bed shear stress, and deposited at low bed shear stress, in line with what was expected. Again, it is clear that a dynamic equilibrium has not been reached as an increasingly amount of mud is stored in the fluff layer. The bed composition reflects the erosion of mud from the bed by which the percentage mud decreases in time and the bed (transport layer) become more sandy. The figure also shows small bed level changes out of phase with the bed shear stress reflection sedimentation and erosion.

Figure 4.24 shows that the total sediment masses are conserved and that mud is eroded from the bed.

Figure 4.25 compares the composition with and without the fluff layer. In case of the presence of the fluff layer, mud is stored in the fluff layer and less mud (and more sand) is contained in the transport layer.

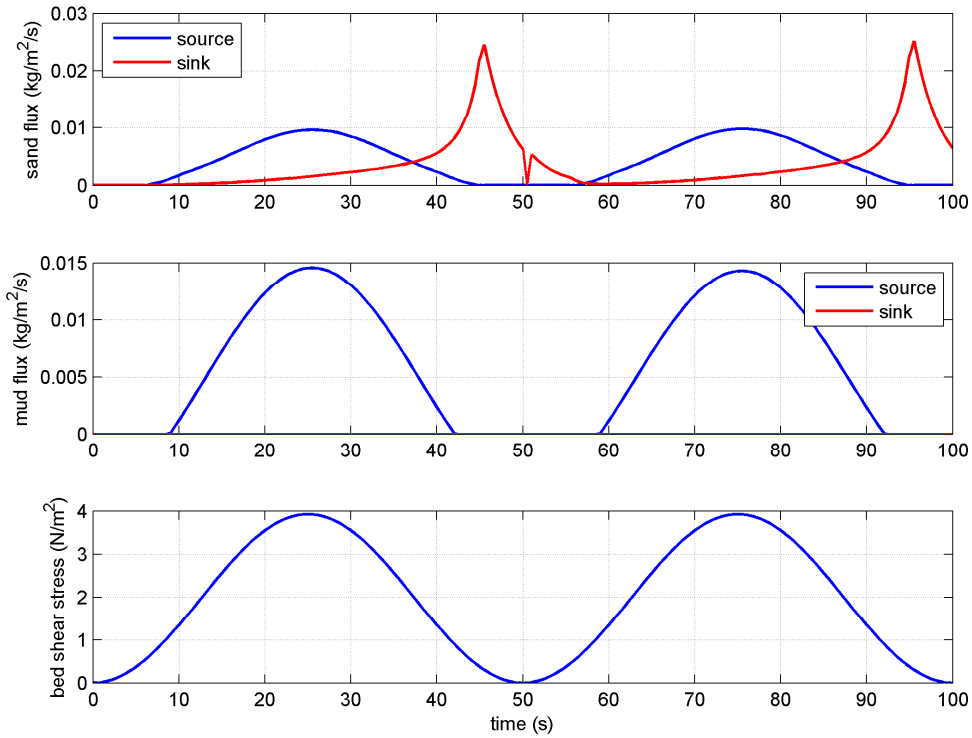


Figure 4.19 Bed shear stress, mud flux (between the bed and the water column) and sand flux in time.

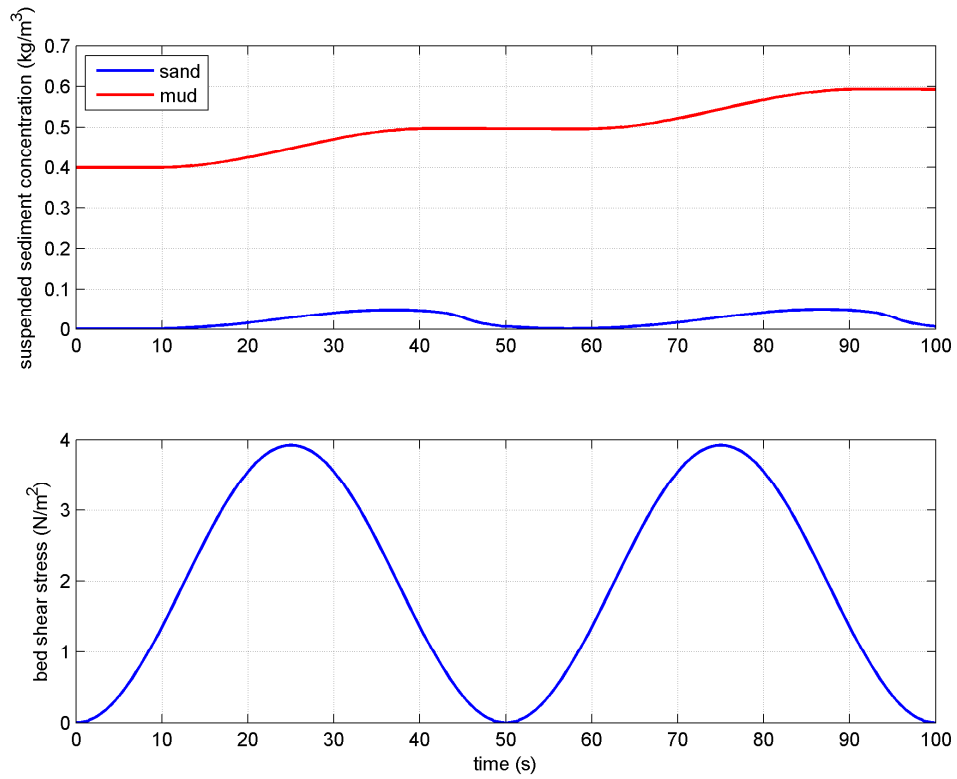


Figure 4.20 Bed shear stress and mud and sand concentration in the water column.

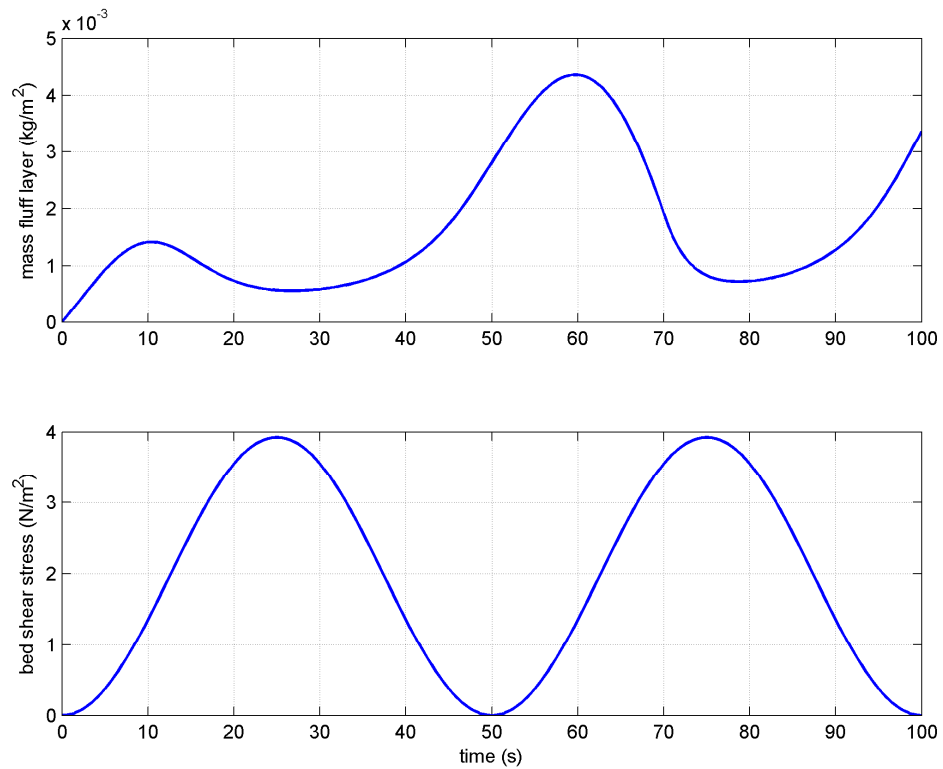


Figure 4.21 Bed shear stress and mass fluff layer in time.

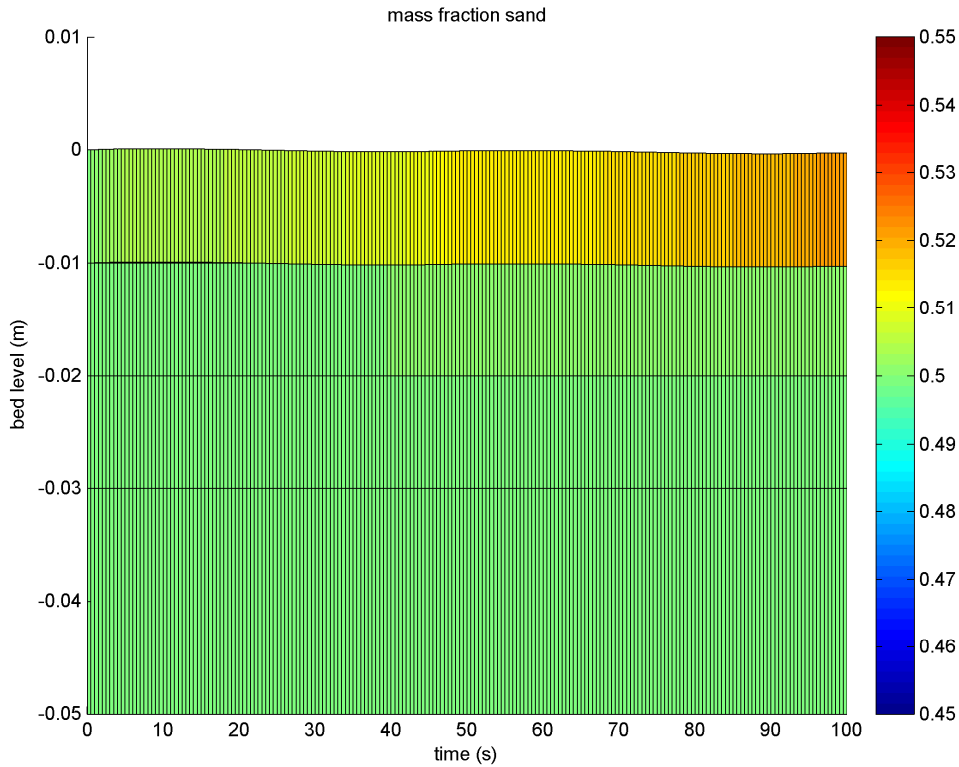


Figure 4.22 Mass fraction sand per bed layer.

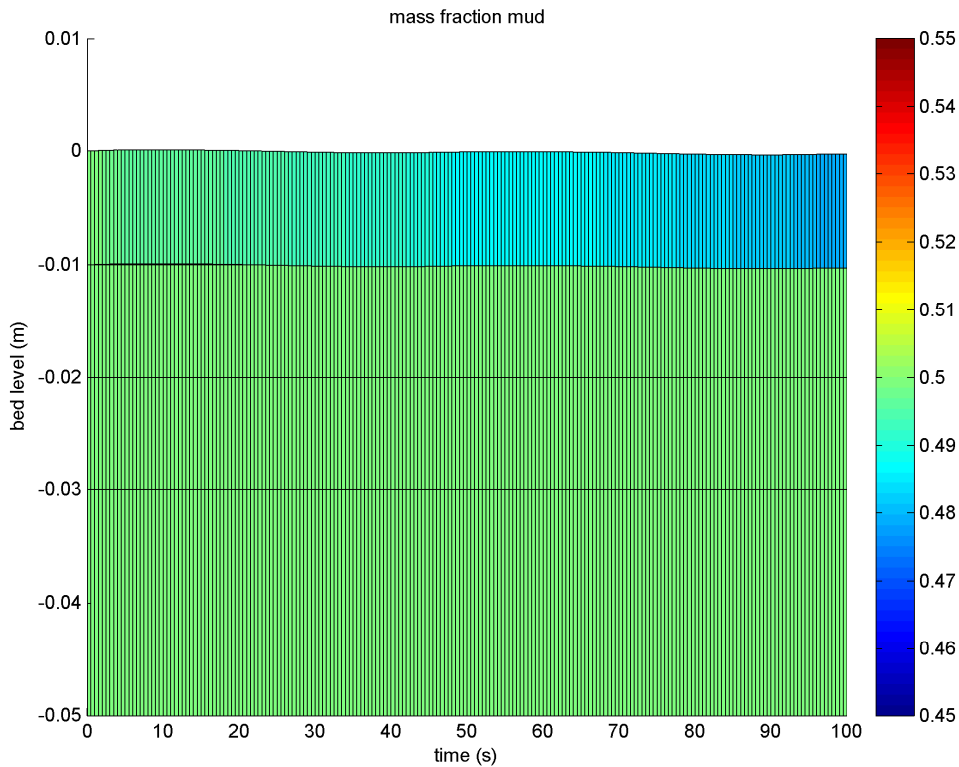


Figure 4.23 Mass fraction mud per bed layer.

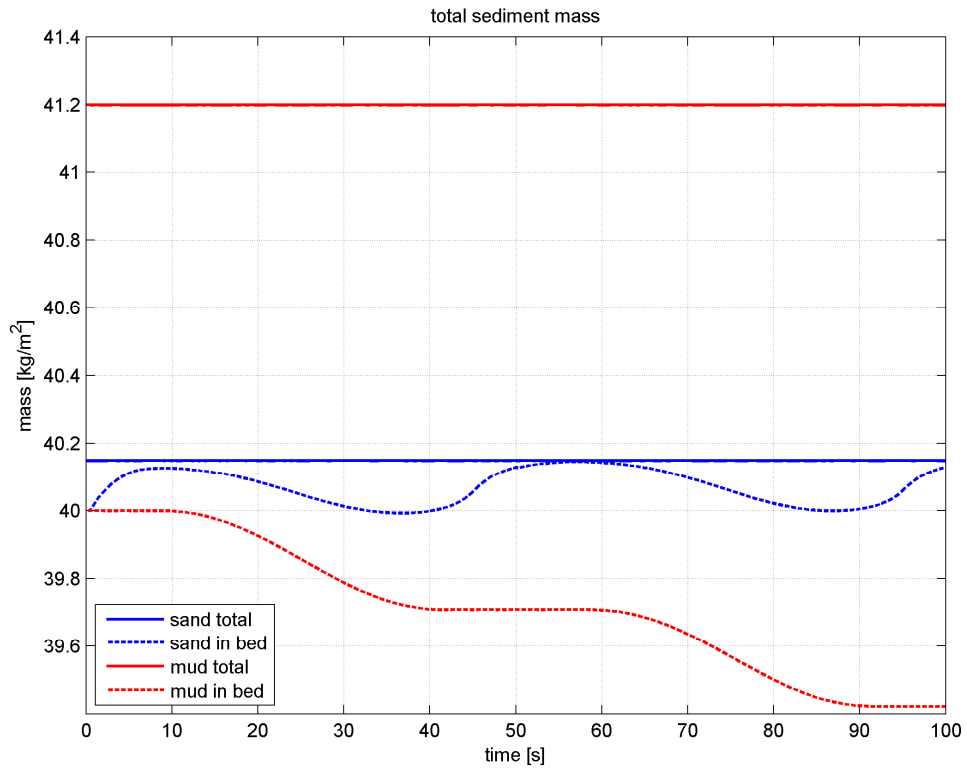


Figure 4.24 Mass sand and mud fraction in bed and total sand and mud mass.

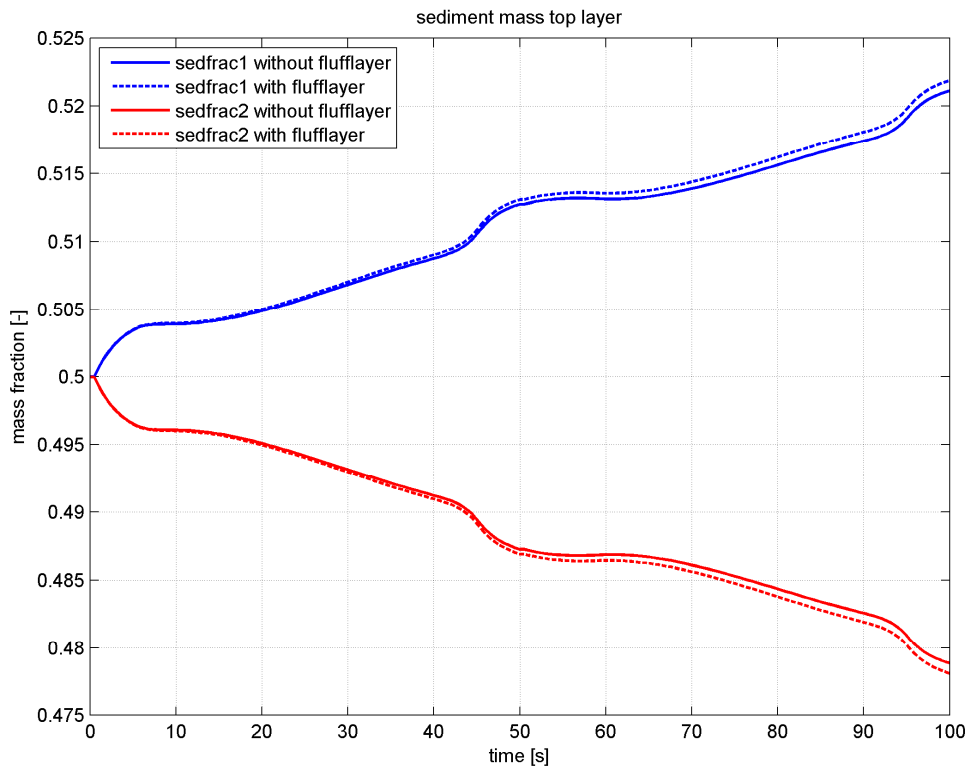


Figure 4.25 Mass fraction sand (sedfrac1) and mud (sedfrac2) in top bed layer with and without fluff layer.

## 4.5 Test 4: Sand-mud interaction

The final test is on sand-mud interaction. In the following examples there is no exchange of the sediment with the bed and there is no fluff layer. We define two sediment fractions, sand and mud, with the following properties:

- $D_{50} = [0.20, 0.05]$  mm
- $\rho_s = 2650 \text{ kg/m}^3$ ,  $\rho_{s,dry} = 1600 \text{ kg/m}^3$
- $w_s = [2.0, 0.1]$  cm/s
- $C = [0.01, 0.01] \text{ kg/m}^3$  (constant)
- Constant bed composition [50%,50%]

For the mud fraction:  $M_b = 1 \times 10^{-5} \text{ kg/m}^2/\text{s}$ ,  $\tau_{cr,dep} = 1000 \text{ Pa}$  and  $\tau_{cr,dep} = 1.0 \text{ Pa}$ . We will vary the critical mud fraction that distinguished between the non-cohesive and cohesive regime  $p_{m,cr}$  (keyword pmcrit). Furthermore, we take  $\beta = 1$  as the empirical constant for the critical bed shear stress for erosion.

Figure 4.26 shows the erosion velocity for the sand and mud fraction, defined as  $E_{vel} = E_{flux} / (m^* \rho_{s,dry})$  with  $E_{flux}$  the erosion flux [ $\text{kg/m}^2/\text{s}$ ] and  $m$  the mass fraction, for  $p_{m,cr} = -1$  (no sand-mud interaction),  $p_{m,cr} = 0.3$  and  $0.6$ .

Without sand-mud interaction ( $p_{m,cr} = -1$ ), sand and mud are eroded separately with a relative high erosion rate for the sand fraction and a low erosion rate for the mud fraction. Note that the critical bed shear stress for the sand fraction is still affected by the presence of mud using the equation proposed by Van Rijn (2007):

$$\tau_{s,cr} = \tau_{s,cr,0} (1 + p_m)^\beta$$

For the case  $p_{m,cr} = 0.6$  (given that  $p_m = 0.5$ ) we are in the non-cohesive regime. In this regime accounting for sand-mud interaction has no influence on the erosion of sand (blue and black lines are on top of each other). However, mud is now eroded proportional to sand, reflected in the same erosion velocity. With  $p_{m,cr} = 0.3$  we enter the cohesive regime and sand is eroded proportional with the mud and so the erosion velocity for the sand and mud fraction are the same again. Now, the values are lower as the erosion velocity follows from interpolation between the erosion velocity in the non-cohesive regime (which is computed using pm) and the erosion velocity in the fully mud regime ( $p_m = 1.0$ ). Alternatively, the erosion velocity in the non-cohesive regime could be computed using  $p_{m,cr}$ , but this option is not (yet) included in the computational code.

Figure 4.27 shows that the power  $\beta$  in the bed shear stress calculation has a strong effect on the erosion velocity of the sand and mud fraction in the non-cohesive and cohesive regime.

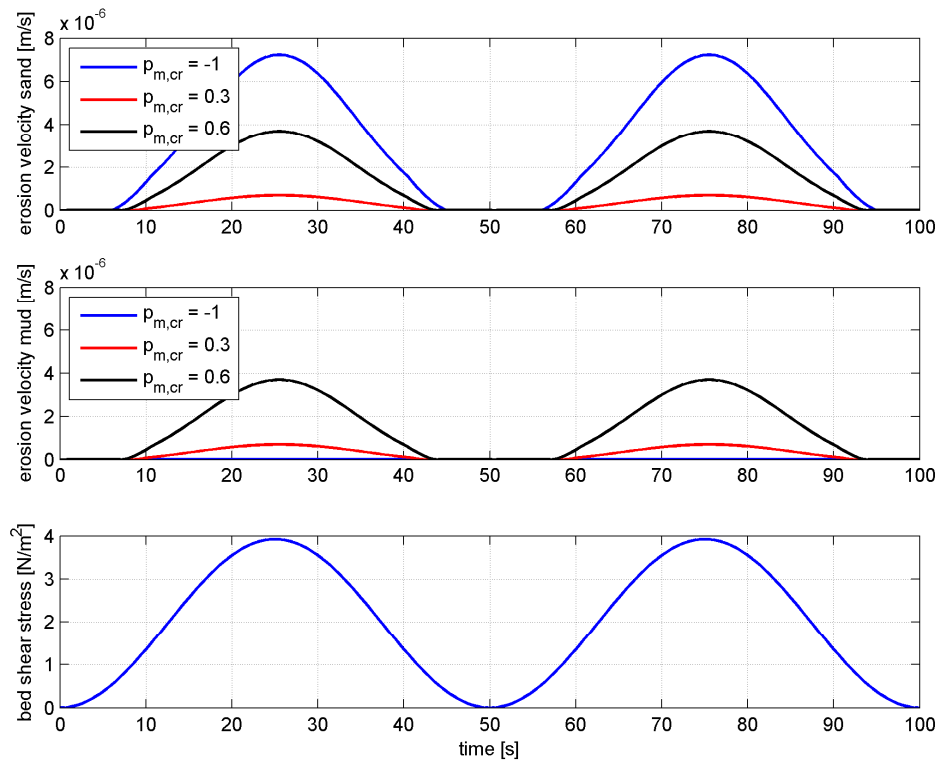


Figure 4.26 Bed shear stress and erosion velocity of the sand and mud fraction in time for different values of  $p_{m,cr}$ .

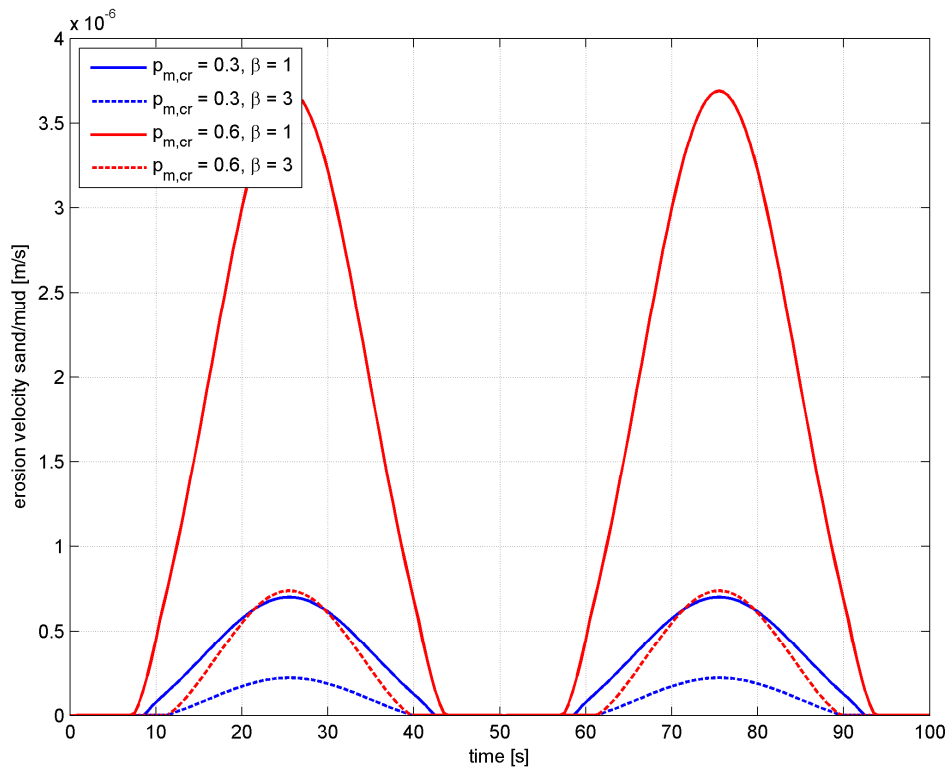


Figure 4.27 Effect power  $\beta$  in the bed shear stress calculation on the erosion velocity of the sand and mud fraction.



## 5 Practical Application

### 5.1 Introduction

This study includes a sensitivity analysis for testing the response and the sensitivity to change in parameter settings of the new Sand-Mud (SM) model implemented in Delft3D.

The Sand Mud module was developed and implemented as part of the wider Building with Nature joint industry initiative. This module focuses on the implementation of the newest seabed / water interface process into a open source module that can be coupled with (all) the numerical models that aim at dealing with water / bed interactions, morphological simulations, suspended particulate matter (SPM) prediction, water quality, etc. This module particularly focuses on the interaction between mud and sand in the seabed, and in the exchange of sediment between seabed and water column, and shallow and deeper layers within the seabed itself.

Specifically, during this study three new concepts were developed or extracted from the present literature and implemented in a numerical code:

- a. Sand-mud interaction
- b. Fluff layer concept
- c. Mixing between sediment layers

For a detailed description of these concepts see Chapter 3. This sensitivity analysis especially focuses on a. and b. Tests on bed mixing are discussed in Chapter 4.

This new module was here tested with its application to the Wadden Sea. A new Delft3D-sedonline model was set up on the basis of a former Delft3D-WAQ model (Deltares, 2010). At an earlier stage, the new code was also applied to a schematised tidal basin representing a part of the Dutch Wadden Sea (Scheel, 2012).

A series of seventeen simulations were run starting with the standard Delft3D release version (D3D), and then transitioning to the new SM version. Main object of this testing were:

1. Consistency between SM and D3D;
2. Effect of change in Active Layer Thickness;
3. Effect of Morphology Updating;
4. Behaviour of Fluff Layer; and
5. Effect of changing threshold for cohesive / non-cohesive formulations (critical mud fraction – pcr).

### 5.2 Model and Model Outputs Description

The model is set up on the Wadden Sea including a North Sea portion until about 20 km offshore. The model is set-up for the year 1998, and it is generally run for a one-year only period. Initially, all parameters and boundary conditions are derived from the Delft3D-WAQ Wadden Sea model developed discussed in Deltares (2010).

The model is run with three fractions: Sand, Mud1, Mud2. Sand is non-cohesive, while Mud1 and Mud2 are cohesive. The Sand fraction has a median diameter (D50) of 300  $\mu\text{m}$ . The Mud1 fraction has a settling velocity ( $W_s$ ) of 1 mm/s, and Mud2 of 0.125 mm/s. Both Mud1

and Mud2 have critical shear stress for erosion ( $T_{cr}$ ) of 0.2 Pa and erosion parameter ( $M$ ) of  $1e-4$ .

Main output of the models were bed composition and SPM time series at different location, and spatial distribution of mud, SPM and mass in the fluff layer. Plots and maps were generated for visual observation. Time series, when possible, were compared to available data.

### 5.3 Parameters Setting and Variations

Parameters variation can be divided in five groups to study the model behaviour with respect to:

1. Consistency between SM and D3D;
2. Effect of change in Active Layer Thickness;
3. Effect of Morphology Updating;
4. Behaviour of Fluff Layer; and
5. Effect of changing threshold for cohesive / non-cohesive formulations (critical mud fraction – pcr).

All parameters settings are depicted in Table 5.1.

The two different versions of the model (D3D and SM) are selected depending on the executable utilized. However, Sand-Mud interaction is turned on only when the critical mud fraction for cohesive behaviour (pcr) is specified. Therefore, when not specified D3D and SM version should use the same physical and numerical processes and therefore should give the same results.

1. This analysis was obtained simply by running the same model setting and boundary conditions on different executables, without specification of pcr. Particularly, Runs 4 and 5 are identical in input and boundary conditions and should be most closely compared.

2. The active layer thickness was varied herein: full deposit, 0.5 cm, 50 cm and 5 cm (Runs 6 through 9 respectively). Specifically Runs 7 through 9 have identical parameters (but active layer thickness) and should be compared.

3. The morphological updating was turned on and off for simulations run with the SM module, with and without pcr specification. Aim is the analysis of sensitivity of morphological updating and different behaviour with respect to pcr specification. Runs 10 and 12 have morphological updating on, and Runs 9 and 11 do not specify pcr.

4. The Fluff Layer is included (and pcr not specified). In Run 13 the parameters utilized for the Fluff Layer are the same as calibrated in the previous Delft3D-WAQ model (assuming correct units conversions). Runs 14 and 15 vary these parameters by a factor 10 lower and larger. In Run 19  $T_{cr}$  is varied.

5. Pcr is active and varied. The default Pcr is 0.3 (Run 11). The same model is run for pcr of 0.1, 0.2 and 0.5 (Runs 16 through 18 respectively).

Run	Model	Group	% Sand	% Mud 1	% Mud 2	Thick AL	Morphology	pcr	ParFluff0	ParFluff 1	TcrFluff
3	D3D	1	99	0.5	0.5	Deposit	OFF	x	x	x	x
4	D3D	1	94	3	3	Deposit	OFF	x	x	x	x
5	SM	1	94	3	3	Deposit	OFF	x	x	x	x
6	SM	1/2	94	3	3	Deposit	OFF	x	x	x	x
7	SM	2	80	10	10	0.005	OFF	x	x	x	x
8	SM	2	80	10	10	0.5	OFF	x	x	x	x
9	SM	2/3	80	10	10	0.05	OFF	x	x	x	x
10	SM	3	80	10	10	0.05	ON	x	x	x	x
11	SM	3/5	80	10	10	0.05	OFF	0.3	x	x	x
12	SM	3	80	10	10	0.05	ON	0.3	x	x	x
13	SM	4	80	10	10	0.05	OFF	x	5.01E-04	1.16E-04	0.05
14	SM	4	80	10	10	0.05	OFF	x	5.01E-03	1.16E-03	0.05
15	SM	4	80	10	10	0.05	OFF	x	5.01E-05	1.16E-05	0.05
16	SM	5	80	10	10	0.05	OFF	0.1	x	x	x
17	SM	5	80	10	10	0.05	OFF	0.2	x	x	x
18	SM	5	80	10	10	0.05	OFF	0.5	x	x	x
19	SM	4	80	10	10	0.05	OFF	x	5.01E-04	1.16E-04	0.02

Table 5.1 List of parameters for the entire set of simulations included in this sensitivity study and described in this report.

## 5.4 Results

For consistency, the results of the different test runs are evaluated per each group, as described in section above. Results are evaluated considering SPM concentrations, bed composition and mass of fines in the fluff layer when applicable.

Results are reported as time series and maps. Time series of SPM are compared to data collected at the stations of Doove Balg Oost, Doove Balg West, Blauwe Slenk, and Vliensroom (even if for brevity, comparative results with data are reported here mainly wfor Blauwe Slenk). Time series are also reported for other locations in the Wadden Sea including in proximity of mud flats, in channels, near shore and near islands for comparison (Figure 5.1).

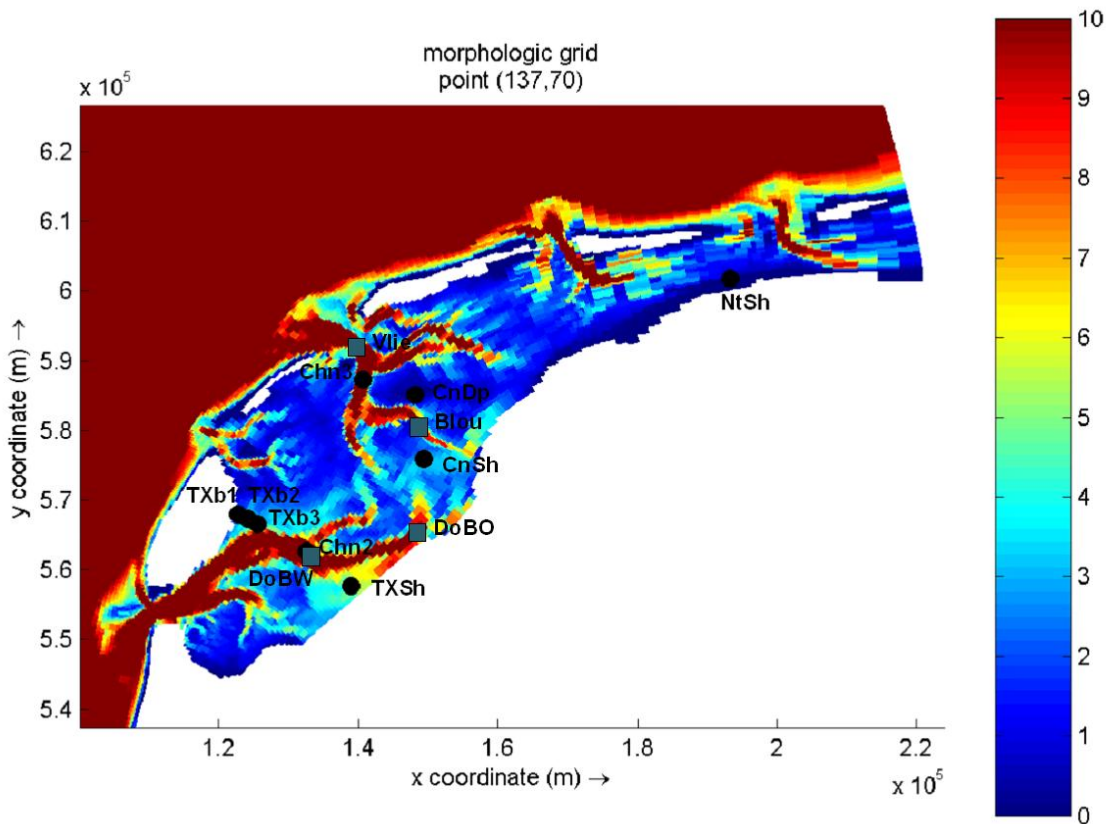


Figure 5.1 Locations of stations for where SPM data are available in 1998 (grey squares) and selected locations for comparison (black dots).

## 5.4.1 Group 1

Runs 3 and 4 computed made with D3D, while Runs 4 and 5 are computed with the Sand Mud (SM) module. This group is mainly done to compare the results of the D3D version with the new SM version. Theoretically, D3D and SM should be identical unless the critical mud fraction parameter (*pcr*) is specified. In these runs *pcr* is not specified. From a visual comparison of Run 4 and Run 5 for both bed composition and SPM (Figure 5.2 and Figure 5.3 respectively), results appears identical. Figure 5.4 shows a detailed comparison between the two model results for SPM. The magenta line does show a little discrepancy between the two model results, however of a much smaller order of magnitude with respect to the actual modelled concentration.

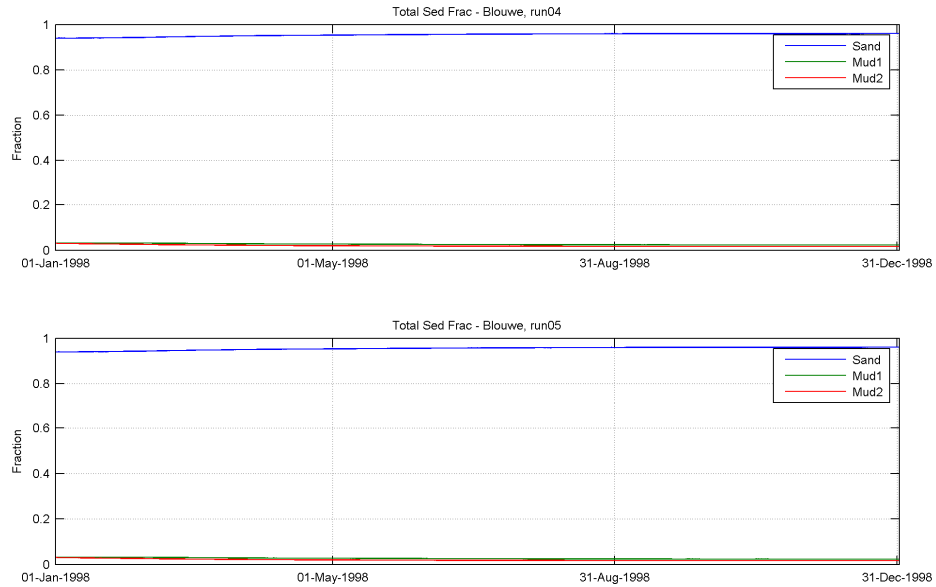


Figure 5.2 Bed composition time series for Station Blouwe Slenk for Run 4 and Run 5.

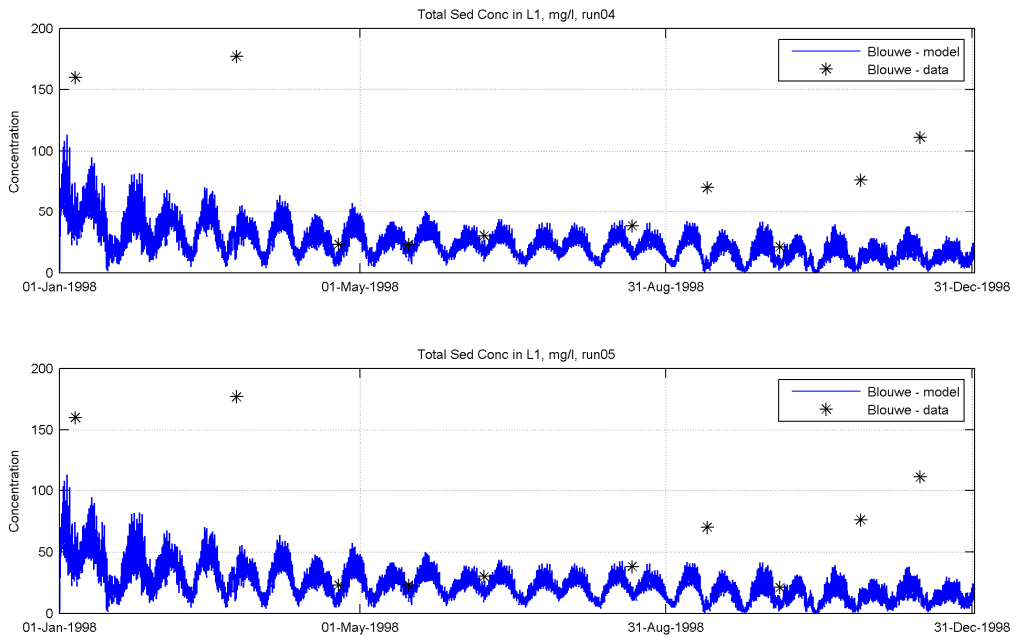


Figure 5.3 SPM time series for the Station Blouwe Slenk for Run 4 and Run 5. Blue line is model results, black stars are measured data.

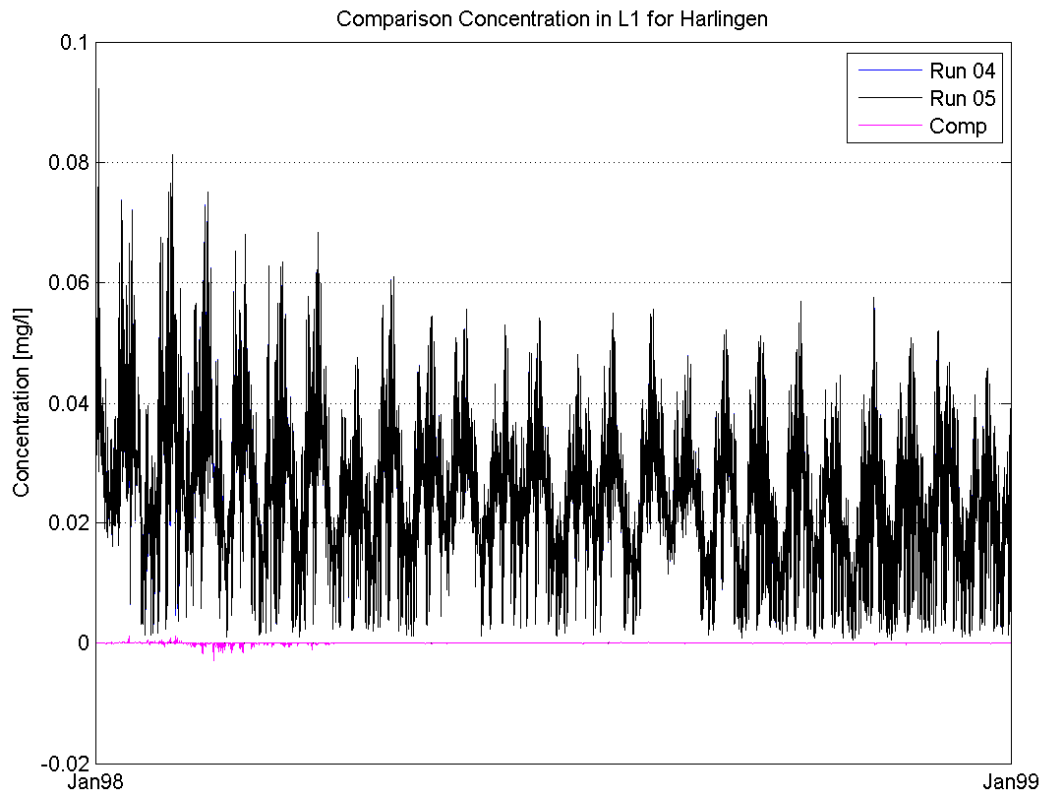


Figure 5.4 Detailed comparison of Run 4 and Run 5. In black and blue the modelled SPM concentration. In magenta their difference.

#### 5.4.2 Group 2

Main aim of this group of runs is to analyse the effect of Active Layer Thickness on bed composition and SPM. The active layer is effectively the layer of the seabed that reacts directly to the hydrodynamic forcing. It's sediment composition is well mixed. For example, if a certain mass of fines (mud) is eroded from the active layer, this will become sandier. However, a thin active layer will become sandier than a thicker active layer, given the same mass of eroded fines. Thinner active layers are therefore expected to have a quicker response to external forcing.

Figure 5.5 shows the bed composition for Station Blauwe Slenk for Runs 7 through 9. The initial sand fraction is 80%, while the initial mud fraction is 20% (10% for each mud fraction). The Active Layer Thickness for Run 7 is 0.5 cm, for Run 8 it is 50 cm and for Run 9 it is 5 cm. All runs tends to increase sand fraction with time to reach a similar value after one year, however adaptation of Run 7 is much more rapid. In addition, Run 7 is much more sensitive to short scale fluctuation.

Figure 5.6 and Figure 5.7 show seabed composition in two lower energy locations where mud tends to accumulate, specifically near the shore and in a mud flat. Both figures show the seabed becoming muddier from a constant initial sand fraction of 80%, and particularly highlight the different time scale of seabed response due to different active layer thickness.

Both the runs with active layer thickness of 0.5 cm and 5 cm reach similar end values after one year, but the 5 cm case is about 3 times slower. As within the channel, also near shore the 0.5 case is much more sensitive to short scale fluctuations. Moving toward the shoreline the hydrodynamic energy probably decreases further so that also the 0.5 cm scenario becomes rather static, while the 5 cm scenario loses any major short scale variation. Similarly to the previous location, here end values after one year are similar, and time for adaptation is about 3 times larger for the 5 cm active layer thickness. In both cases, the 50 cm layer thickness scenario (centre in the figures) reacts much slower and fails to adapt to final values after one year. This confirms the impression that 50 cm active layer thickness for this environment is likely to large.

Comparison with actual data (unavailable at the time of this report) will help determining which is the most appropriate active layer thickness. It is here assumed that 5 cm is a reasonable estimate, and this thickness is kept for the other sensitivity runs.

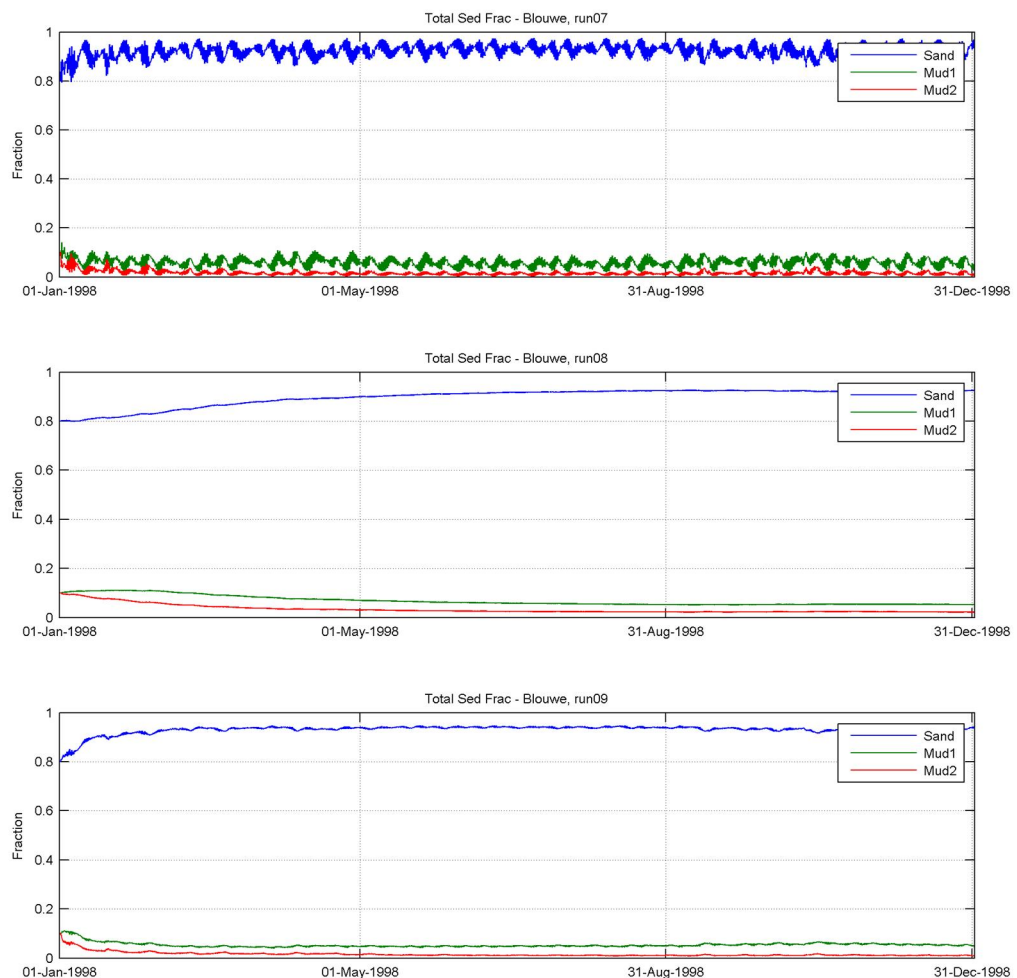


Figure 5.5 Bed composition time series for Station Blouwe Slenk for Runs 7 through 9.

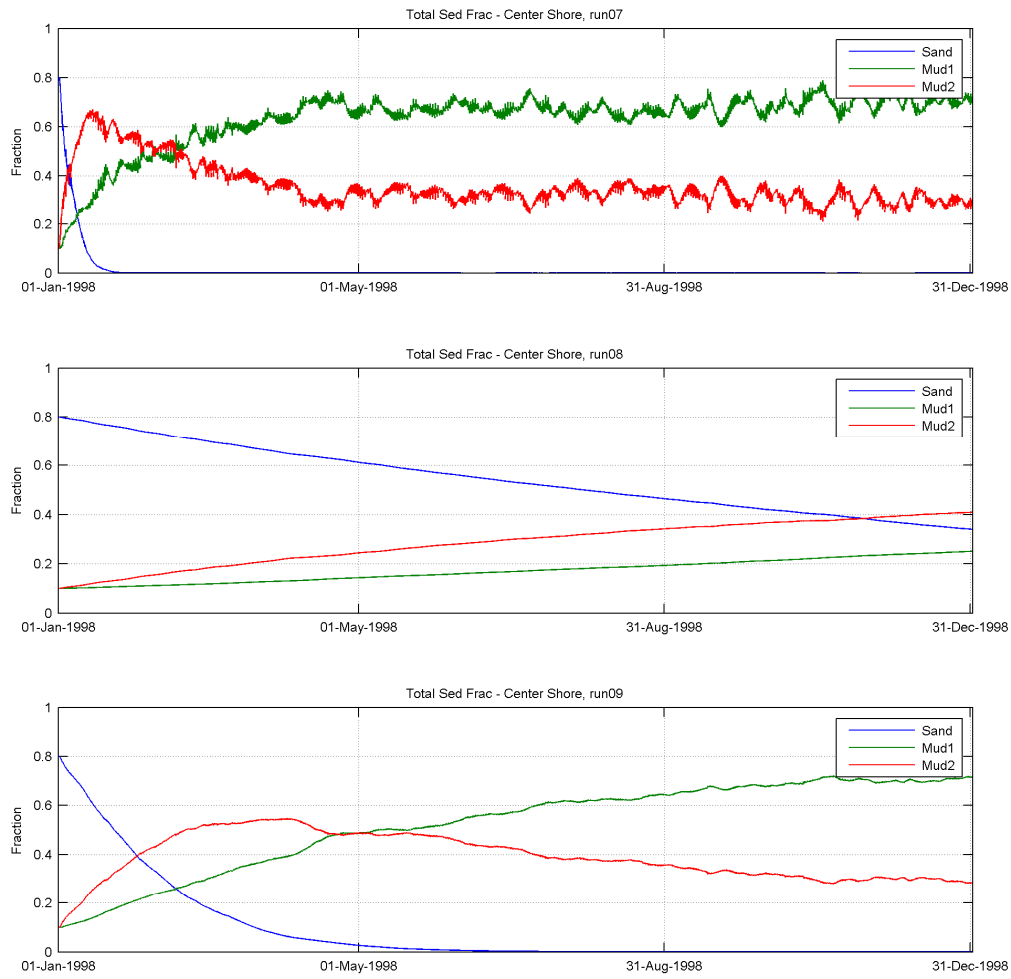


Figure 5.6 Bed composition time series for a near shore location (CnSh) for Runs 7 through 9.

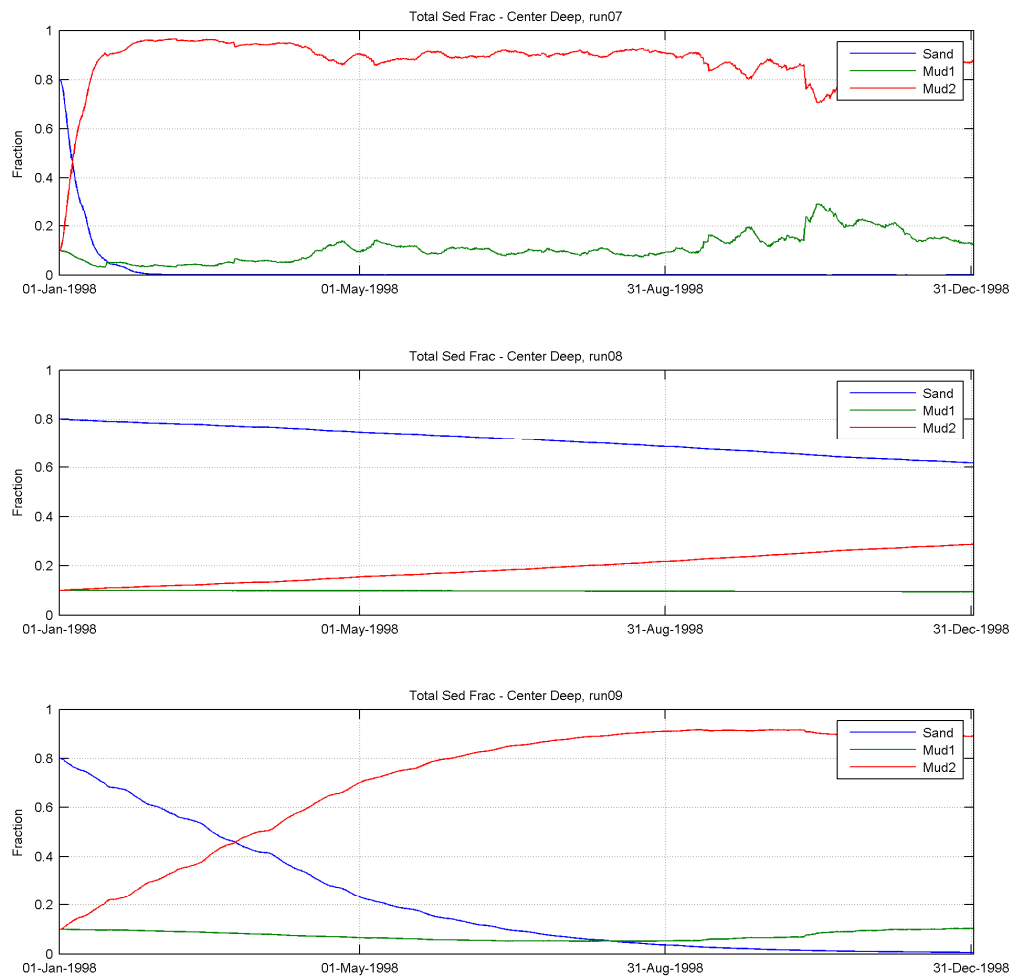


Figure 5.7 Bed composition time series for a tidal flat location (CnDp) for Runs 7 through 9.

Figure 5.8 shows the SPM for the same runs at the same location as Figure 5.5 (Blouwe Slenk). Here the amplitude and time scale of SPM variation is similar in the three runs, however Run 8 shows higher values. This may be caused by the large abundance of fine sediment in the bed and available to be resuspended, but also to three-dimensional effect, such as mud being transported from nearby areas.

Spatial distribution of sediment concentration (Figure 5.9) indicates however generally higher suspended sediment concentration in most of the model domain for Run 8. This reinforces the assumption that more sediment may be resuspended due to the larger fine sediment availability in a thicker active layer. It is however recommended to verify this hypothesis further.

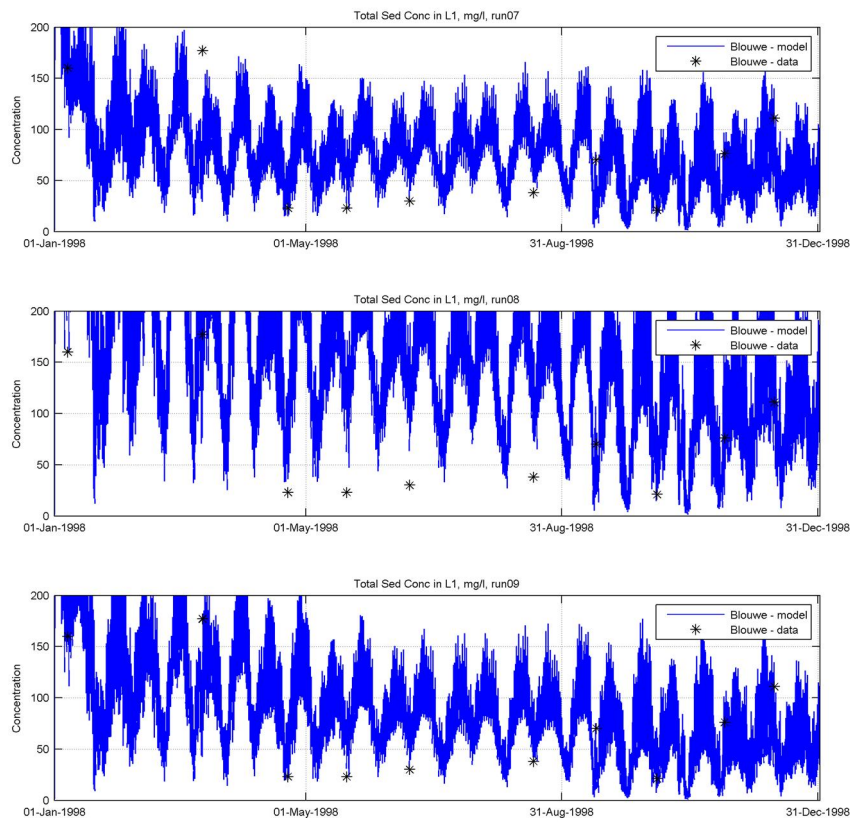


Figure 5.8 SPM time series for the Station Blauwe Slenk for Runs 4 through Run 9. Blue line is model results, black stars are measured data.

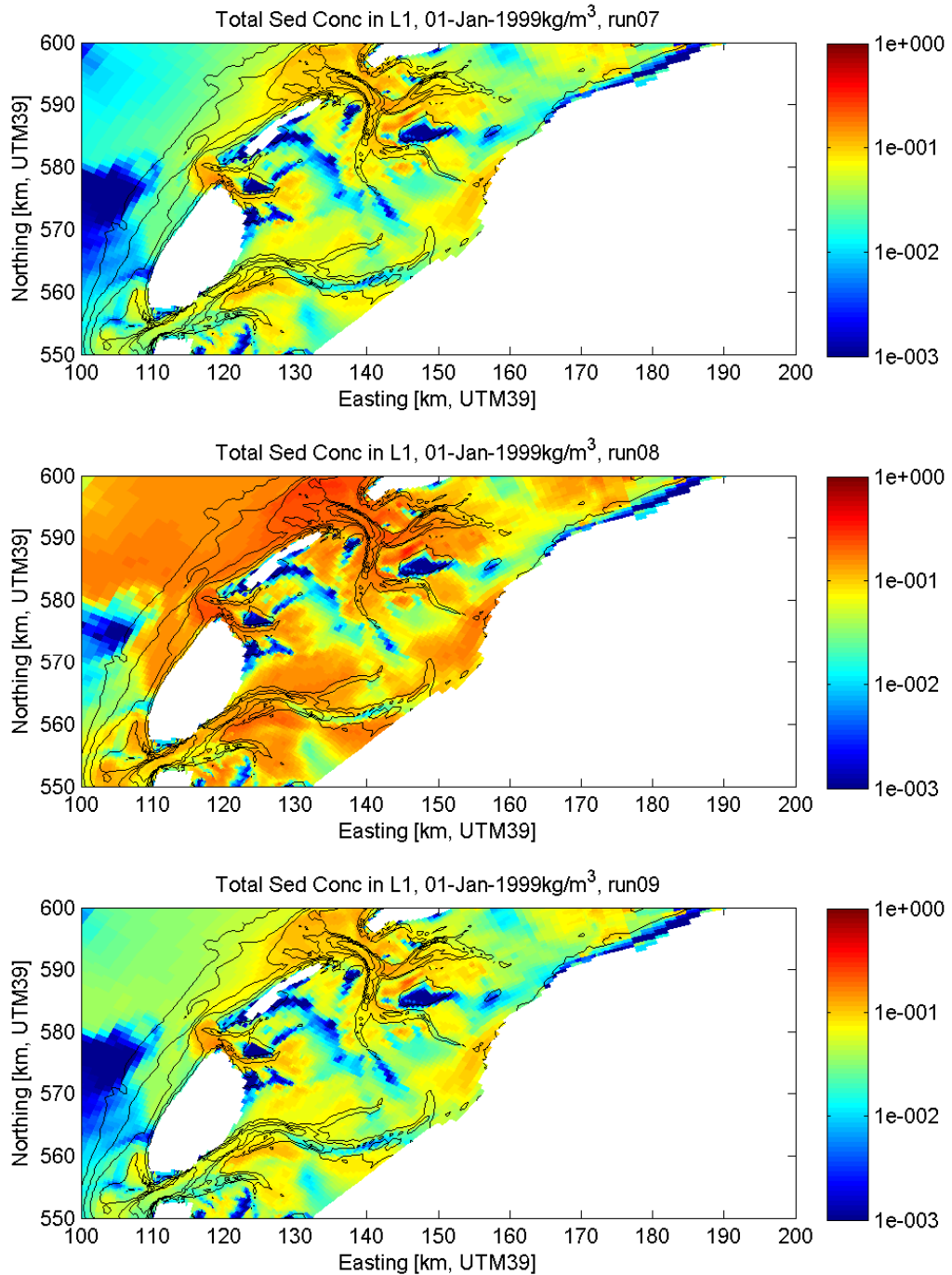


Figure 5.9 Sediment concentration near the water surface for Runs 7 through 9 after 1 year of simulation. The colour scale is logarithmic.

### 5.4.3 Group 3

Group 3 aims at assessing the effect of morphological update on bed composition, and at comparing the effect of including pcr. Runs 9 and 10 do not specify pcr, while pcr of 0.3 is specified in Runs 11 and 12. Pcr indicates the transition between cohesive and non-cohesive regime in the new SM module. When pcr is not specified, then the sand-mud interaction process is turned off. In Runs 10 and 12 the morphological update is turned on, meaning that bed level changes are active in the model. It is common knowledge that bed level change influences the bed sediment composition, especially when this is not in equilibrium.

Figure 5.10 shows the bed composition time series for Runs 9 through 12 for Station Blauwe Slenk. Comparison of Run 9 with Run 10 and Run 11 with Run 12 shows that morphological update has a minor influence on bed composition. However, comparison Run 9 versus Run 11 (or 10 vs. 12) shows a significant contribution of pcr. Being pcr equal to 0.3, and being the mud fraction in the bed at Blauwe Slenk always lower than 20%, here the SM module follows the non-cohesive regime formulation. In this regime, mud is eroded proportionally to the sand. In the standard D3D instead, mud is always eroded following the Partheniades-Krone formulation. Both D3D and SM use the same formulation for sand in the non-cohesive regime. Runs 11 (and 12) shows more mud in the bed with respect to Runs 9 (and 10) meaning that less mud is eroded from the bed with the SM formulation. Being the formulation different, this is not expected in a uniform or 1D model. Assuming that the module works correctly, the most likely explanation for this difference is three-dimensional effects, meaning that mud is entrained from adjacent cells which fall under the cohesive behaviour (see section below on pcr).

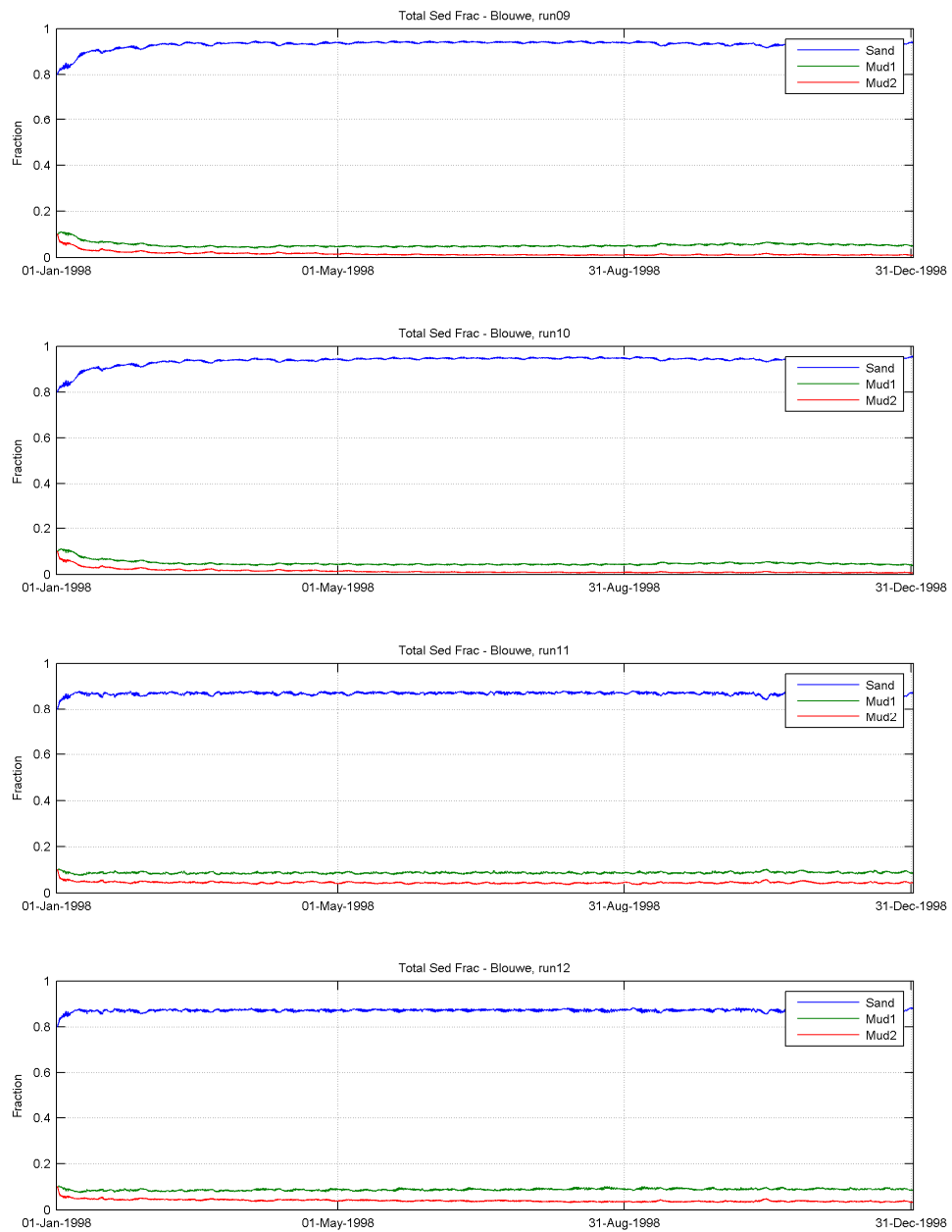


Figure 5.10 Bed composition time series for Station Blauwe Slenk for Runs 9 through 12.

Similarly, SPM values are lower in Run 9 than Run 11 (Figure 5.11). In a 1D closed single cell system, one would expect lower SPM if more mud is retained in the bed. This is not the case in these simulations with open boundaries.

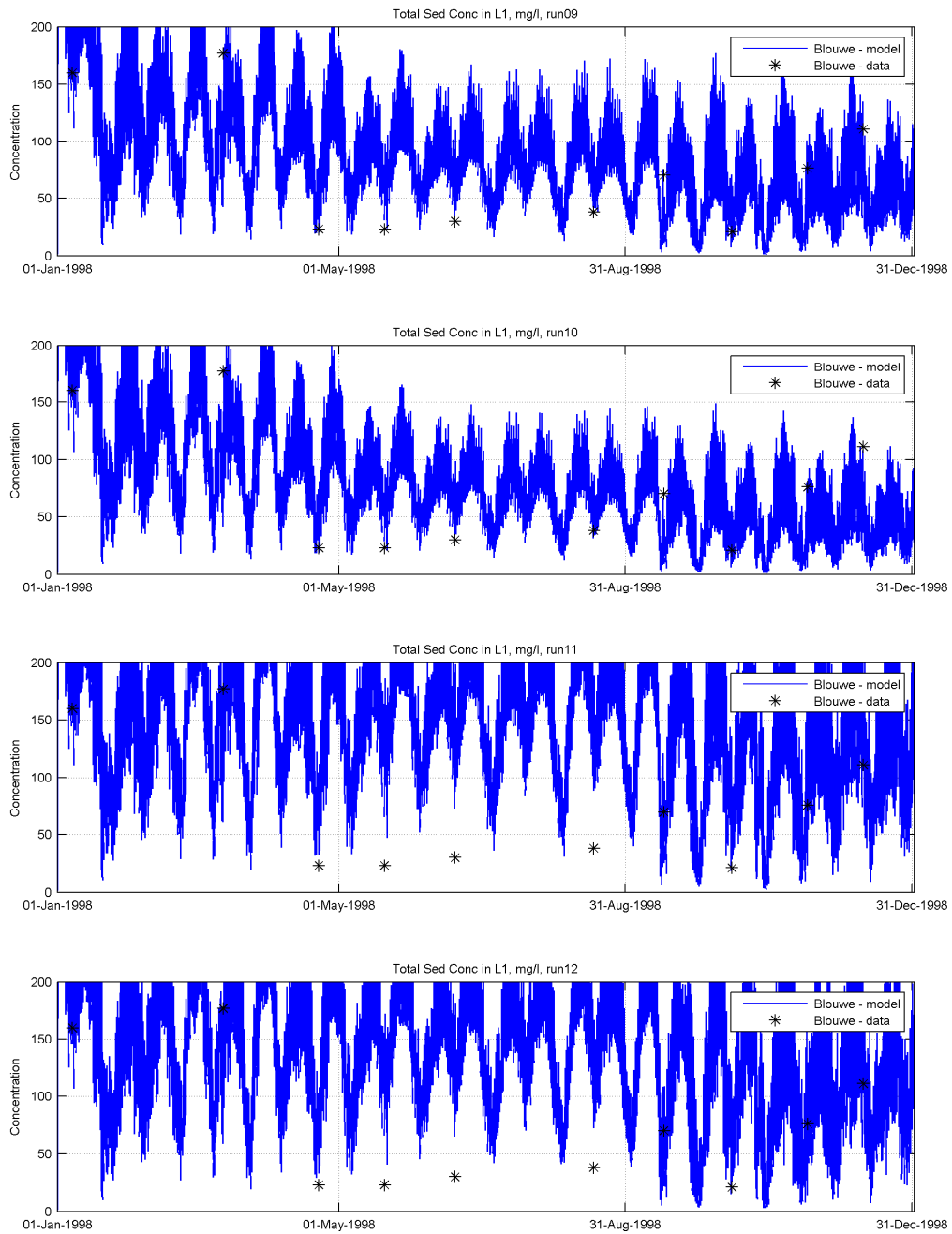


Figure 5.11 SPM time series for the Station Blauwe Slenk for Runs 9 through Run 12. Blue line is model results, black stars are measured data.

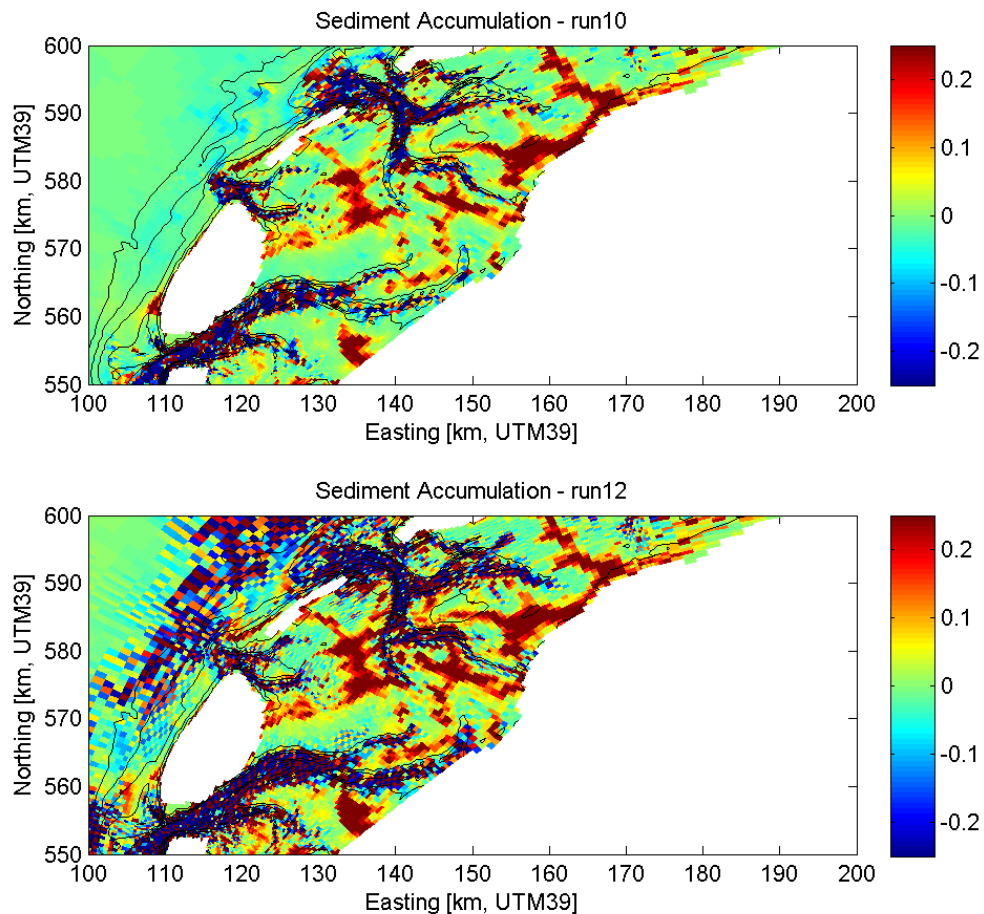


Figure 5.12 Bathymetric change for Run 10 and Run 12. Colorbar is in meters

Bathymetric change (Figure 5.12) shows general results in line with expectations: tendency to deposition in the mud flat areas and tendency of erosion in the channels. Run 12 (SM with pcr) however, shows more pronounced instabilities, especially in the areas of erosion. It is recommended to further investigate this behaviour with specific respect to morphological change.

#### 5.4.4 Group 4

Aim of this group is the functioning and sensitivity of the Fluff Layer. Four runs (13, 14, 15 and 19) are run including the Fluff Layer. The Fluff Layer is a thin layer included between the water column and the seabed, that serves as a (short-term) storage of fine sediments. Cohesive fractions (mud) hosted in the Fluff Layer are easier to resuspend than in the seabed. This layer effectively is responsible for quicker response to SPM variation in the water column, while the underlain seabed is responsible for long-term storage and release of fine sediment.

In Runs 13 through 15 the erosion parameters of the Fluff Layer formulation (Deltares, 2011b) are varied, while in Run 19 the critical shear stress for erosion of the Fluff Layer is changed with respect to Run 13 (Table 5.1). Run 13 is chosen as the reference, and the fluff layers values are taken from previously calibrated Wadden Sea models. It is however to be noted that previous Wadden Sea models were carried out with Delft3D-WAQ, therefore in principle a new calibration is needed.

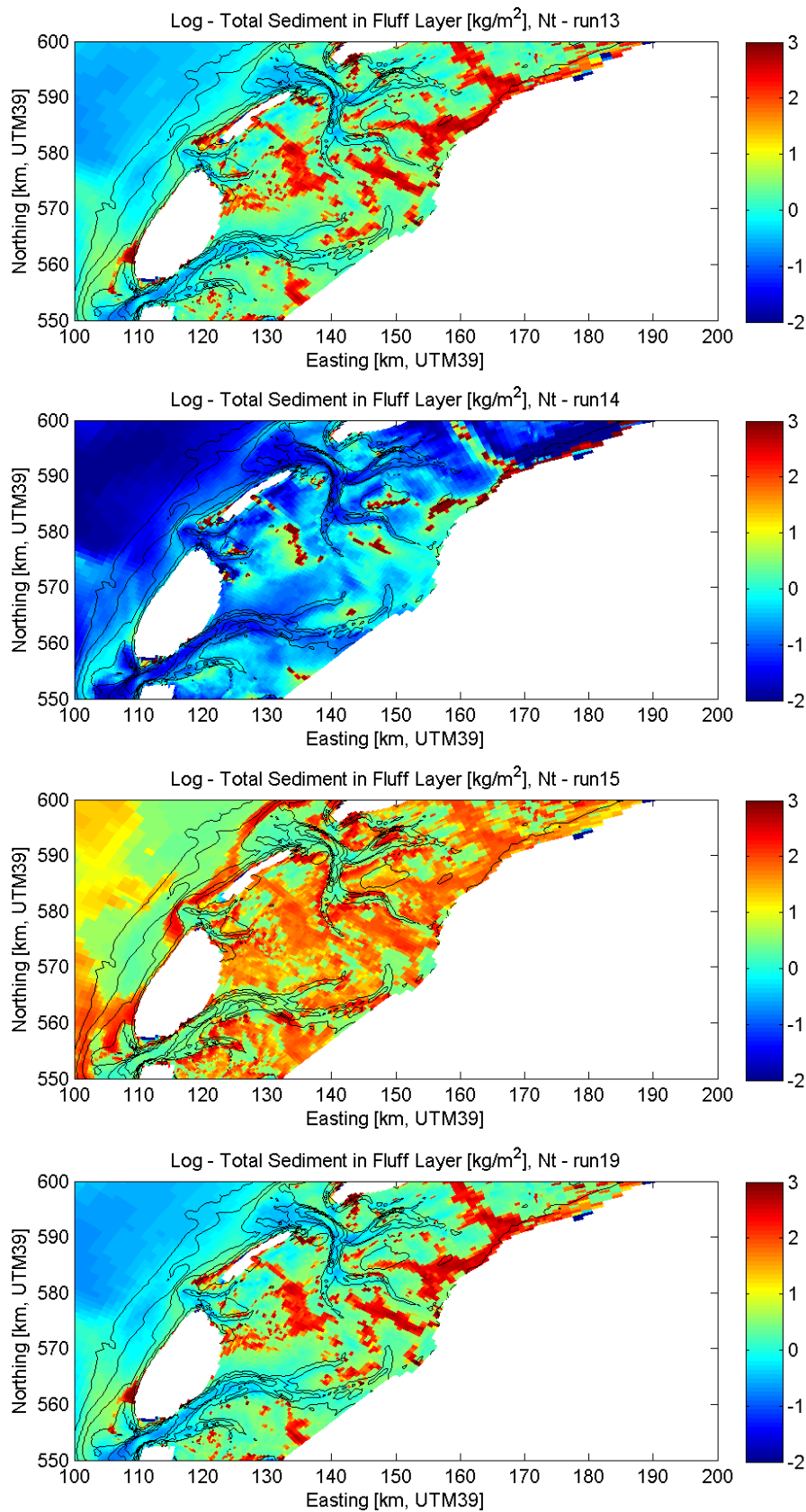


Figure 5.13 Sediment in the Fluff Layer for Runs 13, 14, 15 and 19 at the end of 1 year simulations, in  $\text{kg/m}^2$  and presented in logarithmic scale.

From Figure 5.13 it is evident how change in fluff layer parameters determines quite a difference in sediment mass contained in the Fluff Layer. In general, larger mass of sediment is contained in the Fluff Layer near the flat areas regions, which is expected. Run 14 (smallest erosion parameters) shows the largest spatial variation of mass in the fluff layer. Run 15 (largest erosion parameters) shows the opposite. Consequently, Run 15 shows a general deprivation of mud from the top seabed layer (Figure 5.14).

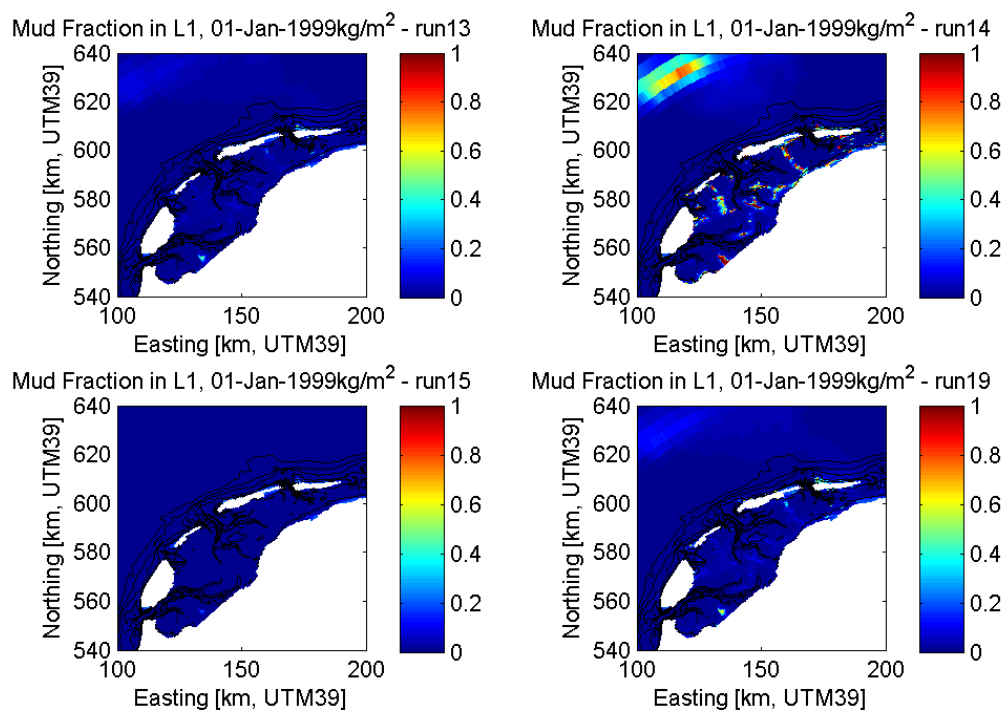


Figure 5.14 Mud fraction in the top layer (Runs 13, 14, 15 and 19) after 1 year of simulation.

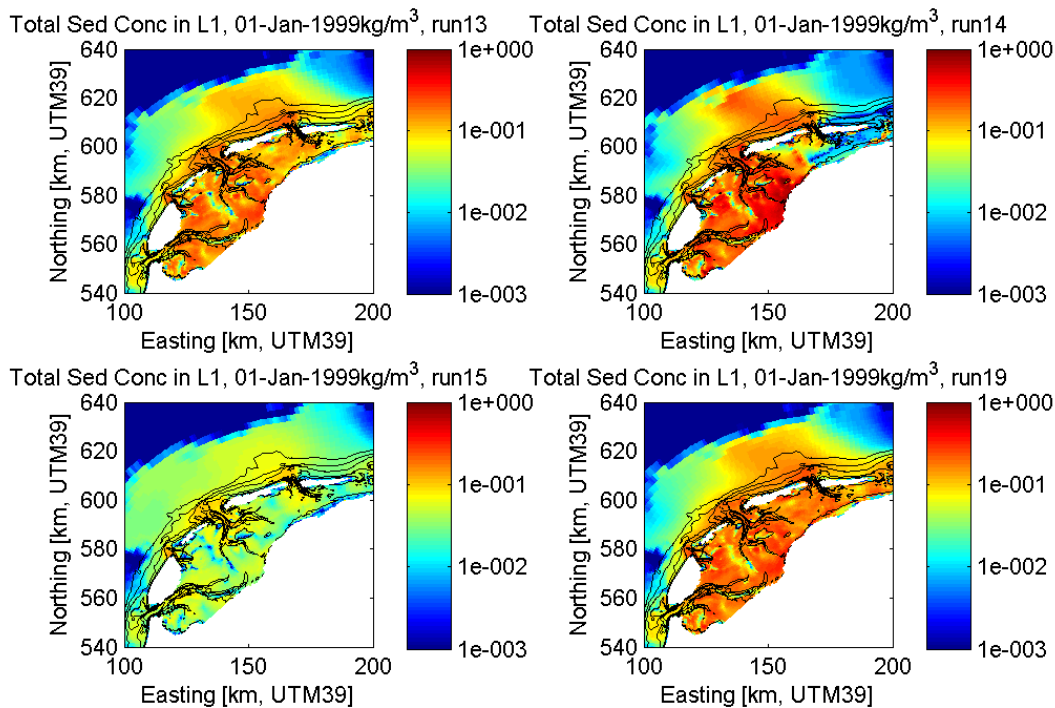


Figure 5.15 Sediment concentration near the water surface for Runs 13, 14, 15 and 19, after 1 year of simulation. The color scale is logarithmic.

Spatial distribution of SPM (Figure 5.15) is consistent with mass in the Fluff Layer and seabed composition: when larger fines mass is trapped in the Fluff Layer (Run 15), less fines are available for the bed (mostly sand indeed, even in the tidal mud flats) and for the water column (lower SPM). Vice versa is valid as well. When a closer look is given Blauwe Slenk Station, (Figure 5.16) Run 15 appears to best match SPM concentration. All other sets of parameters appear to overestimate the SPM concentrations. It is however to be said that this figure focuses on a single point in a tidal channel, therefore definitive conclusion cannot be extrapolated. It appears therefore likely that Fluff Layer runs in general demands for further calibration to best match bed and SPM observations.

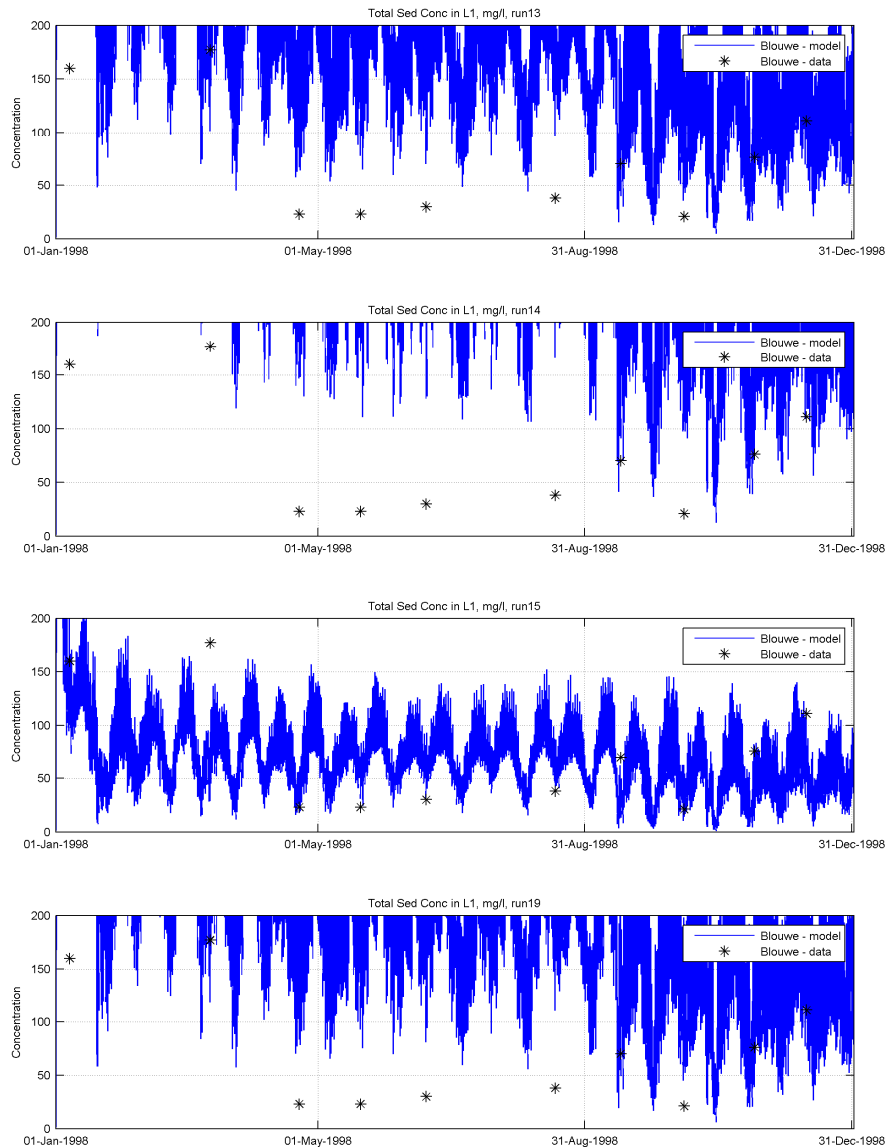


Figure 5.16 SPM time series for the Station Blauwe Slenk for Runs 13 through Run 19. Blue line is model results, black stars are measured data

#### 5.4.5 Group 5

Aim of this group of simulations is to investigate the effect of different pcr. Pcr is the critical mud fraction in the seabed that distinguished cohesive from non-cohesive behaviour. For computational cells with mud fraction in the bed lower than pcr the non-cohesive formulation is used. Where and when mud fractions are higher than pcr than the regime is switched to cohesive. In the SM module, pcr is the parameters that drives this transition. When pcr is not specified, as in the other runs, than the standard D3D formulation is used and sand-mud interaction is not included. The fluff layer is not active in these simulations.

In the new SM formulations,  $pcr$  plays a role only in the cohesive sediment regime. In the non-cohesive sediment regime, the formulations are independent from  $pcr$ . It is therefore expected no change in bed composition or SPM when  $pcr$  is varied within the non-cohesive regime.

In the test simulations, the initial sand fraction is 80% in all scenarios and whole domain, meaning that the mud fraction is of 20%. In all cases, sand fraction at Blauwe Slenk (in a tidal channel) seems to increase immediately after the beginning of the simulations (Figure 5.17), causing the mud fraction to decrease below 20% (or 0.2). This means that at this location all runs but Run 16 are in non-cohesive regime. In a 1D simulations (or in a uniform domain) Runs 11, 17 and 18 are therefore expected to give identical results. In practice as  $pcr$  increases, so does the mud fraction in the seabed. This trend is valid for Run 16 as well. Identical results, but for a near shore muddier location (Figure 5.18) shows a somewhat different trend: all runs with low  $pcr$  tends to become completely muddy within four months, while the larger  $pcr$  run maintains some sand in the seabed. It is likely that this area is mostly depositional, while the Blauwe Slenk Station mostly erosional. It is possible that less (mud) deposition occurred in Run 18 with respect to the other runs. That may explain the lower mud content.

Figure 5.19 shows the mud fraction distribution for a wider area. These figures are in agreement with what highlighted above, especially with respect to the near shore and tidal flat areas. Larger mud fractions in the seabed is observed for all runs with  $pcr$  less than 0.5. These low- $pcr$  runs tends to show very similar mud distribution. Run 18 ( $pcr = 0.5$ ) instead shows major differences. In this case, a larger portion of the domain falls under non-cohesive regime (all seabed cells with mud fraction lower than  $pcr$ ). The areas with large mud distribution are significantly reduced. This may lead to conclude that non-cohesive regime is more effective in resuspending mud.

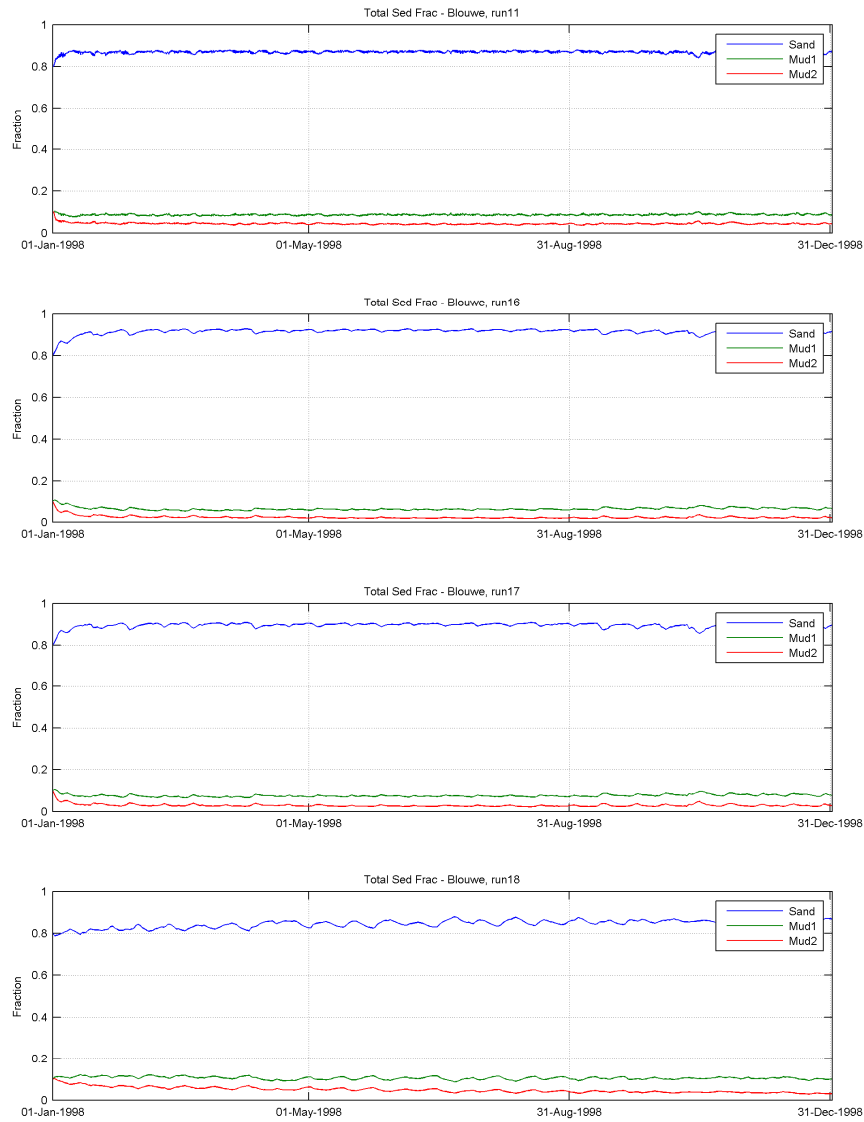


Figure 5.17 Bed composition time series for Station Blauwe Slenk for Runs 11, 16, 17 and 18 ( $p_{cr} = 0.3, 0.1, 0.2$  and  $0.5$  respectively).

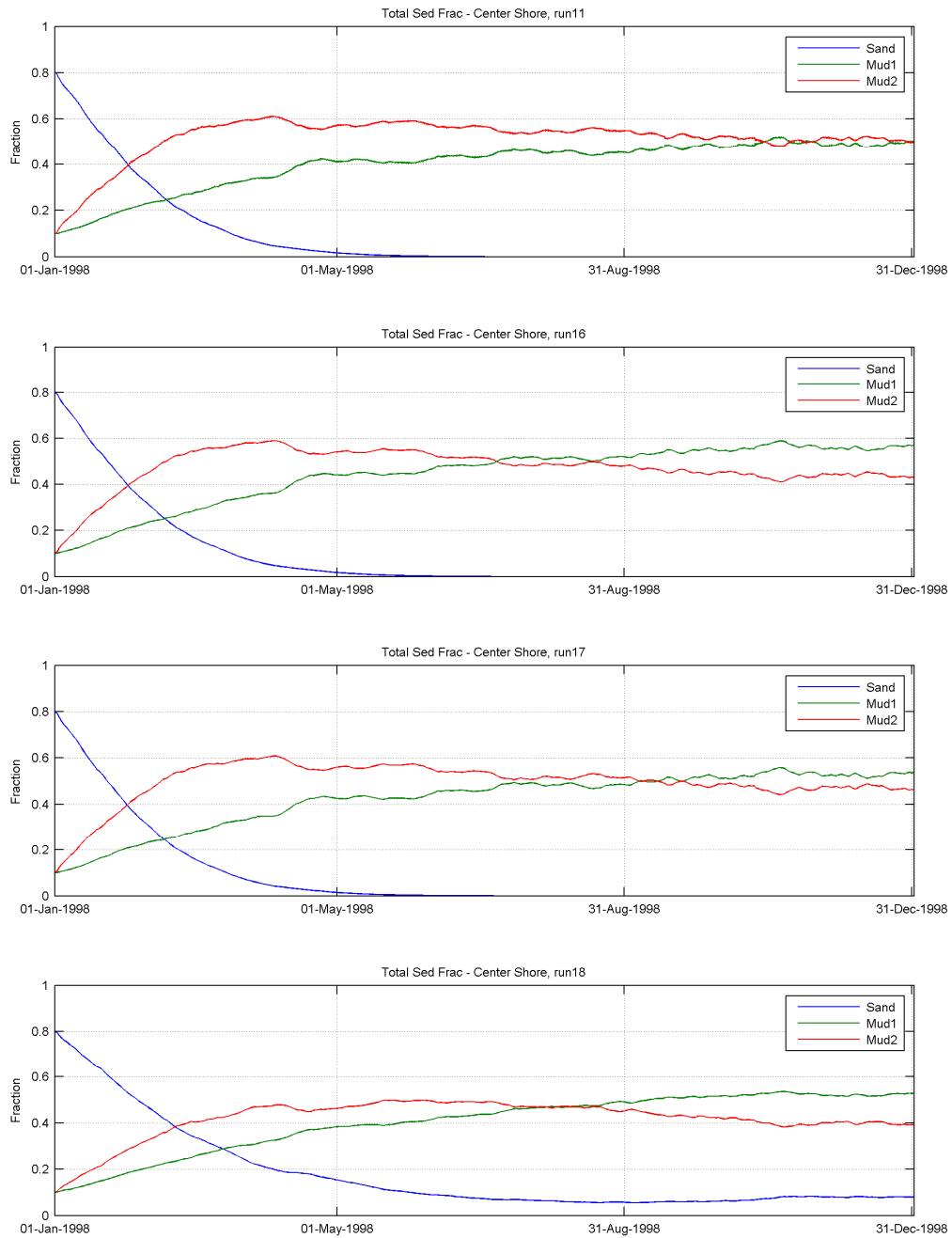


Figure 5.18 Bed composition time series for a Near Shore location (ChSh) for Runs 11, 16, 17 and 18 ( $pcr = 0.3, 0.1, 0.2$  and  $0.5$  respectively).

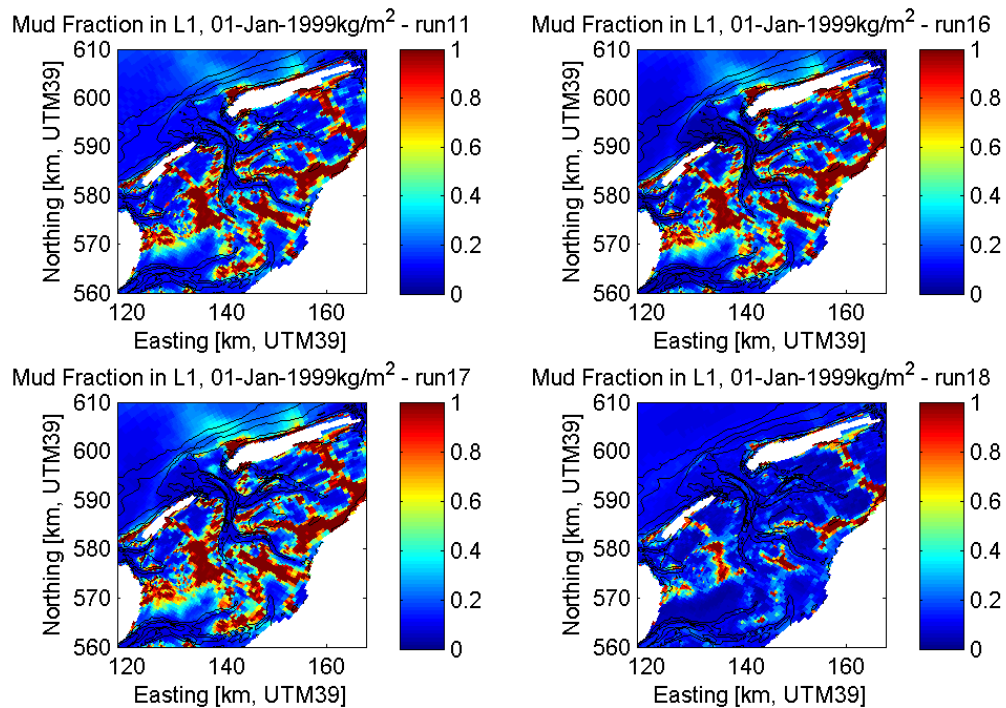


Figure 5.19 Mud fraction in the top layer (Runs 11, 16, 17 and 18,  $pcr = 0.3, 0.1, 0.2$  and  $0.5$  respectively) after 1 year of simulation.

When evaluated with respect to SPM (Figure 5.20) Runs 11, 16 and 17 show similar SPM concentration values and distribution. However, when  $pcr$  is 0.5 (Run 18) the SPM is generally lower throughout the domain, and areas of very low concentrations are observed. This reinforces the observation that larger SPM is, in the medium – long period, related to larger mud availability in the seabed. Run 18 generally shows lower mud availability in the system. This can only be explained with net export of mud from the system during the yearlong simulation.

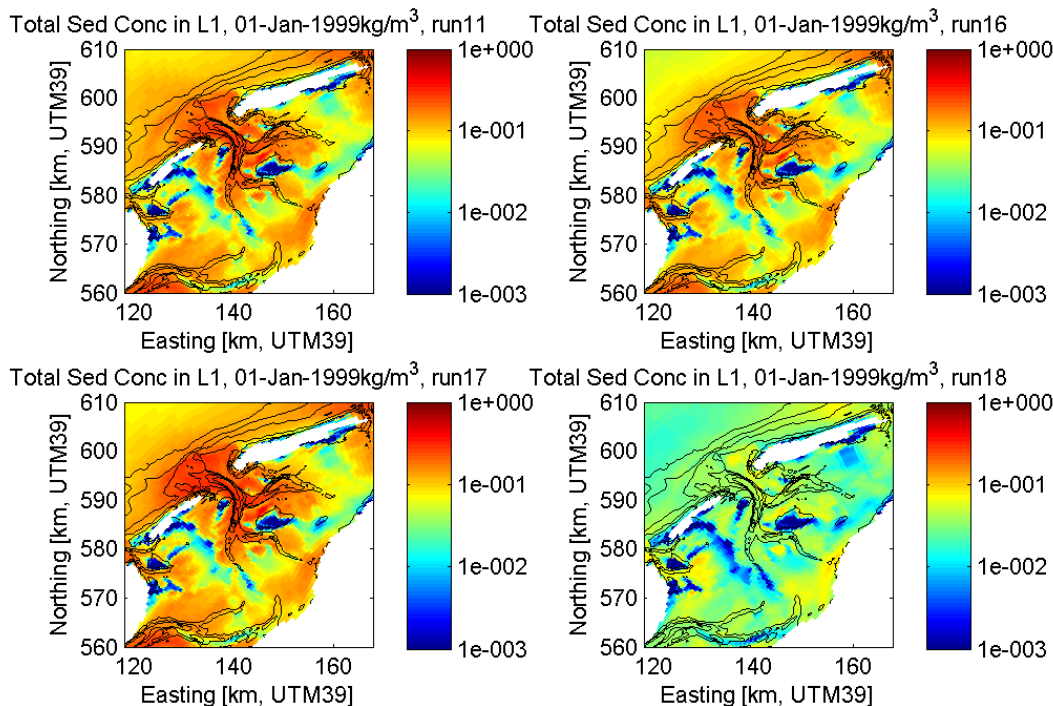


Figure 5.20 Sediment concentration near the water surface for Runs 11, 16, 17 and 18 after 1 year of simulation. The color scale is logarithmic.

Concluding, pcr does influence the bed composition in the seabed. Variation of pcr in the range of 0.1 through 0.3 did not show significantly different results. Instead pcr of 0.5 shows reduction in muddy areas and low SPM. Therefore non-cohesive regime appears to be more effective in resuspending mud, hence, in the long run, decreasing the mud availability in the system.

## 5.5 Conclusions

A sensitivity analysis composed of seventeen simulations were carried out for the Wadden Sea to test the performance of the new SM module and its sensitivity to change in selected parameter settings. Five main settings were tested and divided in five groups aiming at the assessment of:

1. Consistency between SM and D3D;
2. Effect of change in Active Layer Thickness;
3. Effect of Morphology Updating;
4. Behaviour of Fluff Layer; and
5. Effect of changing threshold for cohesive / non-cohesive formulations (critical mud fraction – pcr).

The version of Delft3D that includes the SM module when pcr is not specified appears to reproduce the standard release D3D results. Only minor differences on much smaller order of magnitude with respect to significant outputs are noticeable.

An important parameter to model bed sediment composition, and consequently SPM concentrations is the Active Layer Thickness. As expected the results are very sensitive to this parameters. In general, the thinner the active layer, the quickest the response to hydrodynamic forcing. A 0.5 cm active layer captures variation on the scale of the single tide, while a 5 cm layer captures general seasonal trends. A 50 cm active layer seems not too capture seasonal trends correctly as it carries significant inertial effect given the hydrodynamic conditions of this system. Thicker active layer guarantees larger fines availability for erosion. Larger SPM is simulated in this case. In general the most appropriate active layer thickness depends on the system, and hydrodynamic forcing, and correct assessment demands for bed composition data coupled with SPM recording. All this is not currently available. However, for the Wadden Sea, an Active Layer Thickness of 1 – 5 cm appears appropriate.

Effect of morphological updating was also tested in this study. It appears that its effect is not very significant with respect to other more influential parameters. It is however to be noticed that increase in instabilities were observed when pcr was imposed as input parameter. It is therefore recommended to further investigate the implementation of pcr with respect to morphological update.

The Fluff Layer was also tested in few runs. Initial parameters of the Fluff Layer were derived from the calibrated Delft3D-WAQ previous model. The Fluff Layer appears to be quite sensitive to its parameters, at least in the yearlong run. In general, some (depending on the parameters chosen) mass of fine sediment is trapped in the Fluff Layer. As a consequence, (much) less fine sediment (mud) remains in the seabed. In the simulations run with these arbitrary non-calibrated parameters, too little mud appears to remain in the bed, and possible to high SPM were observed. In general the Fluff Layer seems to work properly, but calibration is recommended to capture the correct behavior of the system.

Finally, the effect of pcr is evaluated . In theoretical terms, pcr is expected not to influence the non-cohesive behavior at locations where the mud fraction in the seabed is lower than pcr itself (non-cohesive conditions). This is not observable directly from these simulations. These simulations indeed include areas of little and large mud fractions (the interested by cohesive and non-cohesive behavior) and open boundaries. Therefore it is difficult to make an exact comparison. However, it is generally observed that when pcr is larger (pcr = 0.5) areas of large mud fraction and SPM in the water column are both reduced. It appears therefore that wider non-cohesive regime tends to deplete mud from the system. It appears that mud is easier resuspended and outputted from the Wadden Sea to the North Sea.

In general it appears that the bed is the long term storage of fine sediment, and drives the behavior of the system both as far as bed composition and SPM. Active Layer Thickness, Fluff Layer and Pcr all influence seabed / water column interaction and are therefore important for correct simulation of the physical process. They are all indeed responsible for bed composition (i.e. fines availability in the bed) and consequently SPM. It also appears that as fines are suspended, they tend to be outputted from the system, as given identical initial conditions, when less mud is found in the bed, then lower SPM concentration are also simulated (after one year of simulation).



## 6 Dissemination

The objective of the present BwN project was not only to develop the sand-mud bed module, but also to promote its application in a wider community. To this end, the following initiatives have been unfolded:

- Invitation and participation of a wider audience of potential users to the progress meetings.
- Collaboration with TU Delft on the development of the module and with NIOZ on its application.
- Organisation of a workshop on June 29, 2012 at Deltares (Delft) for a wider group of potential users. The invitation was distributed within the whole NCK community.
- Application of the bed module in the [PACE](#) project, a scientific programme between The Netherlands and Germany.
- Dissemination of the bed module within the Open Earth community.
- Incorporation as one of the tools in the EDD (Ecodynamic Design manual) on the Ecoshape portal.
- An abstract on water-bed exchange has been submitted the next Battelle conference on sediment remediation, including results from the bed module.

Overall, the following institutes participated in at least one of these initiatives and have first-hand information on the bed module:

Deltares, TU Delft, NIOZ, Boskalis, Van Oord, UNESCO-IHE, Utrecht University, Royal HaskoningDHV, Svasek, Witteveen + Bos, Grontmij, Helmholtz-Centre Geesthacht, Leibniz Institute for Baltic Sea Research, DHI.

The sand-mud bed module will be part of the standard version of Delft3D, thus guaranteeing its future maintenance.



## A References

- Creutzberg, F., and H. Postma (1979). An experimental approach to the distribution of mud in the southern North Sea.--Neth. J. Sea Res. 13 (1): 99-116.
- Delft3D-Flow user manual. Delft, The Netherlands  
(<http://oss.deltares.nl/web/opendelft3d/manuals>)
- Dellapenna, T. M., S. A. Kuehl and L. C. Schaffner (1998). Sea-bed Mixing and Particle Residence Times in Biologically and Physically Dominated Estuarine Systems: a Comparison of Lower Chesapeake Bay and the York River Subestuary. *Estuarine, Coastal and Shelf Science* 46, 777–795
- Dellapenna, T. M., S. A. Kuehl, L. C. Schaffner (2003). Ephemeral deposition, seabed mixing and fine-scale strata formation in the York River estuary, Chesapeake Bay. *Estuarine, Coastal and Shelf Science* 58, p. 621–643
- Deltares (2010). Mud modelling in marine systems. Results 2010. Deltares report 1202283.
- Forster, S., R. N. Glud, J. K. Gundersen and M. Huettel (1999). In situ Study of Bromide Tracer and Oxygen Flux in Coastal Sediments. *Estuarine, Coastal and Shelf Science* 49, p. 813–827.
- Galappatti, R., 1983. A depth integrated model for suspended transport. Tech. rep., Delft University of Technology, Delft, The Netherlands.
- Gibbes, B., C. Robinson, H. Carey, L. Li, D. Lockington (2008a). Tidally driven pore water exchange in offshore intertidal sandbanks: Part I. Field measurements. *Est. Coast. Shelf Science* 79, p. 121-132
- Gibbes, B., C. Robinson, L. Li, D. Lockington, H. Li (2008b). Tidally driven pore water exchange in offshore intertidal sandbanks: Part II. Numerical simulations. *Est. Coast. Shelf Science* 80, p. 472-482.
- Harris, C.K. and P.L. Wiberg (1996). Approaches to quantifying long-term continental shelf sediment transport with an example from the Northern California STRESS mid-shelf site. *Cont. Shelf Res.*, Vol 17, No 11, pp 1389-1418.
- Heberta, A. B., F. J. Sansone, G. R. Pawlak (2007). Tracer dispersal in sandy sediment porewater under enhanced physical forcing. *Continental Shelf Research* 27 2278–2287.
- Houwing, E.J. (1999). Determination of the critical erosion threshold of cohesive sediments on intertidal mudflats along the Dutch Wadden Sea coast. *Estuar. Coast. Shelf Sci.* 49, 545–555.
- Huettel, M. and Webster, I. T. (2001). Porewater flow in permeable sediment. In Boudreau, B. P., and B.B. Jorgensen (eds): *The benthic boundary layer*. Oxford University Press, New York, p. 144-179.
- Huettel, M., and Gust (1992). Impact of bioroughness on interfacial solute exchange in permeable sediments. *Marine Ecology Progress Series* vol 89, p. 253-267.
- Huettel, M., W. Ziebis, and S. Forster (1996). Flow-induced uptake of particulate matter in permeable sediments. *Limnol. Oceanogr.*, 41(2), p. 309-322
- Huettel, M., W. Ziebis, S. Forster, and G. W. Luther (1998). Advective transport affecting metal and nutrient distributions and interfacial fluxes in permeable sediments. *Geochimica et Cosmochimica Acta*, Vol. 62, No. 4, pp. 613–631.
- Jacobs, W., W.G.M. van Kesteren and J.C. Winterwerp (2005). Strength of sediment mixtures as a function of sand content and clay mineralogy. INTERCOH.
- Jacobs, Walter (2006). Eco-morphology of estuaries and tidal lagoons: literature review and experiments on sand-mud mixtures, TU-report No. 1-06.
- Kleinmans M.G., O. Montfort, P.J.T. Dankers, L.C. van Rijn, W. Bonne (2005). Mud dynamics on the shoreface and upper shelf, Noordwijk, the Netherlands. In L.C. van Rijn, R.L. Soulsby, P. Hoekstra, and A.G. Davies: *Sandpit, sand transport and morphology of offshore mining pits*. Aqua Publications, the Netherlands, p. Z.1-Z.15.

- Krishnappan, B.G. and P. Engel (2006). Entrapment of fines in coarse sediment beds. Proc. River Flows 2006. Feirreira, Alves, Leal and Cardoso (Eds). Taylor and Francis Group London, ISBN 0-415-40815-6. pp. 817–824.
- Laane, R.W.P.M., H.L.A. Sonneveldt, A.J. Van der Weyden, J.P.G. Loch, G. Groeneveld (1999). Trends in the spatial and temporal distribution of metals (Cd, Cu, Zn and Pb) and organic compounds (PCBs and PAHs) in Dutch coastal zone sediments from 1981 to 1996: a model case study for Cd and PCBs. *Journal of Sea Research* 41, p. 1–17
- Lee, H II and R. C. Swartz (1980). Biological processes affecting the distribution of pollutants in marine sediments, part II: Biodeposition and Bioturbation. In: Baker, R.A. (ed): Contaminants and sediments Vol. 2: analysis, chemistry and biology. Ann Harbor Science Publishers Inc., Michigan, U.S.
- Marinelli, R.L., R. A. Jahnke, D. B. Craven, J. R. Nelson, and J. E. Eckman (1998). Sediment nutrient dynamics on the South Atlantic Bight continental shelf. *Limnol. Oceanogr.* 45 (3), p. 550-557.
- Mastbergen, D.R. and van den Berg, J.H. (2003) Breaching in fine sands and the generation of sustained turbidity currents in submarine canyons. *Sedimentology* 50, 625–637.
- Mitchell, J.K. (1976). *Fundamentals of Soil Behaviour*. University of California, Wiley, Berkeley.
- Mitchener, H. and Torfs, H. (1996). Erosion of sand – mud mixtures. *Coastal Eng.* 29, 1–25.
- Paarlberg, A.J., M.A.F. Knaapen, M.B. de Vries, S.J.M.H. Hulscher, Z.B. Wang. Biological influences on morphology and bed composition of an intertidal flat. *Estuarine, Coastal and Shelf Science* 64, p. 577-590
- Panagiotopoulos, I., Voulgaris, I.G. and Collins, M.B. (1997). The influence of clay on the threshold of movement on fine sandy beds. *Coastal Eng.* 32, 19–43.
- Precht, E., Huettel, M. (2004). Rapid wave-driven advective pore water exchange in a permeable coastal sediment. *Journal of Sea Research* 51, 93–107.
- Prooijen, B. van, T. van Kessel, M. van Ledden (2007). Modelling of fine sediment in a sandy environment – the coastal zone of the Netherlands, submitted to: IAHR 2007 Conference.
- Prooijen, B., J.C. Winterwerp, A stochastic formulation for erosion of cohesive sediments, submitted to *Journal of Geophysical Research*.
- Raudviki, A.J. (1990) *Loose Boundary Hydraulics*, 3rd edn. Pergamon Press, Oxford.
- Reimers, C. E. H. A. Stecher, G. L. Taghon, C. M. Fuller, M. Huettel, A. Rusch, N. Ryckelynck, C. Wild (2004). In situ measurements of advective solute transport in permeable shelf sands. *Continental Shelf Research* 24 p. 183–201.
- Riedl, R. J., N. Huang, and R. Machan (1972). The subtidal pump: a mechanism of interstitial water exchange by wave action. *Marine Biology* 13, p. 210 – 221.
- Rijn, L. C. van, 1984a. Sediment transport, Part II: suspended load transport." *Journal of Hydraulic Engineering* 110 (11): 1613{1640. 339, 362
- Rusch, A., M. Huettel and S. Forster (2000). Particulate Organic Matter in Permeable Marine Sands—Dynamics in Time and Depth. *Estuarine, Coastal and Shelf Science* 51, p. 399–414.
- Rutgers van der Loeff (1981). Wave effects on sediment water exchange in a submerged sand bed. *Netherlands journal of sea research* 15 (1): 100-112.
- Rutgers van der Loeff, M. M. (1980). Nutrients in the interstitial waters of the Southern bight of the North Sea. *Netherlands journal of sea research* 14 (2), p. 144-171.
- Sanford, L. P. (2008). Modeling a dynamically varying mixed sediment bed with erosion, deposition, bioturbation, consolidation, and armoring. *Computers & Geosciences* 34, p. 1263–1283
- Scheel, F. (2012). Simulating and classifying large-scale spatial sand-mud segregation using a process-based model for a tidal inlet system. A process-based assessment on the relation between different forcing conditions and large-scale spatial sand-mud segregation. MSc-thesis Delft University of Technology. (<http://repository.tudelft.nl>)
- Suijlen, J.M. and Duin, R.N.M. (2001). Variability of near-surface total suspended matter concentrations in the Dutch coastal zone of the North Sea. *Climatological study on the*

- suspended matter concentrations in Dutch coastal zone of the North Sea. Climatological study on the suspended matter concentrations in the North Sea. Report RIKZ/OS/2001.150X.
- Thibodeaux, L. J. and J. D. Boyle (1987). Bedform-generated convective transport in bottom sediment. *Nature*, Vol. 325, p. 341-343.
- Torfs, H. (1995). Erosion of mud/sand mixtures. PhD thesis, Katholieke Universiteit Leuven, Leuven.
- Turner, I.L., and G. Masselink (1998). Swash infiltration-exfiltration and sediment transport. *J. Geoph. Res.*, Vol 103 (C13),p. 30.813–30.824
- van Heteren, S., P. Kiden, and J.M.M. Hettelaar (2007). Inventarisatie slibgehalte Noordzeebodem tussen Cadzand en Den Helder. TNO-rapport 2007-U-R0584/C
- van Kessel, T. (2002). Modelling of sand-mud mixtures. Steps towards implementation into standard version Delft3D, Report Z2840, WL | Delft Hydraulics.
- van Kessel, T., J. C. Winterwerp, B. van Prooijen, M. van Ledden, and W. Borst (subm.). Modelling the seasonal dynamics of SPM with a simple algorithm for the buffering of fines in a sandy bed. submitted to *Cont. Shelf Res.*
- van Ledden, M. (2003). Sand-mud segregation in estuaries and tidal basins. PhD thesis, Delft University of Technology, 221 p.
- van Ledden, M., van Kesteren, W.G.M. and Winterwerp, J.C. (2004) A conceptual framework for the erosion behaviour of sand-mud mixtures. *Cont. Shelf Res.* 24, 1–11.
- Van Rijn, L. C. (1984). Sediment transport, Part II: suspended load transport." *Journal of Hydraulic Engineering* 110 (11): 1613{1640. 339, 362
- van Rijn, L. C. (2007). Unified view of sediment transport by currents and waves, Part I, II, III and IV, *Journal of Hydraulic Engineering, ASCE*, Vol. 133, No. 6 and 7.
- Webster, I. T. (2003). Wave Enhancement of Diffusivities within surficial sediments. *Environmental fluid mechanics* 3, p. 269-288.
- Wilson, A.M., M. Huettel, S. Klein (2008). Grain size and depositional environment as predictors of permeability in coastal marine sands. *Estuarine, Coastal and Shelf Science* 80, p. 193–199.
- Winterwerp, J.C., van Kesteren W. (2004). Introduction to the physics of cohesive sediment in the marine environment. *Developments in Sedimentology* 56, Elsevier, Amsterdam.



## **B Considerations on a generic water-bed exchange module**

---

# Considerations on a generic water-bed exchange module

---

Bram van Prooijen, B.C.vanProoijen@TUDelft.nl

DRAFT June 22, 2012

## 1 INTRODUCTION

We describe and discuss a general bed exchange module. General implies that there are several options in numerical sense (framework, time-integration, ...) and in physical sense (erosion formulations, deposition, mixing, ...). General also implies that it can be used for different systems (e.g. rivers with gravel and sand, estuaries with sand and mud, or coastal systems). Furthermore, general implies that the module can be coupled to different model systems (1D, 2D and 3D flow/wave models). Finally, general implies that the software is freely available under GNU-GPL license ([www.gnu.org/licenses/gpl.html](http://www.gnu.org/licenses/gpl.html)). At present several packages already exist that can cope with multiple sediment fractions and different bed layers: ROMS (Warner et al. [2008]) Delft3D (Deltares), or MIKE (DHI). Furthermore, stand-alone bed-modules are developed, e.g. Harris and Wiberg [2001], SEDTRANS (Li and Amos [2001], and Neumeier et al. [2008]), Sanford [2008], Armanini [1995]. Although these modules have many things in common, they are all different: some modules have a Lagrangian framework, others an Eulerian one; some are developed for mixtures of sand/mud, others for gravel/sand; some account for only two fractions (resulting with continuity in only one fraction to be resolved), others for multiple fractions; some consider biological mixing, others neglect this; some allow consolidation, others not. In this memo, we consider several choices and show the benefits and drawbacks of the choices made. The module is build such that many choices can still be made.

### 1.1 FRAMEWORK

Aggradation and degradation can be treated in a Lagrangian framework or in an Eulerian framework, see Figure 1.1. In the Lagrangian framework, the thickness of the layers is

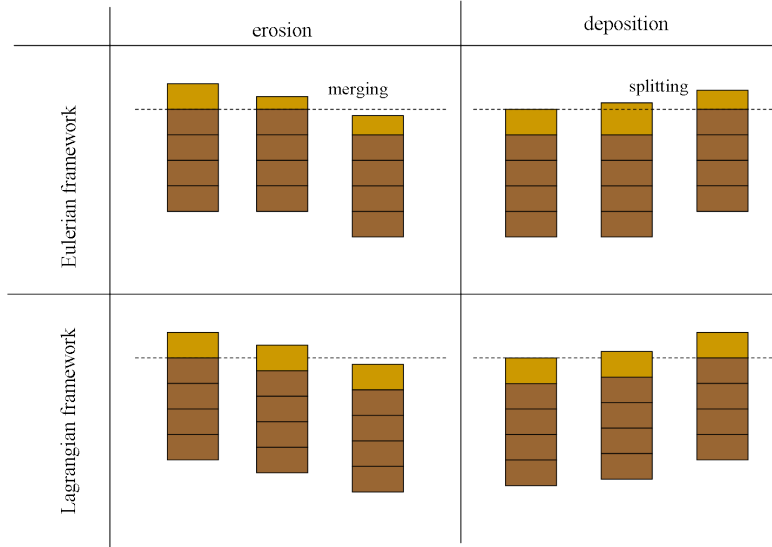


Figure 1.1: Sketch of the change of grid for aggradation and degradation for the Eulerian and Lagrangian framework.

constant and the set of layers moves with the aggradation/degradation by means of an artificial advection velocity, see Van Ledden et al. [2004]. The advantage of this method is that the grid itself does not change. This means that the thicknesses of the cells can vary over the depth. In many cases it is desirable to have a high resolution near the bed surface and a coarser resolution at a larger depth. The drawback is that, depending on the numerical scheme, the movement of the grid results in artificial diffusion between the layers. Stratification will then be smoothed. This can partly be encountered by applying a sophisticated numerical scheme in space.

In the Eulerian framework, the position of the layers is kept constant. Such an approach is for example followed in Warner et al. [2008] and Sanford [2008]. The aggradation/degradation is accounted for by changing the thickness of the top layer. In case the top layer becomes too thick due to deposition, it will be split. In case the thickness tends to zero due to erosion, the layer is merged with the second layer.

The drawback of the Eulerian framework is that the top layer has no fixed thickness. As this thickness has a significant effect on the time scales of the system, it is desirable to have a top layer with a constant thickness, or a even multiple top layers with constant thickness. This implies a combination of the Eulerian and the Lagrangian framework. In this paper we propose a mixed framework that in its limits results on the one hand in a fully Lagrangian framework and on the other hand in a fully Eulerian framework.

## 1.2 SEDIMENT TRANSPORT FORMULATIONS

Sediment transport is generally subdivided into bed load transport and suspended load transport (see Einstein [1950] or Van Rijn [1993]). Although it is difficult to make this

distinction properly in real flows, it is generally done for numerical simulations. The mass balance in the top layer of the bed is:

$$\frac{\partial m_{n,k=1/2}}{\partial t} = D - E + q_{in} - q_{out} + F_2 \quad (1.1)$$

with  $m_n$  the mass of sediment fraction  $n$  in the top layer ( $k = 1/2$ ), deposition rate  $D$  depending on the sediment concentration of fraction  $n$  in the water  $c_n$ , erosion rate  $E_n$ , depending on bed shear stress  $\tau$ , bed load transport  $q$  and  $F_{f2}$  representing the exchange with the second layer, through face 2 (f2).

The distinction between bed load and suspended load has significant consequences for the numerical implementation of the water-bed exchange. In case of suspended load transport, the flux between water and bed is fully defined in a single grid cell, whereas in case of bed load transport, the flux between water and bed also depends on adjacent cells.

Many bed load transport formulations ( $q$ ) exist for non-cohesive sediments, see García [2006] for a recent and extensive overview. Erosion rates for suspended load of non-cohesive sediments are often based on the determination of a near-bed concentration, see Garcia and Parker [1991] for a comparison of formulations for this concentration. Most of the formulations relate the near-bed concentration to the bed shear stress, the critical bed shear stress and the grain diameter. More difficulties arise in case the sediment particles interact. This can be caused by either cohesive forces in case of clay particles or by hiding/exposure effects. Erosion rates for cohesive sediments are generally of the form  $E = M(\tau_b - \tau_c)^r$ , with  $r = 1$  and empirical parameters  $M$  and  $\tau_c$ . Hiding and exposure requires the interaction between different fractions. Here interaction can take place between bed load transport and suspended transport. Bigger particles can be transported as bed load, and smaller particles are then winnowed as suspended load.

## 2 MODEL SET-UP: 1DV BED MODULE

As mentioned in the introduction, two frameworks can be adopted. In this section we show that the same code can be used for both frameworks. We start with the Eulerian framework with a variable top layer thickness, continue with an Eulerian framework with a constant top layer thickness and a variable thickness for the second layer and conclude with multiple layers with constant thickness. If all layers have a constant layer thickness, the Lagrangian framework is obtained. We only consider water-bed fluxes in a single cell, i.e. suspended sediment transport. In case of bed load transport, processes in the neighboring cells have to be taken into account. This is not elaborated here yet.

### 2.1 FRAMEWORK: EULERIAN AND/OR LAGRANGIAN

The bed is subdivided in a finite number of layers ( $N_{lay}$ ) and each layer contains a finite number of fractions ( $N_{frac}$ ). Only the top layer thickness increases due to aggradation and decreases due to degradation. Note that the lower layers ( $2:N_{lay}$ ) do not change directly. The number of layers has then no influence on the computation time. They

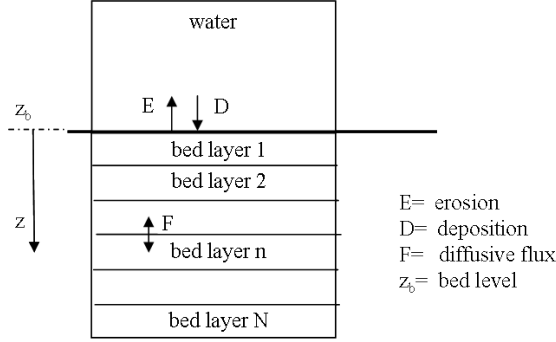


Figure 2.1: Sketch of the framework framework with definitions of fluxes and indices.

only become important in case of erosion, and later on in case of mixing (bioturbation or migration of bedforms).

The mass of the sediment per fraction and per layer, defined by  $M_{i,j}$ , is the principle variable with index  $i$  referring to the layer and index  $j$  referring to the fraction. Help variables are the layer thickness  $\Delta_i$  and the mass fraction  $p_{i,j}$ :

$$\Delta_i = \frac{1}{\rho_s \phi_s} \sum_{j=1}^{N_{frac}} M_{i,j} \quad (2.1)$$

$$p_{i,j} = \frac{M_{i,j}}{\sum_{j=1}^{N_{frac}} M_{i,j}} \quad (2.2)$$

with  $\phi_s$  the solid volume fraction. The solid volume fraction is kept constant, but may later on be coupled to a consolidation model.

The sediment balance equation of the top layer reads:

$$\frac{\partial M_{1,j}}{\partial t} = D_j - p_{1,j} E_j + q_{j,in} - q_{j,out} + F_{f2} \quad (2.3)$$

In case of continuous degradation, the top layer might fully erode. To prevent negative mass in the top layer, the top layer can be merged with the second layer. On the other hand, in case of continuous aggradation, the top layer can be split to prevent the top layer to be too thick. These aspects will be discussed in Section 2.4. The bed level change is then defined by:

$$\frac{\partial z}{\partial t} = \frac{1}{\rho_s \phi_s} \sum_{j=1}^{j=N_{frac}} [D_j - p_{1,j} E_j + q_{j,in} - q_{j,out}] \quad (2.4)$$

In many cases, it is desirable to have a constant top layer thickness. In general, the top layer will be defined much thinner than the lower layers. The above set of equations

will then be slightly different as the second layer will vary in thickness. The top layer moves with a celerity  $\frac{\partial z}{\partial t}$  downwards. The equation for the top layer becomes in case of a constant thickness:

$$\frac{\partial M_{1,j}}{\partial t} = -p_{f2,j} \sum_{j=1}^{j=N_{frac}} [D_j - p_{1,j}E_j + q_{j,in} - q_{j,out}] + D_j - p_{1,j}E_j + q_{j,in} - q_{j,out} \quad (2.5)$$

with the subscript  $p_{f2,j}$  referring to the mass fraction at the interface between the first and the second layer. As the thickness of the top layer is constant, the second layer is variable. The sediment balance equation for the second layer becomes:

$$\frac{\partial M_{2,j}}{\partial t} = p_{f2,j} \sum_{j=1}^{j=N_{frac}} [D_j - p_{1,j}E_j + q_{j,in} - q_{j,out}] \quad (2.6)$$

The system can be extended to multiple constant top layers. If all layers have a constant thickness, a Lagrangian framework is obtained. The equation for the top layer is equal to Eq. 2.5. The sediment balance for the lower layers with constant thickness read:

$$\frac{\partial M_{i,j}}{\partial t} = \frac{\partial p_{i,j}}{\partial z} \sum_{j=1}^{j=N_{frac}} [D_j - p_{1,j}E_j + q_{j,in} - q_{j,out}] \quad (2.7)$$

The sediment balance in the variable layer is given by:

$$\frac{\partial M_{iv,j}}{\partial t} = p_{fv,j} \sum_{j=1}^{j=N_{frac}} [D_j - p_{1,j}E_j + q_{j,in} - q_{j,out}] \quad (2.8)$$

with  $iv$  the the index of the variable layer. By the choice of  $iv$ , the type of framework is set.  $iv = 1$  gives the Eulerian framework and  $iv = N_{lay}$  gives the Lagrangian framework.

## 2.2 SPATIAL DISCRETIZATION

It is expected that the sediment distribution in the active layer can differ significantly from the lower layer. For example winnowing plays a role. The mass fraction at the interface between the top layer and the second layer can therefore best be discretized by the first-order upwind scheme as described above.

In case of multiple layers with constant thickness, the first order upwind scheme will result in numerical diffusion. In case of stratification, the bed will be mixed due to the up and down movement of the grid. A higher order scheme might be desirable. Note that Van Ledden [2003] used a central difference scheme in combination with the  $\theta$ -method for time-stepping. This is only possible in case of two fractions, as only one fraction has to be resolved in combination with mass conservation.

### 2.3 TIME-STEPPING

The mass balance equations for the sediment in the bed and for the sediment in the water column form a coupled set of equations. In general, the mass in the bed layer is much larger than the mass in the water column. The time scale of changes in the bed is therefore much larger as well. The equation can therefore be solved in a decoupled way. The decoupling of the equations makes implicit time stepping complicated. Furthermore, the balance equations for the bed cannot be solved implicitly for more than two fractions. It is desirable to solve the deposition term in the transport equation in an implicit way as instabilities will otherwise occur, especially for very shallow water. This would imply that the transport equation has to be solved first. On the other hand it is desirable to resolve the bed balance equations first as erosion can be limited by the availability of sediment.

The erosion rate is restricted by the availability of sediment in the top layer and is then determined by:

$$p_{1,j}E_j = \text{MIN} \left( p_{1,j}E_j - \gamma D_j + q_{j,out} - \gamma q_{j,in}, \frac{M_{1,j}}{\Delta t} \right) \quad (2.9)$$

with  $\gamma$  a coefficient between 0 and 1. Often,  $\gamma = 0$  is assumed, see e.g. Warner et al. [2008]. For some situations, close to equilibrium, this would be too restrictive. As at this stage, the deposition term is not known, the explicit deposition term could be used to restrict the erosion rate.

The erosion rate is included in the transport equation, where the deposition term is treated in an implicit way, using the  $\theta$ -method. The resulting implicit deposition term is included in the mass balance equations for the bed:

$$\frac{S_{1,j}^{n+1} - S_{1,j}^n}{\Delta t} = -p_{3/2,j}^n \sum_{j=1}^{j=N_{frac}} \left[ D_j^{n+\theta} - p_{1,j}^n E_j \right] + D_j^{n+\theta} - p_{1,j}^n E_j \quad (2.10)$$

$$\frac{S_{i,j}^{n+1} - S_{i,j}^n}{\Delta t} = \Delta_i \frac{\partial p_{i,j}^n}{\partial z} \sum_{j=1}^{j=N_{frac}} \left[ D_j^{n+\theta} - p_{1,j}^n E_j \right] \quad (2.11)$$

$$\frac{S_{iv,j}^{n+1} - S_{iv,j}^n}{\Delta t} = p_{iv-1/2,j}^n \sum_{j=1}^{j=N_{frac}} \left[ D_j^{n+\theta} - p_{1,j}^n E_j \right] \quad (2.12)$$

### 2.4 TREATMENT OF SPLITTING AND MERGING OF THE BED CELLS

In case of degradation, the thickness of the variable layer decreases and might become negative. To circumvent a negative layer thickness, the variable layer is merged with the lower layer when a certain thickness is reached, e.g. 10% of the original thickness. The old lower layer becomes variable layer and all underlying layers move one layer upwards. A similar procedure is followed for continuous aggradation. Then, the variable layer is split and all underlying layers move one layer downwards. To keep the same number of layers, a layer is added at the bottom in case of degradation and removed in case

of aggradation. There are different ways to deal with the lower layer: (1) The lower layer is split or merged with the layer above; (2) a new layer is added or the lower layer is removed. We prefer the second option as for the first option a deformed grid is generated in case of severe erosion. Furthermore, degradation can not go further than the predefined depth. A drawback of the second method is that in case of high aggradation, the information of the lower stratification is lost. Note however that this is the case for the first option as well as the lower layers are merged.

## 2.5 MIXING IN THE BED

Up till now, we only considered the changes in sediment fraction due to erosion and deposition. In reality, there will be interaction between the layers due to physical and biological mixing processes (bioturbation). In principle these can be non-diffusive. However, we start with diffusive interaction. The finite volume approach as used with a central difference scheme:

$$\begin{aligned} \frac{M_{i,j}^{n+1} - M_{i,j}^n}{dt} &= D - E - F_{i-\frac{1}{2},j}^n + F_{i+\frac{1}{2},j}^n \\ F_{i+\frac{1}{2}} &= \rho_s \phi_s K_{i+\frac{1}{2}} \frac{p_{i+1}^n - p_i^n}{\Delta z} \end{aligned} \quad (2.13)$$

with diffusivity  $K$ , which can be depth dependent.  $K$  is defined at the interfaces between the layers. As diffusion is a very slow process ( $K \simeq \text{cm}^2/\text{year}$ ) compared to the erosion/deposition, it can be treated in an explicit way.

## REFERENCES

- A. Armanini. Non-uniform sediment transport: Dynamics of the active layer. *Journal of Hydraulic Research*, 33(5):611–622, 1995.
- H.A. Einstein. The bedload function for sediment transportation in open channels. *Technical Bulletin ASCE no. 1026*, 1950.
- M Garcia and G Parker. Entrainment of bed sediment into suspension. *Journal of Hydraulic Engineering*, 117(4):414–435, APR 1991. ISSN 0733-9429.
- Marcelo H. García. Asce manual of practice 110—sedimentation engineering: Processes, measurements, modeling, and practice. volume 200, pages 94–94. ASCE, 2006. doi: 10.1061/40856(200)94. URL <http://link.aip.org/link/?ASC/200/94/1>.
- CK Harris and PL Wiberg. A two-dimensional, time-dependent model of suspended sediment transport and bed reworking for continental shelves. *Computers & Geosciences*, 27(6):675–690, JUL 2001. ISSN 0098-3004.
- MZ Li and CL Amos. SEDTRANS96: the upgraded and better calibrated sediment-transport model for continental shelves. *Computers & Geosciences*, 27(6):619–645, JUL 2001. ISSN 0098-3004.

- Urs Neumeier, Christian Ferrarin, Carl L. Amos, Georg Umgiesser, and Michael Z. Li. Sedtrans05: An improved sediment-transport model for continental shelves and coastal waters with a new algorithm for cohesive sediments. *Computers & Geosciences*, 34(10):1223–1242, OCT 2008. ISSN 0098-3004. doi: 10.1016/j.cageo.2008.02.007.
- Lawrence P. Sanford. Modeling a dynamically varying mixed sediment bed with erosion, deposition, bioturbation, consolidation, and armoring. *Computers & Geosciences*, 34(10):1263–1283, OCT 2008. ISSN 0098-3004. doi: 10.1016/j.cageo.2008.02.011.
- M. Van Ledden. *Sand-mud segregation in estuaries and tidal basins*. Phd-thesis, TU Delft, 2003.
- M Van Ledden, ZB Wang, H Winterwerp, and H de Vriend. Sand-mud morphodynamics in a short tidal basin. *Ocean Dynamics*, 54(3-4):385–391, JUL 2004. ISSN 1616-7341. doi: 10.1007/s10236-003-0050-y.
- L. Van Rijn. *Principles of sediment transport*. Aqua publications, 1993. ISBN 90-800356-2-9.
- John C. Warner, Christopher R. Sherwood, Richard P. Signell, Courtney K. Harris, and Hernan G. Arango. Development of a three-dimensional, regional, coupled wave, current, and sediment-transport model. *Computers & Geosciences*, 34(10):1284–1306, OCT 2008. ISSN 0098-3004. doi: 10.1016/j.cageo.2008.02.012.